8/10/98

DOE/SF/19645--T12

Final Report

HIGH TEMPERATURE MATERIALS TECHNOLOGY RESEARCH FOR ADVANCED THERMIONIC SYSTEMS

DE-FG03-93SF19645-94

Submitted to

U.S. Department of Energy

Office of Defense Energy Project

by

Ralph H. Zee
Materials Engineering Program

M. Frank Rose
Space Power Institute

Auburn University, AL 36849

Tel: (334) 844-3320
Fax: (334) 844-3400

P3 final

DISCLAIMER

TABLE OF CONTENTS

	ABSTRACT	1
1	INTRODUCTION	3
2..	OBJECTIVES	5
3.	LITERATURE REVIEW	6
	3.1. Operating Conditions of Advanced Thermionic Emitter	6
	3.2. Development of Candidate Materials	8
	3.3. Microstructural Evolution	9
	3.4. Creep of Tungsten and Tungsten Alloys	17
	3.5. Creep of Refractory Metal and Alloy Single Crystals	30
	3.6. Summary	33
4.	CREEP MODELING OF PARTICLE STRENGTHENED TUNGSTEN ALLOYS	34
	4.1. Problem of Previous Studies	34
	4.2 Model Selection and Its Improvement	34
	4.3 Creep Modeling of Particle Strengthened Tungsten Alloys	40
5.	EXPERIMENTAL PROCEDURES	47
	5.1. Materials and Sample Preparation	47
	5.2. Creep Testing Equipment and Creep Testing Procedures	48
	5.3. Creep under Different Microstructures	54
	5.4. Parameters to be Determined	54
	5.5. Microstructural Characterization of the Crept Specimens	57
6.	RESULTS AND DISCUSSION	58
	6.1. Creep of Recrystallized W-0.37HfC	58
	6.2. Creep of As-Received W-0.37HfC	61
	6.3. Verification of the Creep Model for Dispersive Carbide Strengthened Tungsten Alloys	64
	6.4. Recrystallization Study of Crept Specimens	69
	6.5. Discussion	83
7.	CREEP MODELING OF SINGLE CRYSTALLINE SOLID SOLUTION TUNGSTEN AND MOLYBDENUM ALLOYS	89
	7.1. Stress Analysis for Deformation of B.C.C Single Crystalline Cylindrical Tube	89
	7.2. Creep Modeling of Tungsten and Molybdenum Single Crystalline Solid Solution Alloys	95
8.	CONCLUSIONS	117
	8.1. Carbide Particle Strengthened Tungsten Alloys	117
	8.2 Solid Solution Tungsten and Molybdenum Alloys	117
	REFERENCES	119

ABSTRACT

Tungsten and tungsten alloys are candidate materials for the thermionic emitter in the space nuclear power convertor. This emitter needs to possess high dimensional stability at temperatures over 2000 K in order to maintain a long service life. The cause for the dimensional instability under high temperature is due to the internal pressure generated by the nuclear fuel inside the emitter cylinder during operation.

In this work, the creep behavior of HfC strengthened tungsten alloys was studied. An ultrahigh vacuum, high precision creep test system was constructed for this purpose so that the samples could be heated up to 3000 K for heat treatment and creep strain could be measured from the creep sample inside the UHV chamber. Creep tests were conducted in tungsten strengthened with 0.37 percent of HfC at temperatures between 2000 K to 2500 K for durations up to 8 weeks. To explain the creep behavior observed in this dispersion strengthened alloy, a creep model was proposed which accounted for the presence of HfC particles in the form of a back stress generated by these particles. This model was verified by the creep test data of W-0.37HfC alloys tested under both extruded and recrystallized microstructural conditions. According to this model, the steady state creep of this type of alloys was expected to increase with time due to coarsening of HfC particle and recrystallization of the alloys under high temperatures. In contrast, conventional simple power law creep model only predicts a constant steady state creep for these materials, which does not represent the microstructural evolution of the materials.

The creep of solid solution alloys such as W-Re, W-Nb and W-Hf and Mo-Nb was also studied. These materials are expected to be more stable in creep properties due to the absence ofcoarsening particles. These solid solution alloys, in their single crystalline state, are reported

possessing better corrosion resistance over their polycrystalline counterparts. Existing creep data of both solid solution tungsten and molybdenum alloys were re-analyzed. The data of these alloys showed two distinct different creep mechanisms: Class I and Class II. The dominating creep mechanism at low stresses could be explained by the Takuchi-Argon model (Class I). At higher stresses, the data could not be explained by any of the existing creep models. A creep model was thus proposed that contained a shift factor due to the effect of the solute in these alloys. In this model, the Class II creep behavior of these solid solution alloys were found as a function of the alloy concentration and atomic size mismatch.

1. INTRODUCTION

Efficiency in direct power conversion systems depends strongly on temperature. During the past decade, there is a concerted effort to develop high temperature thermionic emitter materials in thermionic nuclear power converter. The search has been concentrated on materials based on high temperature creep resistant refractory alloys. An advanced emitters are expected to function at temperatures between 1700 K and 2100 K for ten years under an equivalent stress of about 10 MPa. The high emitter operating temperature as well as the very small cesium gap between the emitter and the collector (needed for the high conversion efficiency) require the development of extremely stable materials. Furthermore, the emitter materials must also be compatible with the hostile nuclear environment present in thermionic systems. The conductive nature of the emitter excludes the possibility of using traditional refractories due to their insulating nature. Pure refractory metals were found to be too weak for such applications due to their low strength at high temperature. Strengthening agents of either solid solution atoms or second phase particles must be added to improve the high temperature mechanical properties. Results from previous studies have shown that the greatly enhanced high-temperature strength observed in tungsten was due to these two strengthening methods.

The prediction of long term creep behavior of materials such as tungsten alloys requires the understanding of dominating creep process with regards to applied stress and temperature. On the other hand, creep properties of a material is sensitive to microstructure. To provide a better creep prediction for the emitter materials, the evolution of the microstructure must be included. From this point of view, two fundamental approaches can be used to acquire the life time evaluation of the emitter. One method is to measure the dimensional stability of emitters made of tungsten alloys under real service conditions, which is both time and resource

consuming. In this case, alloys with different compositions must be tested with different microstructures so that an optimal candidate can be selected. Another approach is to correlate microstructure with short time creep results and to predict real life performance based on the effect of microstructural evolution on properties. The time needed for this latter approach is significantly shorter than the former one. The accuracy of the latter approach depends on the interpretation of short term creep data in light of controlling microstructural parameters. The reliability also depends on the correct prediction of the possible major microstructural changes which occur over long time. Recent studies on microstructural evolution in the candidate emitter materials under the condition relevant to the working conditions of the emitter have made this latter approach possible. However, no creep model is available that can perform the life time evaluation with considering microstructural changes.

In this study, research efforts were devoted to (a) develop creep model(s) that incorporate the microstructural effects and material parameters to the life time prediction of thermionic emitter for different type of tungsten alloys; (b) establish a high temperature creep test chamber and use it to test the candidate materials under conditions similar to the service environment of the emitter; (c) verify the model(s) with the experimental results.

2. OBJECTIVES

The effect of microstructure on the creep behavior of tungsten alloys is important to the application of the long term thermionic emitters. Changes in the microstructure during long term service may lead to enhanced creep and changes in the creep mechanisms. A mechanistically based creep model containing microstructure parameters will not only describe long term creep behavior, but will also provide guidance for the development of new low-creep materials. The research objectives of this study are to:

1. Design, construct and test a system for high temperature high vacuum creep test with high precision; and use this system to conduct high temperature creep tests of a precipitation strengthened tungsten alloy with different microstructures;

2. Develop mechanistic or semi-mechanistic creep models for both second phase strengthened tungsten alloys and single crystalline solid solution tungsten alloys.

3. LITERATURE REVIEW

3.1. Operating Conditions of Advanced Thermionic Convertor

Thermionic nuclear power sources are being considered for long term space applications. To realize the long service life, increasing the service life of thermionic fuel elements is essential. In each fuel element, the heat required for thermionic electron emission from the emitter is generated by nuclear fission of the UO_2 fuel. As shown in Figure 3.1[1], the nuclear fuel pellets are clad in a thermionic emitter cylinder. This cylinder is subject to internal pressure up to 10 MPa due to fuel swelling under neutron irradiation. The cladding creep radially toward the collector leading to a possible internal electrical short circuit at high temperature. Because of the tight tolerance (about 0.2 mm) between the emitter and collector in the fuel element and its high operating temperature, high creep deformation resistance for the thermionic emitter materials is a key factor in the success of these power systems. A typical design of fueled thermionic emitter tube requires a 10 year life at 2000 K during which only 1% radial creep deformation of the emitter is allowed. Thus the average creep rate should be less than 3×10^{-11} s^{-1} over 10 years.

Figure 3.1 shows a schematic for a typical thermionic emission fuel element. The shape of a single unit emitter cylinder resembles that of a thin wall tube. The typical dimensions are 15 mm outside diameter, 1 mm thickness, and 100 mm long. In this case, the radial creep rate $\dot{\varepsilon}_r$ can be calculated by the geometrical parameter and creep relation under simple uniaxial creep condition, which can be expressed as[2]

$$\dot{\varepsilon}_r = (3/2)(\dot{\varepsilon}_{uniaxial}/\sigma_{eff})\sigma_{ij} \tag{3.1}$$

where $\dot{\varepsilon}_{uniaxial}$ is the creep rate obtained under the uniaxial condition, σ_{eff} is the effective stress for creep, σ_{ij} is the deviatoric stress tensor.

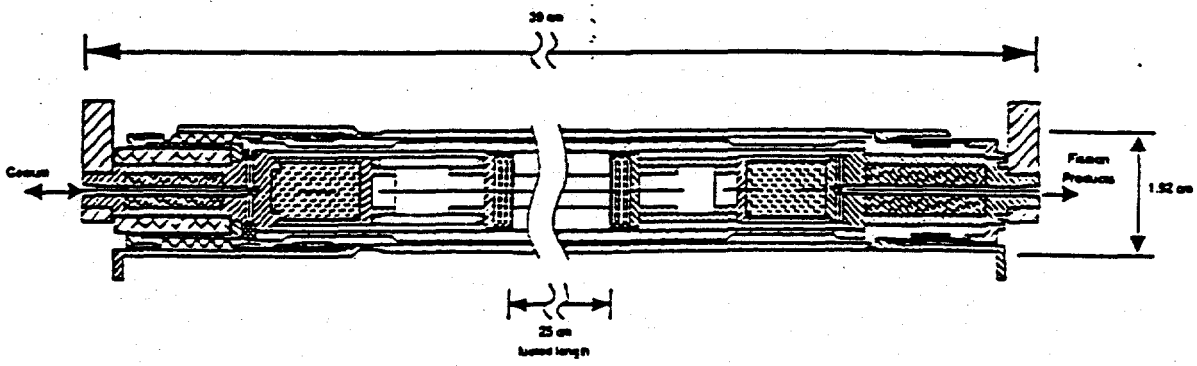

Figure 3.1. Schematic of a thermionic fuel element [1].

3.2. Development of Candidate Materials

The development of particle strengthened tungsten for high temperature aerospace applications began in the late 1950's. Pure refractory metals were found to be too weak for such applications due to their low strength at high temperature. Based on the previous efforts of Raffo et al.[3], Klopp et al.[4,5,6], Rubenstein[7] and Witzke[8] in the search of strong structural materials for space and nuclear applications above 1644 K (2500 °F), tungsten alloys strengthened with fine dispersoids have been proposed to for use in the next generation of thermionic energy conversion (TEC) systems[9,10,11]. In these materials, second phase particles, such as HfC or ThO_2 with high melting point, were introduced into the W matrix[12,13]. Table 3.1 gives some of the high melting refractory materials[14]. In these alloys, dispersed carbides or oxides retard the motion of dislocations and the growth of grains or subgrains, and thus improve the mechanical properties at high temperature[5]. All of these alloys show superior high temperature mechanical properties and creep resistance over pure W at 2200 K [12,15]. However drastic strength loss occurs at higher temperature due to particle coarsening in the precipitation strengthened (PS) tungsten alloys[16].

Another approach to obtain stronger materials than pure tungsten is solid solution strengthening[12]. The alloying atoms for this purpose are Re, Ta, Nb, and Hf. The addition of small amounts of Re in W can also greatly improve the room temperature ductility for fabrication without sacrificing the high temperature mechanical properties of W alloys[4,7,12]. Grain growth also occurs after recrystallization in the solid solution W alloys at high temperature over long periods of time. Stability of the microstructure is thus a major factor that prevents these alloys from long time high temperature service. Recent development of single crystalline substitutional solid solution tungsten alloys has provided both strengthening and long term

thermal stability[17]. But the theories for the creep properties of these single crystalline alloys are insufficient to guide the development of such new alloys.

Table 3.1. Melting Temperatures of Refractory Materials

Metal (symbol)	Tungsten (W)	Tantalum (Ta)	Molybdenum (Mo)	Niobium (Nb)	Rhenium (Re)
Melting Point, K	3695	3290	2896	2750	3459

Material (Formula)	Hafnium Carbide (HfC)	Zirconium Carbide (ZrC)	Thoria (ThO_2)	Tantalum Carbide (TaC)	Titanium Carbide (TiC)
Melting Point, K	4163	3303	3573	4153	3433

3.3 Microstructural Evolution

Microstructural changes occur when the HfC strengthened alloys were exposed to high temperature. There are two major types of microstructural changes: HfC particle coarsening and recrystallization. This two changes will affect the yield strength σ_y of a HfC particle strengthened tungsten alloy through[18]

$$\sigma_y = \sigma_0 + 2\,G\,b\,/\,L \qquad (3.2(a))$$

where G is the shear modulus, b is the Burgers vector, L is the mean planar center-to-center particle spacing, σ_0 is the yield strength of the material in the absence of particles which can be

expressed in the Hall-Petch relation [19]

$$\sigma_0 = \sigma_i + K_y d_G^{-1/2} \qquad (3.2(b))$$

where σ_i is friction stress, K_y is Petch slope and d_G is the grain diameter of the material for different type of tungsten alloys. When coarsening of the HfC particles occurs, the particle radius r increases. Thus for a constant particle volume fraction f_v, interparticle spacing L increases according to [20]

$$L = (3\pi/2f_v)^{1/2} r \qquad (3.3)$$

which results in a decrease in the Orowan stress (σ_{Oro})[21]

$$\sigma_{Oro} = (Gb/L) \qquad (3.4)$$

of the material. On the other hand, when recrystallization occurs, dislocation density decreases, leading to a decrease in the friction stress σ_i (the base yield strength of the material), because σ_i is proportional to the square root of the dislocation density. During grain growth, the diameter of the grains increases resulting in a drop in the term $d_G^{-1/2}$. It is through this combination of microstructure changes (coarsening of particle and recrystallization) that reduces the yield strength of a cold worked particle strengthened material. In pure tungsten, grain growth has also been reported to increase the steady state creep rate. According to Klopp et al.[22], for the steady state creep of arc-melted tungsten also increases with grain diameter through the relationship

$$\dot{\varepsilon} = K_c \sigma^{5.8} d_G^{0.43} \quad (3.5)$$

where $\dot{\varepsilon}$ is steady state creep rate and σ the applied stress. The coefficient K_c is a material's constant which depends on temperature through the term $\exp(-Q_c/RT)$, where Q_c is the activation energy for creep, R the gas constant, and T the absolute temperature. The microstructural effect on the creep of tungsten and tungsten alloys will be reviewed in detail in latter sections of this chapter.

3.3.1 HfC Particle Coarsening

The driving force for the particle coarsening is caused by minimizing the free energy of the system via a reduction in the total particle surface area. Large particles grow at the expense of the smaller ones. Ardell derived a general equation to describe such particle coarsening behavior as[23]

$$r^3 - r_0^3 = k_{coarsen} t \quad (3.6)$$

where r and r_0 are the particle radius at time t and at the onset of coarsening respectively, $k_{coarsen}$ is the coarsening rate which is expressed as

$$k_{coarsen} = 8\gamma D C_e V_m^2 / 9RT \quad (3.7)$$

In Equation (3.7), γ is the interfacial free energy of the particle-matrix interface, D is the diffusion coefficient of the coarsening rate-limiting solute which contains the term $\exp(-Q_{coarsen}/RT)$. The parameter $Q_{coarsen}$ is the activation energy of coarsening. In Equation (3.7), C_e is the correspondent solute concentration that is in equilibrium with a particle of infinite size, V_m the molar volume of the precipitate.

In W-Re-HfC and W-HfC alloys, the coarsening of the HfC particles has been studied independently by Klopp and Witzke[5], Chen[24] and Ozaki[25] using similar methods. The particle size was measured using transmission electron microscopy (TEM) techniques. In their work, the particle radii were expressed by the Equation (3.6); but different $k_{coarsen}$ values were obtained. Their results are summarized in Table 3.2.

Table 3.2. Summary of the Coarsening Studies for HfC.

Author(s)	Klopp and Witzke[5]	Chen[24]	Ozaki[25]
$k_{coarsen}T$ (m^3K/s)	$1.2\times10^{-13}e^{-615000/RT}$	$1.5\times10^{-17}e^{-307000/RT}$	$1.3\times10^{-12}e^{-480700/RT}$

The activation energy for coarsening ranges from 293 kJ/mole to 615 kJ/mole. There are differences in other corresponding parameters in the Equation (3.7). As pointed out by Ozaki[25], this discrepancy is due to the statistical error in the particle size measured using TEM. Plotting all three equations in Table (3.2) against reciprocal temperature, the maximum difference in the predicted particle sizes was found varies only a factor of about two at temperatures above 2000 K. It is important to identify the expression with the highest scientific merit. From Klopp's work[5], the controlling factor was considered as the diffusion of Hf

because they found that the activation energy of the coarsening to be 615 kJ/mole which was close to that of the substitution diffusion of the Hf in tungsten (598 kJ/mole from the study of coarsening of HfC by Klopp and Witzke[5]). According to Chen[24], the activation energy of the coarsening was 293 kJ/mole at temperatures between 1955 K and 2500 K. Chen suggested that the controlling factor was the diffusion of carbon in tungsten. Chen based this interpretation on the work of Dainyak and Kostikov[26], where the activation energy of carbon diffusion in tungsten was found to be 224 kJ/mole at temperatures between 1600 K and 2500 K while the diffusion energy of Hf was only 197 kJ/mole at temperatures between 1173-2173 K. The large difference in the reported activation energy of Hf in tungsten critically affects the identification of the controlling factor for the HfC coarsening. Thus the direct diffusion of Hf in tungsten under the condition relevant to the emitter working temperature range was conducted by Ozaki[25]. Ozaki found that Hf lattice diffusion in pure tungsten can be expressed as

$$D\ (m^2/sec) = 10^{-10} \exp(-Q_{lattice}/RT) \tag{3.8}$$

where $Q_{lattice}$ has a value of 334 kJ/mole.

Comparing this lattice diffusion activation energy with that of the coarsening by Ozaki's work (481 kJ/mole)[25], there remains a 146 kJ/mole difference. According to Ozaki, this is due to the fact that the solubility of Hf is also a strong function of solubility behavior of carbon. Based on the W-C phase diagram, the solubility of carbon in tungsten is governed by an energy of solution of 125 kJ/mole. Once carbon has reached its solubility limit in the matrix due to a decrease in temperature, the Hf atoms will also be precipitated out due to the strong binding energy of Hf to C to form HfC. Results from earlier studies have shown that the solubility of Hf

in W is significantly reduced due to the presence of carbon[27]. When temperature increases, carbon solubility increases which leads to the decomposition of HfC. Thus, the temperature depends of the carbon solubility also contributes the coarsening behavior. Taking into consideration of this contribution, the total activation energy of coarsening is about 460 kJ/mole which is close to the observed 481 kJ/mole by Ozaki[25].

Considering the existing error in measuring particle size using TEM, Ozaki provided an particle coarsening equation that based on the above three studies[25], i.e.

$$r(m)=[2.8\times10^{-13}(t/T)\exp(-472340/RT)+r_0^3]^{1/3} \qquad (3.9)$$

which appears to be the best representation to-date describing the coarsening of HfC particles in tungsten alloys.

3.3.2. Recrystallization

As mentioned earlier, recrystallization is another important microstructural change that will affect the emitter material's property during service at high temperature. Recrystallization occurs when a cold worked pure metal is heated up to a temperature that is about 40 to 50 percent of its melting temperature. The driving force of this process is the release of the stored energy from dislocations that are generated in the material by cold work. As a result of the reduction in dislocation density, hardness will drop drastically and so will the yield strength of the material. In pure tungsten, recrystallization occurs at about 1500 K. The recrystallization temperature of the unalloyed tungsten is greatly affected by impurity[4]. The study on recrystallization of electron-beam-melted (EB) tungsten and tungsten-rhenium alloys shows that the electron-beam-

melted tungsten undergoes a 50 percent recrystallization in one hour at temperature of 1477 K which is about 280 K lower than that of the unalloyed arc-melted tungsten (1755 K)[28]. This is because that the purity of the electron-beam-melted tungsten is higher than that the arc-melted (AM) one. In EB-tungsten, alloy atoms of rhenium produce a sharp increase in the recrystallization temperature from 1477 K to 1894 K, an increment of 417 K. This effect saturates at rhenium contents between 4 and 6 at%. At the same time, minimum grain size and grain growth rate were obtained when Re content were between 6 to 24 at%. For EB tungsten, after annealing for 1 hour at 2255 K, the minimum average grain diameter is about 500 μm at 9 at% Re. In contrast, under the same annealing condition, a minimum average grain diameter of 200 μm was obtained at 6% Re for the arc-melted W-Re system. In other solid solution alloys such as W-Ta, W-Hf and W-Nb, their ultimate tensile strength in the cold worked state is higher than that of the corresponding recrystallized state below 2200 K, but approaching the latter with increasing test temperatures. Above 2200 K, the cold worked materials have an ultimate tensile strength very close to that of the recrystallized one[15]. Therefore, solid solution tungsten alloy can be used in the recrystallized condition for long time applications.

Using second phase particles, the recrystallization temperature can be increased further. In W-Re-ThO_2 and W-Re-HfC alloys, Tsao et al. studied the effect of ThO_2 and HfC on the recrystallization of W-Re alloys[29]. The microhardness of the two types of tungsten alloys was plotted against the one-hour annealing temperature. The onset of recrystallization was determined at the temperature where significant softening occurred. The recrystallization temperatures of these alloys range from 1600 to 2000 K for the thoriated alloys depending on Re content. For W-4Re-0.35HfC, the recrystallization temperature is between 2065 and 2180 K depending on the amount of cold work. In their work, the onset of recrystallization was delayed

with increasing Re. For a fixed Re content, the recrystallization temperature decreased with increasing cold work as expected. The thoria particle diameter in their study was about 2 μm, while the HfC particle diameter was 0.1 μm. However, in the W-0.37HfC alloy, the reported starting particle diameter was 4 nm, and the recrystallization temperature was as high as 2673 K[25]. Evidently, the finely dispersed HfC particles increases the recrystallization temperature of the alloy. The effect of particles on the recrystallization behavior of an alloy can be explained by the Zener's theory[30].

According to Zener, there is a retarding force exerted on the migrating grain boundary by a precipitate particle during the recrystallization. This retarding force can be expressed as

$$F_R = 3f_v\gamma/2r \tag{3.10}$$

where γ is the specific interfacial energy of the boundary, and r is the radius of the particle. To continue the recrystallization process under the retardation of the particle, a driving force is needed to maintain the grain boundary migration. This force (F_D) is estimated by

$$F_D = 2\gamma/d_G \tag{3.11}$$

where d_G is the grain diameter. Equating Equations (3.10) and (3.11), yields

$$d_G = 4r/3f_v \tag{3.12}$$

Equation (3.12) illustrates that the final grain size of a recrystallized material is proportional to

the precipitate radius (r) and the reciprocal of its volume fraction (f_v). Small particle radius and large particle volume fraction will yield small final grain size. From this point of view, the coarsening of HfC particles will promote grain growth and lower the recrystallization temperature. Based on this theory and the recrystallization temperature of the W-HfC alloy obtained from the experiments, it is possible to estimate the critical particle radius r_c beyond which recrystallization is unrestricted. According to Equation (3.9), for recrystallization to occur after annealing at 2673 K for one hour, the critical radius is about 60 nm. To reach the same radius at 1800 K, 2000 K, and 2200 K, the times needed are 2.32 years, 40 days and 80 hours respectively. Thus according to Equation (3.8) for the tungsten alloy emitter operating at about 1800 K, the material will creep under two stages: creep under cold worked microstructure, and creep under the recrystallized condition.

3.4. Creep of Tungsten and Tungsten Alloys

In order to predict the lifetime of the emitter materials within the working temperature range and in the condition of low stress, the identification of the dominating creep mechanism is important. Different creep controlling mechanisms display different dependencies of the steady state creep rate on applied stress. In general, when the creep of a pure metal or an alloy is controlled by diffusional creep, the stress exponent (n) of the power law creep equation

$$\dot{\varepsilon} = A_c \sigma^n \tag{3.13}$$

with n equals to 1[31]. When the creep is controlled by dislocation climb and solution drag, n equals to 5 and 3 respectively, according to Sherby and Burke[32]. In Equation (3.13), $\dot{\varepsilon}$ is the

steady state creep, σ the applied stress, A_c a material's constant that depends on absolute temperature (T) through an activation energy Q as described by the Arrenius law, with $A_c=A_c'\exp(-Q/RT)$, where A_c' is a temperature-independent constant, while R is the gas constant.

The fundamental process with which a material creeps may be a function of temperature. Thus determining the dominating creep mechanism under the stress-temperature regime that is relevant to the service condition of the emitter is essential to meaningful life prediction. In order to gain insight on these aspects, the creep behavior of tungsten and tungsten alloys will be compared and reviewed regarding to the stress-temperature-microstructural effects based on information available in the literature.

3.4.1. Creep of Pure Tungsten

The study of the creep behavior of tungsten first started in the lamp industry. Pugh et al. studied the effect of temperature on the stress sensitivity of the creep rate of tungsten[33]. They found that between 1145 K and 1477 K, the stress exponent (n) of the power law creep equation (Equation (3.13)) increased with decreasing test temperature. In the study of Harris and Ellison , the n value changed from 4.5 to 18 and then to 43 when the test temperature was changed from 1644 K to 1088 K and then to 922 K[34]. This increase in the n value was explained as the shift of creep controlling mechanism from fully diffusion control to the fully dislocation glide control.

Klopp and Raffo[28] found that in arc-melted tungsten, even when the creep was fully controlled by diffusion (n=5.8), the activation energy Q also changed with test temperature. They observed that Q=309 kJ/mole between 1922 to 2200 K and Q=585 kJ/mole from 2200 to 2477 K. Similar temperature dependent behavior of the creep activation energy in tungsten was also reported by Robinson and Sherby[35]. They reexamined the creep test results of arc-melted

and powder-metallurgy tungsten by King and Sell[13], Klopp et al.[22], Pugh[36], Green[37], Sutherland and Klopp[38], Gilbert et al.[39], Flagella[40] and Taylor et al.[41]. Using the temperature dependent elastic modulus data, E=E(T), from the work of Armstrong and Brown[42] and Lowrie and Gonas[43], steady state creep rate was plotted against the stress to modulus ratio (σ/E) for every set of data. Robinson and Sherby[35] reexpressed the creep of tungsten by the equation

$$\dot{\varepsilon}=A_c''\exp(-Q_c/RT)(\sigma/E)^n \tag{3.14}$$

where $A_c''=A_c'/E^n$. Taking the logarithm of this equation, the modulus-corrected activation energy for creep was calculated by

$$Q_c|_{\sigma/E} =-R[\partial \ln\dot{\varepsilon}/\partial(1/T)] \tag{3.15}$$

Plotting the calculated Q_c as a function of temperature, Robinson and Sherby[35] found that between 1473 and 2473 K, Q=376 kJ/mole and above 2473 K, Q=585 kJ/mole. The two distinct activation energy values were found to correspond to those for the dislocation core diffusion (378 kJ/mole) and lattice diffusion (585 kJ/mole) respectively in tungsten. In order to provide a unified creep equation for tungsten for the two activation energies, Robinson and Sherby introduced an effective diffusion coefficient D_{eff} which was expressed as

$$D_{eff} = D_L f_L + D_D f_D \tag{3.16}$$

where D_L and D_D are the lattice and dislocation diffusion coefficients respectively, f_L and f_D are the fractions of atoms which participate in lattice and dislocation diffusion respectively. According to their paper, $D_L=5.6\times10^{-4}\exp(-585/RT)$ m^2/s, and $D_D=10^{-8}\exp(-378/RT)$ m^2/s, where the energy is expressed in unit of kJ/mole.

The creep behavior of polycrystalline tungsten is also affected by the microstructure. As shown in Equation (3.5), in the arc-melted tungsten, the creep rate $\dot{\varepsilon}\propto d_G^{0.43}$, while for tungsten made by the powder metallurgy method, $\dot{\varepsilon}\propto d_G^{2}$. This discrepancy in the grain size dependence was discussed by Robinson and Sherby[35]. According to their paper, the creep data of polycrystalline tungsten fall into two categories: creep without subgrain formation and creep with subgrain formation. Without subgrain formation, creep of tungsten can be expressed as

$$\dot{\varepsilon} = S d_G^{2} D_{eff} (\sigma/E)^{7} \tag{3.17}$$

where S is a universal creep constant with a value of 3×10^{48} m^{-4}. This relationship is valid in tungsten made by the powder metallurgy (PM) method. In this case, the reported grain sizes are very small (in the ranges of 10 to 35 μm)[37]. Grain boundary area is sufficiently large to act as source and sink of dislocations so that creep will proceed without forming subgrain. When the grain is sufficiently large, subgrains are formed during creep in order to sustain the creep deformation. Robinson and Sherby proposed that the form of Equation (3.17) was still valid, but the grain diameter in the Equation (3.17) was replaced by the subgrain size λ but with a different value of creep constant, S'[35]. In this case, according to the work of Sherby and Burke, the subgrain size λ depends on stress σ through the relationship[32]

$$\lambda=\beta\sigma^{-1} \tag{3.18}$$

where β is a material constant. Combining Equations (3.17) and (3.18), a fifth power law relationship is obtained for the subgrain forming tungsten. According to Robinson and Sherby[35], all arc-melted tungsten materials obey this fifth power law. When subgrain is created during creep deformation, the effect of grain size becomes minor. Since the fifth and seventh power law relations represent the above two extreme cases, any power value that falls between these two values for tungsten can be explained by the relative contributions of the two microstructural factors. For example, in the work of Klopp et al.[22], n equals to 5.8 for both arc-melted and electron-beam melted tungsten. One can conclude that the subgrain formation dominates, and the grain size dependent is rather week ($\dot{\varepsilon}\propto d_G^{0.43}$). The relation $\dot{\varepsilon}\propto d_G^{0.43}$ holds when the reported grain size ranges from 50 μm to 4 mm. However, the exact condition for the transition between the different stress dependence was not discussed by Robinson and Sherby.

3.4.2. Creep of Tungsten Alloys

3.4.2.1. Creep of Solid Solution Tungsten Alloys

Systematic studies of the high-temperature creep properties refractory metal alloys had been carried out by the National Aeronautics and Space Administration (NASA) Lewis Research Center (LeRC) through the research program of refractory metals since 1963[44]. This program was aimed at searching for refractory metal alloys with useful strength above 1644 K. Various tungsten alloys had been developed and tested for their high-temperature tensile properties, recrystallization temperature, high-temperature creep rupture test, high-temperature step-load creep test, and low-temperature four point bending test. Great improvements were obtained in

the high-temperature creep strength and tensile strength through appropriate alloying[12].

In general, the presence of solid solution atoms in tungsten increases the creep strength. Raffo et al.[3] conducted step-load creep tests at 2200 K of both arc-melted and electron-beam-melted W-Re alloys in the recrystallized condition with Re content up to 6.64 at%. The n values of the power law equation obtained range from 5.3 to 6.1 which are close to the n value of 5.8 for the unalloyed tungsten[22]. They found that the creep rates of the electron-beam-melted (EB) tungsten alloy were higher than those of the arc-melted (AM)tungsten alloy because of the high purity and larger grain size of the electron-beam-melted alloy. They also obtained the creep strength as a function of alloy content for the solid solution tungsten alloys such as W-B, W-Hf, W-Ta, and W-Nb at the creep rate of 10^{-6} s^{-1} at 2200 K. They concluded that the alloy strengthening effect of the solute atoms followed a descending order of B, Hf, Ta, Nb and Re. The strengthening effectiveness of the different solutes has been correlated with the atomic size difference between the solute and tungsten. For all the substitution alloy studied, Hf was found to be the most effective strengthening agent. Consequently the effect of Hf on the creep behavior of tungsten was studied in more detail [12]. Results of this later work show that the creep stress exponents of different tungsten binary alloys are between 5 to 6. This implies a similar creep mechanism for these alloys as that for pure tungsten under the same test condition. However, creep rates of the alloys were reduced due to the presence of the alloying elements. This creep behavior of dilute tungsten was also reported by other investigators. Vandervoort[45] studied the creep of W-5Re alloy made by PM method between 1873 and 2073 K. Creep rates were reported to reduce by a factor of 10 from pure tungsten. This result is consistent with the work of Raffo et al.[3]. The stress exponent n of 5.5 and an activation energy of 435 kJ/mole for creep were also obtained suggesting that the creep was controlled by dislocation core diffusion.

When the rhenium content was increased above 24 at%, creep rates were found to be consistently higher than those containing only 1 to 2% solute despite the majority of the creep rates were still lower than pure tungsten. At the same time, the stress exponent drops to 4.0 for the EB W-24Re alloy at 2200 K[4], 3.8 for PM W-25Re (1773 to 2200 K)[46], and 4.7 for the AM W-26Re alloy[4].

The change in the creep behavior as a function of solute that had occurred in other alloys was discussed by Sherby and Burke[32]. In their paper, the effects of alloying on the creep behavior of solid solution alloys were summarized based on the analysis of extensive creep data. They concluded that the addition of solute atoms not only increased the creep strength, but under certain conditions also led to a change of the stress exponent of the creep equation from 5 to a value of 3 for steady state creep. Thus the steady state creep behavior of solids can be divided into Class II and Class I solids based on the two different stress exponent values of the power law creep equation for the steady state creep of the material. According to Sherby and Burke[32], the stress exponent value n is typically 3 for Class I solids. This type of creep has been found in many high concentration solid solution alloys. On the contrary, Class II solids usually possess higher n values (on the order of 5). Most pure metals and dilute alloys belong to this type of materials. To quantitatively describe the alloying effect on Class I creep in a material, Takeuchi and Argon[47] developed a creep model showing that creep in Class I material is controlled by the viscous glide of edge dislocations under the drag of the solute atmosphere. And the creep rate is inversely proportional to the square of the solute-solvent atom size mismatch parameter (e) as well as solute concentration (C). On the other hand, Weertman[48] developed a model for Class II creep controlled by non-conservative motion of edge dislocations in pure metals.

In tungsten alloys, the above classification has been supported by the creep data of W-

25Re[46]. Single crystalline Mo-Nb alloys exhibit such a transition from Class II to Class I behavior at 1923 K. Tachkova et al.[49] observed that at 1923 K, stress exponent of the steady state creep of the Mo-Nb single crystalline alloys changed from 5.8 to 3 when the Nb weight percentage increased from 1.8 to 3. They also developed an equation that related the steady state creep rate of the alloys to stress and alloy concentration in the following form:

$$\dot{\varepsilon}/\tau^3_{hkl} = BC^{-1.2} \tag{3.19}$$

where τ_{hkl} is the resolved shear stress on the {hkl} plane, B is a constant and C is the concentration of Nb. The exponent (value of 3) in the shear stress term is related to the stress exponent defined earlier. This equation is in agreement with the model developed by Takeuchi and Argon[47]. However it is only valid for Nb concentrations greater than 3%. For concentrations below this critical value, the stress exponent of the alloy was found to increase from 3 to 5.8 which is similar to that of pure molybdenum. Unfortunately, no equation was provided in these previous studies to correlate the dependence of creep deformation on alloy concentration for class II creep of materials. Available data from W-Nb, W-Ta and W-Hf alloys exclusively show Class II creep. However no detailed analysis of the creep behavior has been for these systems.

3.4.2.2. Creep of Particle Strengthened Tungsten Alloys

There are mainly two kinds of particle strengthened tungsten alloys available: carbide-strengthened tungsten alloys (usually referred as precipitation strengthened tungsten alloy) and oxide-strengthened tungsten alloy (usually referred as dispersion strengthened tungsten alloy or

ODS tungsten alloy).

The creep test of carbide strengthened tungsten alloys was conducted for W-Nb-C alloys[3,12]. In the W-Nb-C alloys, the high tensile strength of an extruded W-1.15Nb-1.32C alloy was related to the stabilization of the cold worked structure by the finely dispersed W_2C carbides (0.5 μm in diameter) in the matrix[3]. The influence of carbon addition on the high temperature creep and tensile strength in unalloyed tungsten, W-Nb, W-Ta, W-Ta-Re, and W-Hf alloys was studied[12]. The creep strength of these alloys increased with increasing carbon content, with the best strengthening effects found in the W-Hf-C alloys. The highest creep strength of the W-Hf-C alloys was related to the finest HfC carbide sizes (on the order of 0.05 to 0.2 μm). Hafnium carbide (HfC) possesses the highest melting point 4103 K and the highest energy of formation (the most negative) among all carbides. Therefore HfC is expected to be the most stable compound for carbide strengthening. On the other hand, lower creep strength was obtained in W-C system as compares to that of unalloyed tungsten. The reduction in the creep strength was explain by the increase in the self-diffusion rate of tungsten due to the presence of carbon[12].

The study on the compositional and microstructural influence on the high temperature strength of AM W-Hf-C alloys provided a further identification of the effect of HfC on the high temperature mechanical properties of tungsten[7]. In Rubenstein's work[7], the effect of microstructure on the creep of W-Hf-C alloys was emphasized. The W-Hf-C alloys were found to be heat treatable and the lowest temperature for solution treatment was 2810 K. Different heat treatments led to different microstructures. TEM results indicate that 1) the recrystallized alloys contain equiaxial grains and relatively large HfC particles; 2) in the solution annealed and aged microstructure, fine HfC particles are distributed dispersively in the recrystallized matrix; and 3)

in the swaged and tested W-Hf-C alloys, cells (subgrains) form with straight sides and contain fine HfC particles HfC precipitates either in the cell boundaries or in the cell interiors, and dislocation network stabilized with fine particles can be seen in the subgrain interior. All of the recrystallized or solution annealed and aged alloys were crept at 2200 K. The resultant creep data were interpreted by the simple power law creep. Significant improvement in the creep strength over the pure tungsten and W-Hf binaries was obtained in both recrystallized W-0.48Hf-0.50C and the solution annealed and aged W-0.48Hf-0.50C. The stress exponent can be as high as 10 to 13, as compared to about 5 for AM pure tungsten and W-Hf alloys. This high stress dependence was explained by the presence of fine dislocation structure stabilized by the particles observed within the cell interior. The network density leads to an increase in the internal stress and thus in the high stress dependence. However, no experimental evidence is available to support this hypothesis. Instead, the well formed subgrain has only been found in the swaged samples after tensile test. While in the solution and aged samples, no subgrain formation has been observed even after tensile test. In fact, TEM observation shows only dislocation network stabilized by particles in the solution and aged tensile specimens. Therefore, Robenstein's statement on the high creep stress dependence for the solution annealed alloys may not be valid.

The creep strength increment due to HfC was quantified by a detailed measurement of the HfC diameter in various W-Re-Hf-C alloys[5]. In this study the combined effects of high temperature strengthening due to HfC and the low temperature ductility improvement of rhenium were examined to determine if there was any detrimental interaction between these two factors. Based on the experimental results they concluded that there was no detrimental interaction associated with the HfC induced strengthening at high temperature and rhenium enhanced ductility. In fact, superior creep properties were obtained in the W-Re-Hf-C alloys. The creep

strength of these alloys σ_c is related to the HfC volume percent (f_V), median HfC particle diameter (d) and matrix creep strength ($\sigma_{c(m)}$) through the relationship

$$\sigma_c = af_V^{1/2}/d + \sigma_{c(m)} \tag{3.20}$$

where a is a constant, also called the particle strengthening rate. The strengthening effect of HfC in tungsten was explained by its ability to retard the motion of individual dislocation (defined as direct strengthening) and resist subgrain boundary migration (defined as indirect strengthening). These two strengthening factors have been illustrated by the fact that swaged alloys possesses an extraordinary high creep strength at the median particle diameter of 40 nm. At a grain diameter of 60 nm the extra strengthening disappears in the as-swaged alloy as compared with the solution annealed and aged alloys. This suggests that the indirect strengthening is ineffective when the particle size is beyond a certain critical size.

In general, finer HfC particles were obtained when the tungsten alloys were either solution-annealed or solution-annealed and aged compared to those in the recrystallized condition. Thus materials with better creep strength can be obtained when processed in the former two conditions. The corresponding stress exponent n (Equation (3.13)) of W-Re-Hf-C alloys ranges from 13 to 20 for solution annealed or solution annealed and aged states. These values are higher than that of alloys in the recrystallized or swaged states (6 to 8). Unfortunately, in the studies of Rubenstein[7] and Klopp and Witzke[5], the creep constant A_c of Equation (3.13) was not expressed in terms of the particle diameter and volume fraction of HfC. Consequently the effect of particle coarsening on long term creep of these alloys cannot be determined.

A recent study at Arizona State University has generated more extensive creep data in the temperature range of 1900K to 2783K and stresses between 20 MPa and 100 MPa for W-4Re-0.26HfC[24], W-4Re-0.33HfC[50] and W-3.6Re-0.33ZrC alloys[51]. A typical set of data is shown in Figure 3.2. These data were analyzed based on the creep equation given in Equation

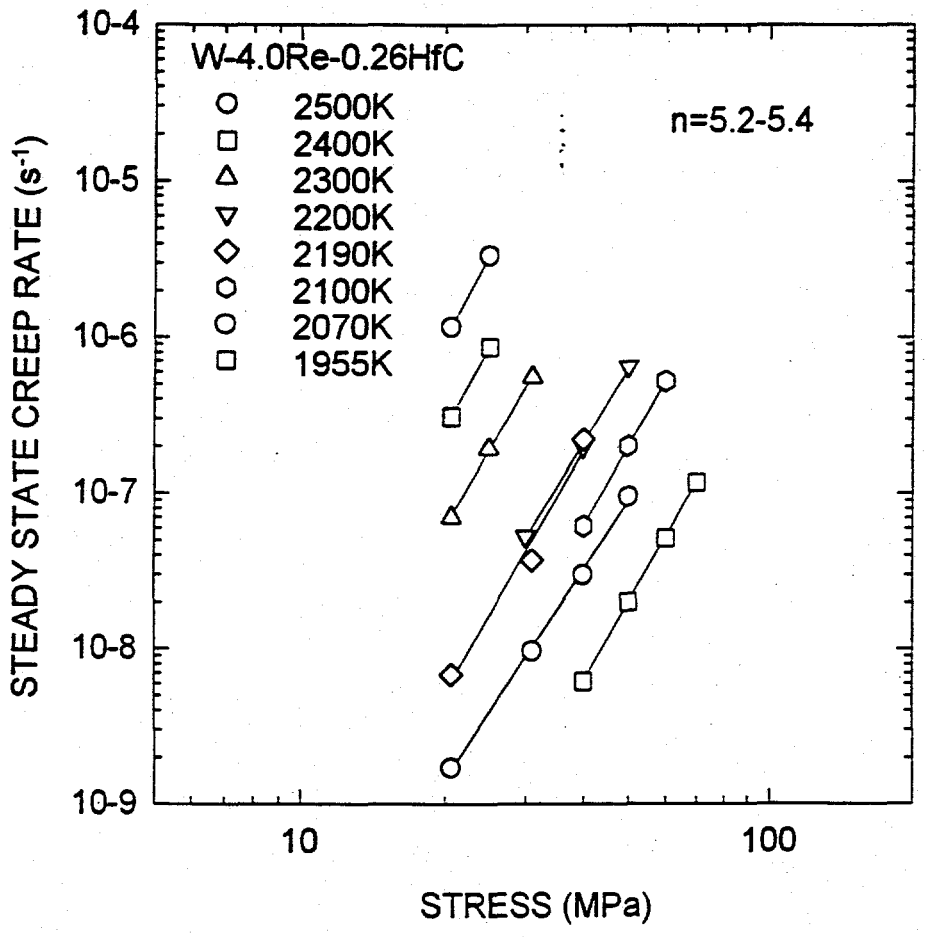

Figure 3.2. Stress dependence of the steady state creep of W-4Re-0.26HfC[24].

(3.13) to produce a stress exponent of 5.2 to 5.4 and the activation energy for creep was also obtained. In W-4Re-0.26HfC, Chen reported two activation energies for creep at two different temperature ranges [24]. At temperatures between 1955 and 2200 K, the activation energy for the W-4Re-0.26HfC alloy was found to be about 439 kJ/mole and from 2300 to 2500 K, the activation energy was 678 kJ/mole [50]. For W-4Re-0.33HfC alloy between 1955 and 2190 K, the activation energy was also reported at around 439 kJ/mole by Luo et al. [51]. This low energy value was related to the dislocation core diffusion in the materials. However, the higher activation energy of 677 kJ/mole obtained for higher temperature is above the highest value for the activation energy for lattice diffusion reported for tungsten (640 kJ/mole)[52]. In W-3.6Re-0.33ZrC, the activation energy is about 456 kJ/mole between 1900 and 2400 K[51]. These studies concluded that the mechanism of creep in these alloys was dislocation creep either controlled by dislocation core diffusion (dominating at low temperature) or by lattice diffusion (dominating at high temperature) Experimental evidence of both direct and indirect strengthening was obtained through TEM observation from the crept W-4Re-0.26HfC and W-3.6Re-0.33ZrC samples. The individual dislocations detected were all edge dislocations. Although particle coarsening was observed in their research, the microstructural change of W-Re-HfC during long term high temperature operation was still ignored by the final creep model[24,51]. Thus, the life time prediction of the emitter was performed under a fixed microstructural condition, which was not consistent with their own research findings.

In W-ThO_2 alloys, thoria is relative inert. It is mainly used for grain size control in the lamp industry because of its melting point of 3490 K which is the highest amongst all metal oxides. Typical alloys are W-1 w/o ThO_2, W-2 w/o ThO_2 and W-Re-ThO_2 with equivalent amount of ThO_2. Because this type of alloys are made by powder metallurgy methods, thoria

tends to segregate on the grain boundaries. Small fraction of the oxide will also be present in the matrix due to grain boundary migration during sintering, thus providing strengthening against creep deformation[24]. In the lamp industry, the addition of rhenium is used to improve the room temperature fabricability, and at the same time, rhenium can also increase the resistance of filament for vibration damage. In the ODS tungsten alloys, the addition of rhenium above 10 percent has been reported to change the creep behavior of the W-ThO_2 alloy from Class II to Class I. This means that in this type of alloys, the contribution of the Re still has a dominating effect through changing the creep behavior of the matrix.

3.5. Creep of Refractory Metal and Alloy Single Crystals

The development of single crystalline alloy provides another alternative for use in the thermionic emitter. One of the problems of carbide strengthened polycrystalline materials is microstructural evolution of the material during service at high temperatures for long periods of time[5,24,25]. The strengthening effect in polycrystalline tungsten alloys strengthened with HfC particles may diminish due to coarsening of the strengthening particles at elevated temperatures. This degradation process is typically represented by an increasing in the steady state creep rate as a function of operating time. During high temperature service, recrystallization will provide additional grain boundary area for easier fuel penetration thus preventing the materials to be in direct contact with nuclear fuel or other components containing potential fast diffusing elements.

The material system based on a single crystalline matrix strengthened by fine inert particles can also provide strengthening and simultaneously eliminate any problems associated with grain boundaries. The successful examples are numerous, and one of these is the single crystalline superalloy turbine blade. However the best superalloys lose their strength at

temperatures above 1300 K and are inappropriate for ultrahigh temperature applications. Single crystalline refractory alloys possess the mechanical strengthened at such ultrahigh temperature. However, the high melting temperature of refractory metals makes the use of crucible for crystal growth difficult if not impossible. Electron beam melting and other non-containment techniques are more appropriate to grow refractory metal and alloy single crystals, albeit at higher fabrication costs. These single crystalline materials have been developed by Nikolev et al.[17]. They selected alloying solutes to form solid solutions which are thermodynamically stable from room temperature to the very high emitter operating temperature of over 1800 K. Figure 3.3 compares the reported creep strength of one of the single crystalline alloys that has been developed with polycrystalline W-4Re-0.33HfC[29]. It is evident from the figure that the solution strengthened single crystals possess better creep resistance than the polycrystalline material.

In the creep study of tungsten single crystal, stress exponent was found to be about 5.8 and the activation energy for creep at 5.8 eV/atom (equivalent to 559 kJ/mole)[53]. Dislocation network and subboundaries were formed during creep between 2073 K and 2823 K.

The creep of single crystalline molybdenum has been reported by numerous authors[49,54,55,56,57]. For single crystalline molybdenum under a uniaxial tensile creep test condition, the stress exponent, n, for power law creep was found to be about 7[57]. In Tachkova's work n was 5.8 as compared to a lower value of 5 for polycrystals[49].

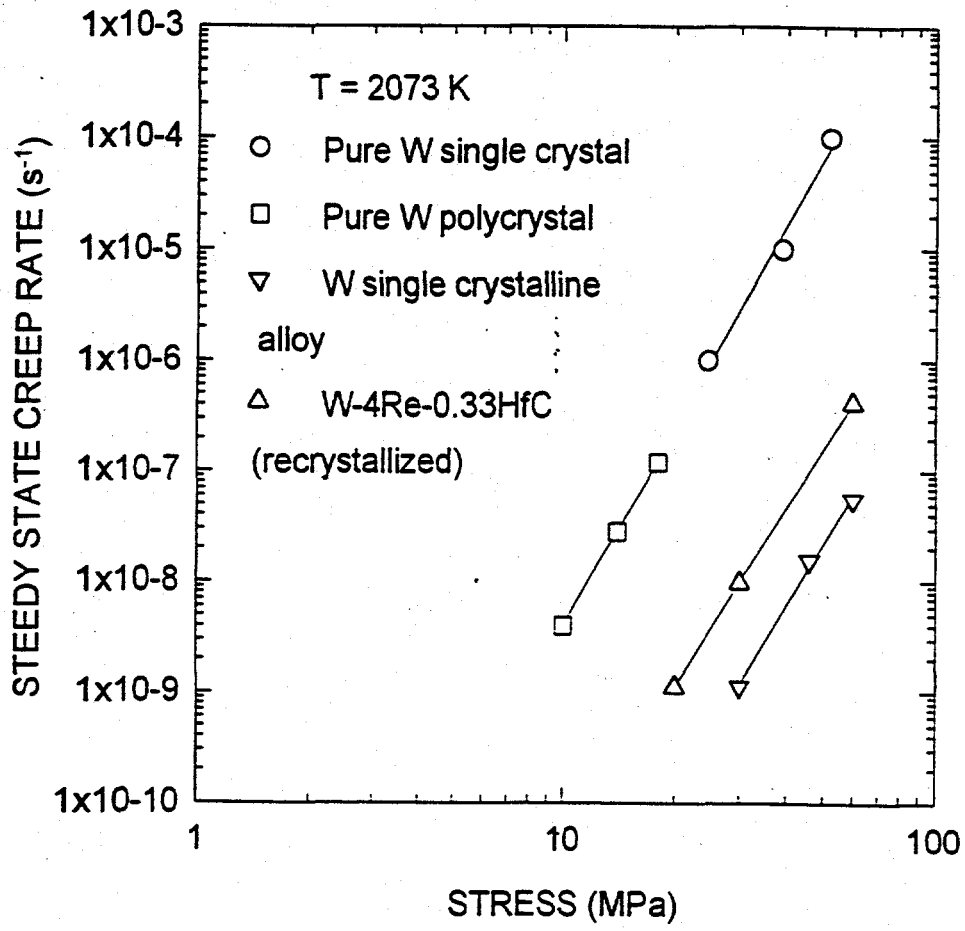

Figure 3.3. Comparison of creep between single and polycrystalline tungsten materials.

3.6. Summary

Extensive creep data, microstructural information and their relationship to high temperature mechanical properties exist for tungsten and its alloys. Most of these results were obtained under the test conditions which targeted at polycrystalline material. The absence of grain boundary also makes fuel penetration significantly slower because no grain boundary exists to provide short circuit diffusion path for the nuclear fuel components[17]. These attributes lead to the current development of high creep resistance single crystalline solid solution strengthened W-based and Mo-based materials for potential thermionic fuel elements applications. However, in Nikolaev's work, the chemical composition and crystalline orientation of their alloy were not reported. On the other hand, the low precision of the strain measurement in the early days precluded the acquisition of low stain rates in a short durations. Therefore the important effects of microstructural changes during long time high temperature operation on creep were predicted with uncertainty. Recent progress on the study of creep of tungsten alloys and the accompanying microstructural evolution investigation under the conditions close to the thermionic emitter service state provides a great deal of insight into the materials property-structure correlation. However, the microstructural change and other material parameters have yet to be explicitly incorporated into the creep equation of particle strengthened tungsten alloys. The governing factors that control creep in solution strengthened tungsten alloys also have not been established. These two problems prevent the performance prediction of the emitter materials for long time high temperature applications. These two issues were the subject of this dissertation.

4. CREEP MODELING OF PARTICLE STRENGTHENED TUNGSTEN ALLOYS

4.1. Problem of Previous Studies

The particle strengthened tungsten alloys have been chosen as candidate materials for advanced thermionic emitter. The strengthening particles in the alloys are expected to coarsen under long-time high temperature exposure. This microstructural evolution and recrystallization will diminish the creep strength of these materials. For this reason, the kinetics for the HfC particle coarsening and the condition for recrystallization have been addressed by several authors[5,24]. However the creep equation used by the authors for life time prediction is still based on a fixed microstructure under relatively short term creep test.

The purpose of this portion of the dissertation is to develop a model that expresses the microstructural variable explicitly in the creep equation of the particle strengthened tungsten alloys.

4.2. Model Selection and its Improvement

The modeling approach taken by this study will be through the comparison between available creep data of tungsten alloys with other particle strengthened alloy systems where creep models have been developed. Early creep data for the W-Re-Hf-C and W-Hf-C alloys cover wide range of compositions and many of them combine both solid solution and particle strengthening together. These alloys shows high stress exponents which range from 5 to 20[5,7]. Figure 4.1 shows the log strain rate versus log stress plot of the creep data obtained from Klopp and Witzke[5] for HfC particle strengthened tungsten alloys. These different n values imply that there is a large variety of mechanisms operating in these alloys. However, any n value larger than 7 does not corresponding to any known creep mechanism[58]. Since all of these data were

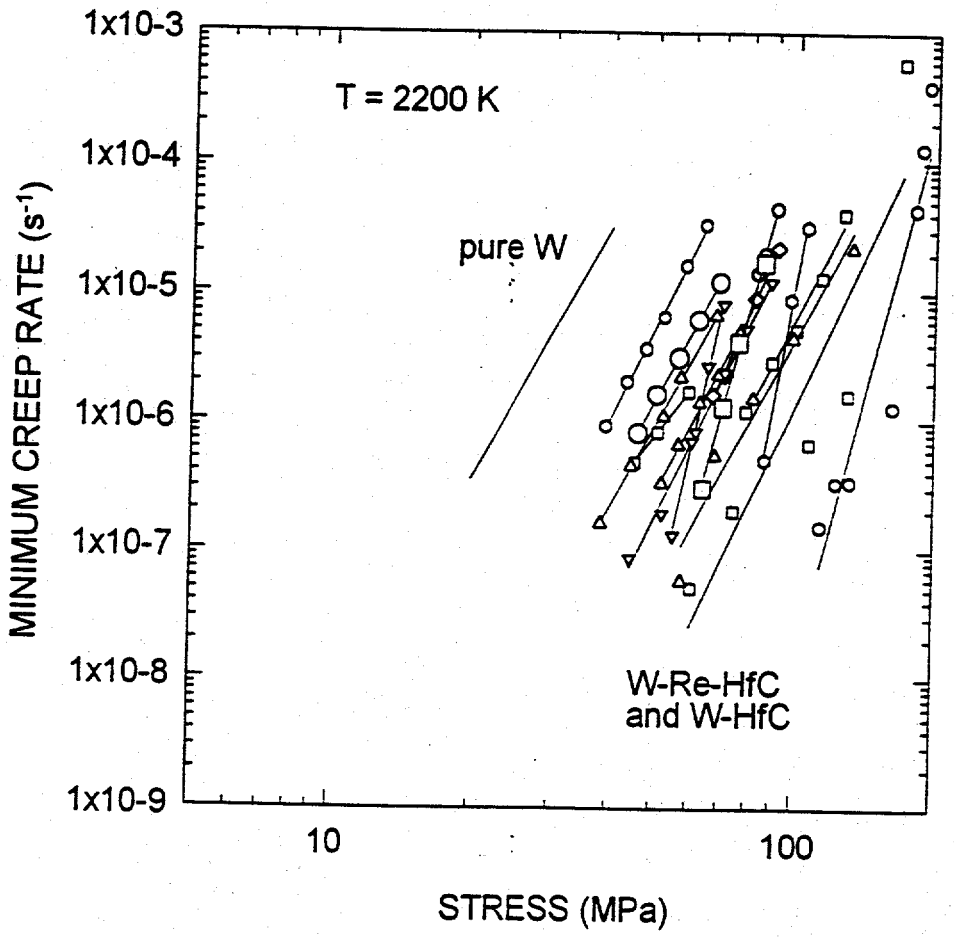

Figure 4.1 Summary of the creep data by Klopp and Witzke[5] and Rubenstein[7].

obtained at 2200 K, the possible dominating creep mechanisms cannot be identified through the activation energy approach.

Studies at Arizona State University[24,50,51] have produced more extensive creep data for the same class of materials under a wide range of test temperatures. They concluded that the creep mechanism was dislocation creep and controlled by the dislocation core diffusion below 2200 K; and above 2200 K, the creep is controlled by lattice diffusion. In their study, three types of materials were used: W-Re-HfC, W-Re-ZrC, and W-Re-ThO_2. The addition of rhenium (approximately 5%) is to enhance the low temperature fabrication property of the materials. Rhenium is highly soluble in tungsten and 5% is believed to have little influenced on the creep behavior. The concentrations of strengthening particles are on the order of 0.2 to 1 mole percent. Creep rates in these materials were investigated in the temperature range of 1900 K to 2873 K and from a stress 10 MPa to 80 MPa. Figure 4.2 shows a typical set of data plotted in a log-log fashion. These data were also analyzed based on the creep behavior given in Equation (3.13).

A survey of the literature on modeling of creep for precipitation strengthened and dispersion strengthened alloys reveals that there are several creep models that were developed in an attempt to contain particle information within the model. Ansell and Weertman[59] developed a model to express the creep rate of PS and DS alloys as

$$\dot{\varepsilon}/D_L = 2\pi(L/b)^2(Gb/kT)(\sigma/G)^4 \qquad (4.1)$$

where L is the interparticle spacing, b the Burgers vector, G the shear modulus of the materials. This model predicts that the creep rate of a particle strengthened alloy depends on the fourth power of the applied stress, which is inconsistent with the high stress exponents observed in

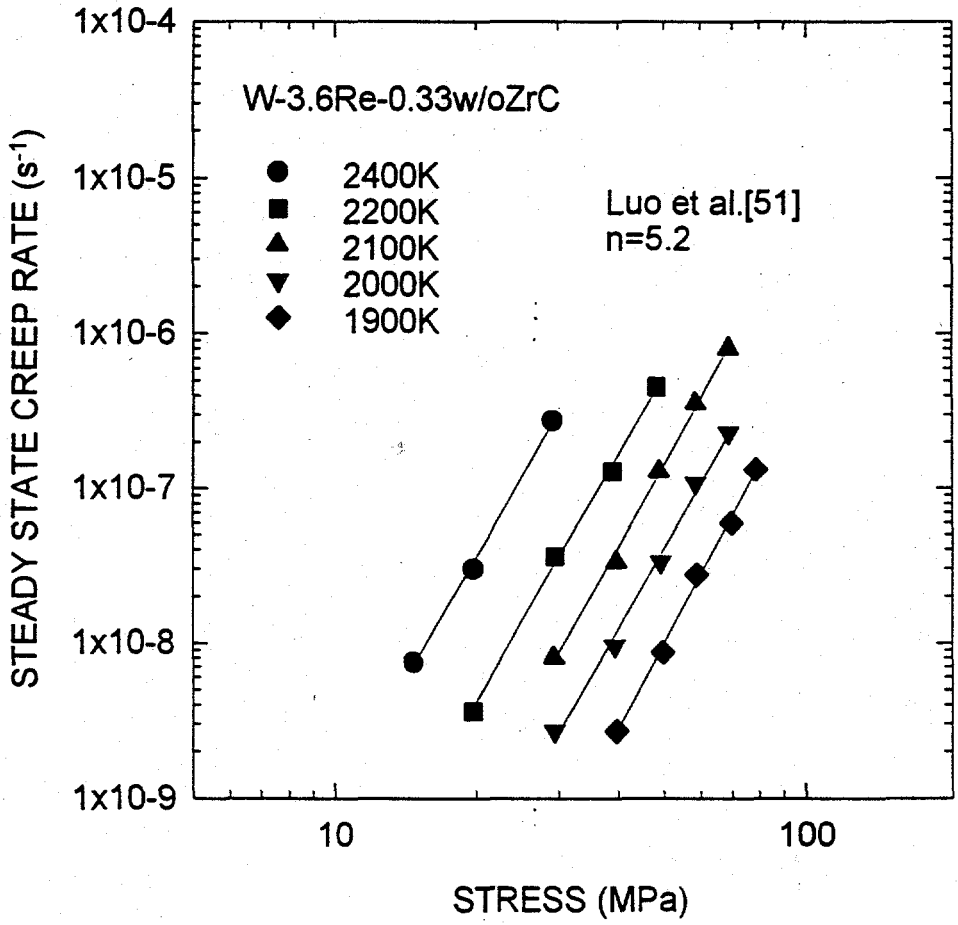

Figure 4.2 Typical creep data by Luo et al.[51].

tungsten alloys and other ODS alloys such as Ni-20Cr-2ThO_2[60]. One approach to model the creep of the alloys with high n values is to plot the normalized steady state creep rate $\dot{\varepsilon}_s/D_L$ against normalized stress σ/E or σ/G in the logarithmic scale. In Ni-20Cr-2ThO_2 single crystal (TD-Nickel), the plot of $\dot{\varepsilon}_s/D_L$ versus σ/E in the logarithmic fashion was found to be nonlinear. Instead, the curve points to the existence of a threshold stress σ_{th} below which dislocation creep does not occur. The physical origin of this threshold is the interaction between the dislocations and the strengthening particles. The threshold stress is proportional to the Orowan stress (Gb/L). If the applied stress is much larger than the σ_{th}, the stress exponent is reduced. Modeling this set of data with the consideration of the threshold stress, a phenomenological equation of the following form was obtained

$$\dot{\varepsilon}/D_L = B(\sigma/E - \sigma_{th}/E)^n \tag{4.2}$$

where B is a creep constant. After reexamining the creep data of TD-Nickel, n is found to be close to 4. This value is in agreement with the stress exponent value which was assigned in the Lagneborg's theory[61] on the creep of dispersion strengthened alloys. In his theory, Lagneborg introduced a back stress σ_p that is due to the particle-dislocation interaction. This creep model can be expressed as

$$\dot{\varepsilon} = A(\sigma - \sigma_p)^4 \tag{4.3}$$

Again A is a creep constant. And this σ_p in Lagneborg's model is proportional to the applied stress through the relationship $\sigma_p = 0.7\sigma$ when the applied stress is less than the Orowan stress.

But this is not true for the W-Re-HfC and W-Re-ZrC alloys. According to the work of Chen and Luo et al., the resulting stress exponent is above 5.2 [24,51]. And the n values obtained from earlier studies are even higher[5,7].

The relation $\sigma_p=0.7\sigma$ in Lagneborg's theory was obtained under the assumption of high volume percent of particles, and the dislocation curvature between the particles induced by the applied stress was also considered helpful to resist the dislocation climb to bypass the strengthening particles. Higher applied stress results in higher back stress. In addition, the higher the stress, the closer the dislocation line increase around the particles, making the climb process more local. However, in tungsten alloys, HfC volume fractions are less than 1% in almost all of the alloys. Thus the Lagneborg's theory is not suitable to describe the creep of the particle strengthened alloys with low volume percent of the strengthening agent and needs to be modified.

When improving the Lagneborg's model, some relevant experimental facts were considered. As mentioned before, the high creep strength of the HfC strengthened tungsten alloys derives from both direct strengthening and indirect strengthening. The creep model should be able to differentiate these factors. In the case of particle strengthened tungsten alloys, TEM results show that movement of individual dislocations is restricted by the particles in both the W-4Re-0.26HfC and the W-3.6Re-0.33ZrC alloys[24,51]. In Ni-20Cr-2ThO_2, the particle-dislocation interaction has been modeled as a threshold stress which is found to be proportional to the Orowan stress of the alloy[60]. The same concept can be used in modeling the direct strengthening of the particles in the tungsten alloys. A modified Lagneborg's creep model was developed by assuming that the back stress be a threshold stress type and is also proportional to the Orowan stress in the manner

$$\sigma_p = \alpha Gb/L \tag{4.4}$$

where α is a constant related to the effectiveness of the particles as strengthening agent, b is the Burgers vector which is 2.74×10^{-10} m for tungsten, G is the temperature dependent shear modulus, L is the inter-particle distance which is also indirectly dependent on temperature and time due to particle coarsening (Equation (3.9)). After considering the temperature effect on the creep constants, the modified Lagneborg creep model can be expressed as

$$\dot{\varepsilon}=(A'DGb/kT)[(\sigma-\alpha Gb/L)/G]^4 \tag{4.5}$$

where D is the diffusivity, A' is a function of indirect strengthening. Combining Equation (3.3) ($L=(3\pi/2f_v)^{1/2}r$) with Equation (4.5), the above model can be expressed as a function of particle volume fraction f_v and average particle radius r,

$$\dot{\varepsilon}=(A'DGb/kT)[(\sigma-0.46\alpha Gbf_V^{1/2}/r)/G]^4 \tag{4.6}$$

4.3. Creep Modeling of Particle Strengthened Tungsten Alloys

The application of this particle strengthened equation to the creep data of HfC, ZrC and ThO_2 is successful, as shown in Figures 4.3 to 4.5. In all these alloys, a constant n value of 4 was used which was appropriate for dislocation creep. In this figures, the y-axis is the fourth root of the creep rate (corresponding to 1/n) and the x-axis is linear stress. The fit was obtained using a least square method based on the particle strengthened creep equation. The activation energy for creep is incorporated in the A term and is related to the slope of the lines in Figures 4.3 to 4.5.

The back stress due to the dispersion particles can be obtained using the x-intercept of the lines in the same figure. For the tungsten alloys strengthened with HfC and ZrC, the particle stress (x-intercepts in Figures 4.3 and 4.4) is a function of temperature whereas ThO_2 particle stress is relatively athermal. Results from microstructure analysis show that the HfC and ZrC are quite randomly dispersed while the thoria particles are segregated at the grain boundaries. Particles at the grain boundaries are ineffective in resisting dislocation motion. The data from thoria strengthened tungsten were therefore not analyzed.

The temperature dependence (through the shear modulus G) of the particle stress in HfC and ZrC containing alloys is given in Figures 4.6 and 4.7 respectively. In these figures, values of 0.274 nm and 0.5 to 2 μm were used for band L respectively. These values were experimentally determined by microstructure analysis[24]. The slope of Figures 4.6 and 4.7 corresponds to α values of 0.094 and 0.1 for the two materials. Theoretically, according to the work of Arzt and Ashby[62], who examined the relationship between threshold stress for creep and material parameters in the shear mode, the threshold stress should range from 0.04 to 0.3 Gb/L depending on different dislocation configurations. Because these α values were obtained for the data under tensile conditions, they should be divided by two in order to compare the theoretical value in the shear mode under the assumption of maximum shear stress state of $\tau_{max}=\sigma/2$. Thus the experimental threshold shear stress of these alloys ranges from 0.047Gb/L to 0.05Gb/L, which is in agreement to the theoretical values which are from 0.04Gb/L to 0.3Gb/L. From the above analysis, the direct strengthening factor is a function of particle morphology. For indirect strengthening, it is expected to be governed by the creep constant A. Indirect strengthening is related to the substructure stabilized by particles. In order to prove this point, it is necessary to compare the A values obtained from the worked structure and the recrystallized structure of the

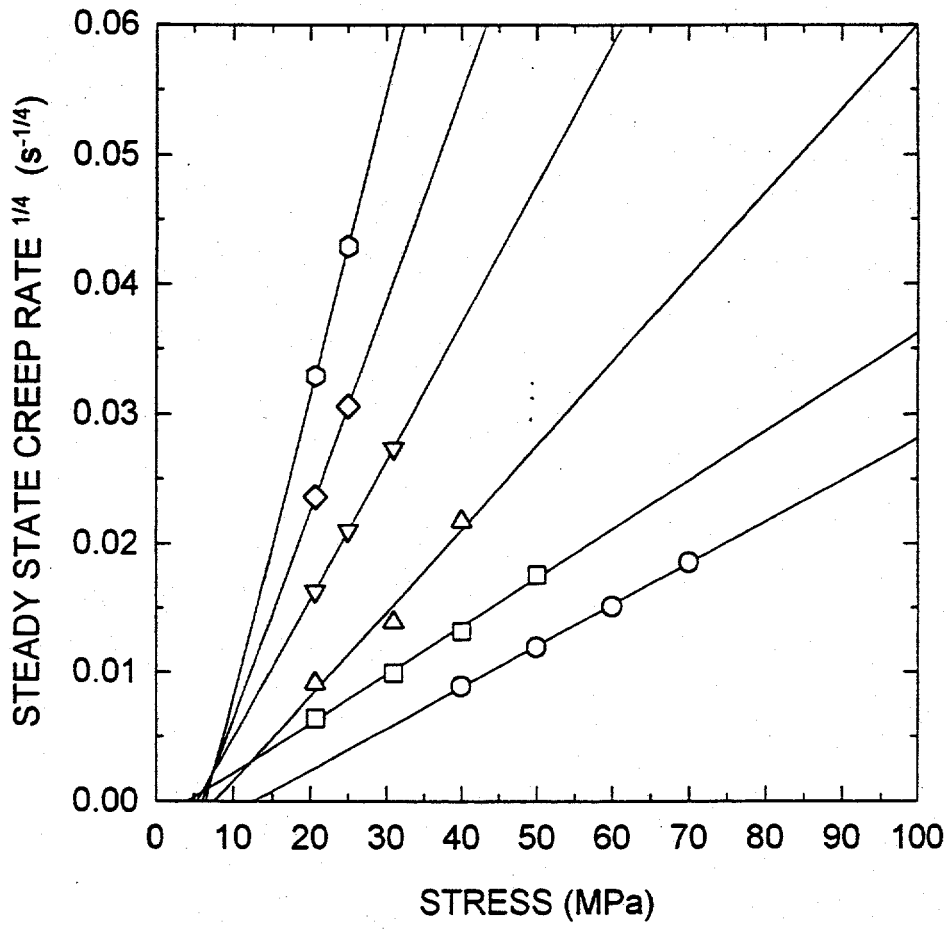

Figure 4.3. Plot of the creep data for tungsten with HfC based on a modified Lagneborg's creep model. The slope of the lines is related to the activation energy for creep and the x-intercept is the particle back stress.

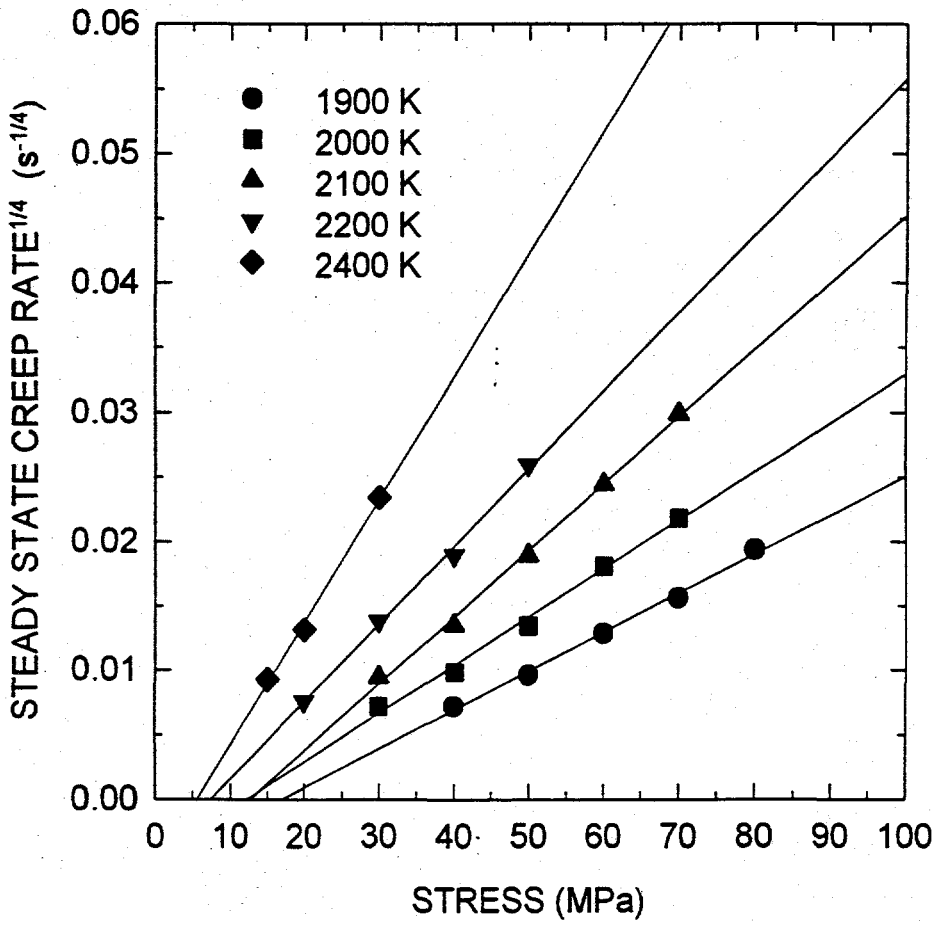

Figure 4.4. Same as Figure 4.3 but for tungsten strengthened with ZrC[51].

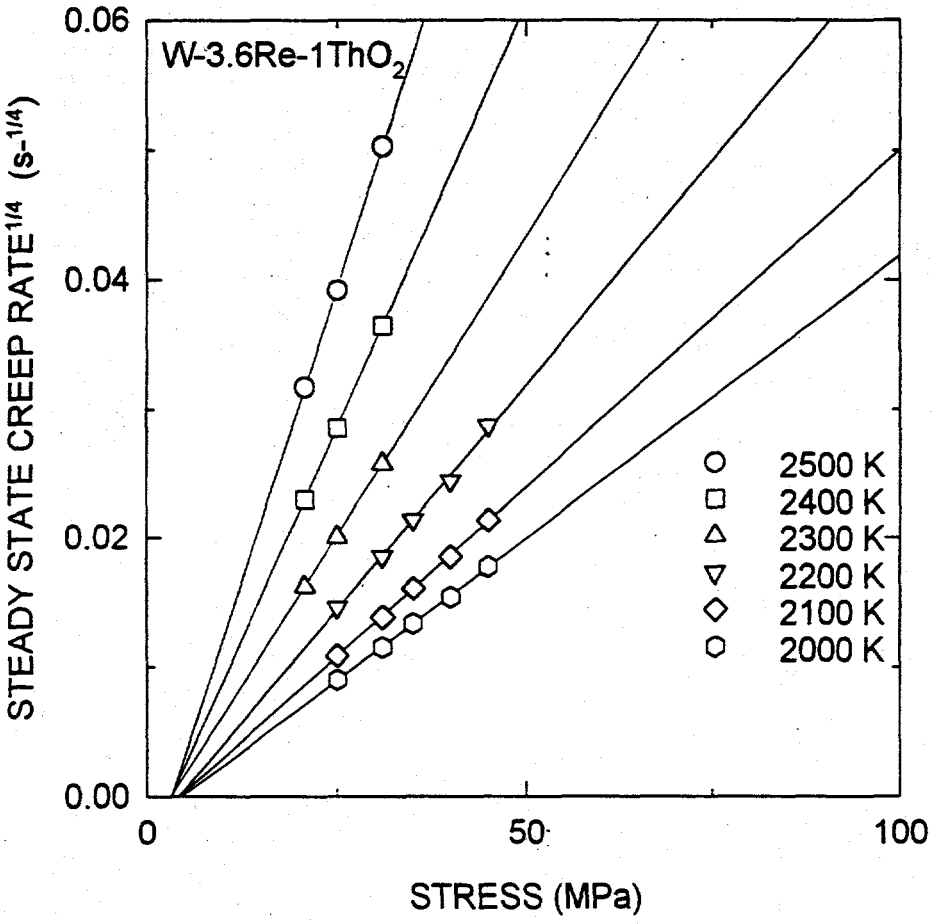

Figure 4.5. Same as Figure 4.3 but for tungsten strengthened with ThO_2[24].

same material. Unfortunately, all the available data were obtained from only one microstructure, either all swaged and all recrystallized. For example, the creep tests of W-4Re-0.26HfC were conducted after recrystallized at 2100 K for one hour plus stay at the test temperature for at least two hours, and that of W-4Re-0.33HfC was conducted after recrystallization for 1.5 hours at 2438 K. For the arc-melted W-3.6Re-0.33ZrC, the test was done after annealing two hours at 2450 K with reported grain size of 110 μm. Therefore, more systematic test need to be done to study the indirect strengthening.

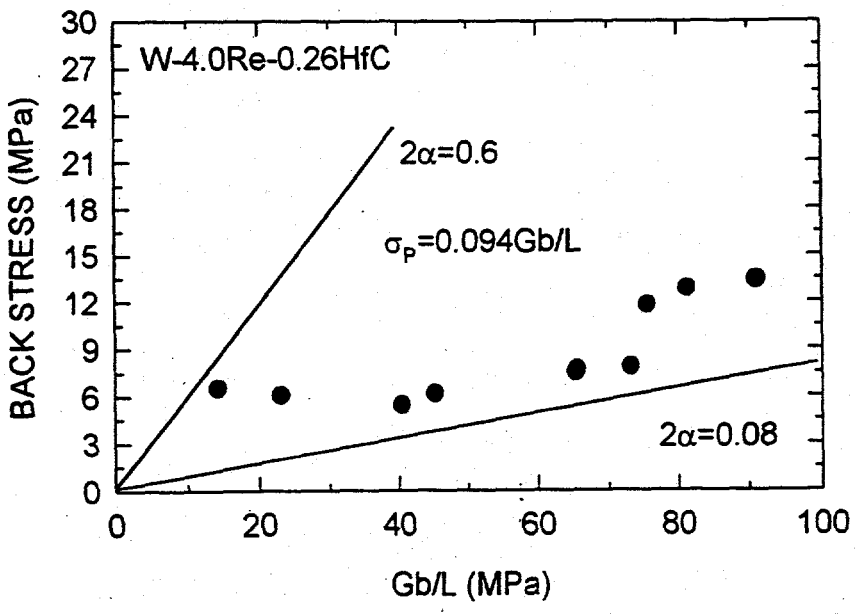

Figure 4.6. Dependence of particle back stress on material parameter in tungsten with HfC.

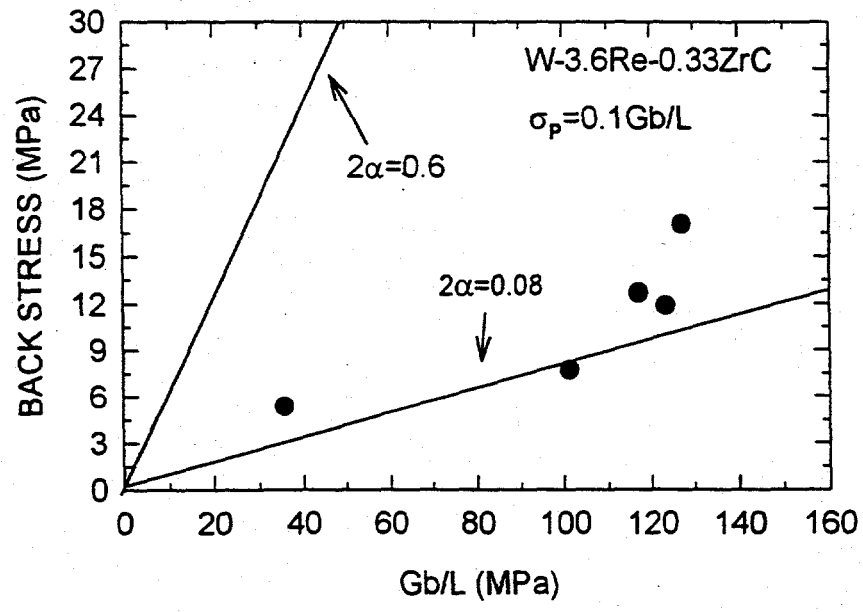

Figure 4.7. Same as Figure 4.6. but for tungsten with ZrC.

5. EXPERIMENTAL PROCEDURES

In this study, an experimental study was designed to verify the semi-mechanistic phenomenological creep model developed in Chapter 4 for carbide particle strengthened tungsten alloys. As mentioned in Chapter 3, a W-HfC emitter with an initial worked microstructure will deform by creep in the as-received condition as well as the recrystallized condition due to coarsening of the HfC particles at temperatures above 1700 K during the 10 year service. Another important reason for conducting creep experiments under these two microstructural conditions is to separate the contribution due to direct and indirect strengthening effects of HfC.

5.1. Materials and Sample Preparation

The material chosen for this research is W-0.37 mol% HfC. This material is close to the optimum HfC content for high temperature mechanical properties according to Klopp, Witzke and Rubenstein[5,7]. Rhenium was not added to the alloy so that the solid solution effect of Re could be eliminated.

The present source of supply for HfC carbide strengthened refractory alloys is Pittsburgh Materials Technology Inc. During material fabrication, the first step was the vacuum arc melting of the three components (tungsten in the form of rods, hafnium in the form of thin foils and carbon yarn) into 38 mm diameter electrodes formed by a water cooled copper mold. The ingot was machined to form a 100 mm long billet and was then encapsulated in a 47 mm diameter Mo cladding for extrusion. Extrusion was accomplished at 2273 K at a reduction ratio of 8:1 to a final diameter 15 mm. The cladding was subsequently removed by dissolving it in nitric acid. With 0.37 mol% HfC precipitated in the pure W matrix, this alloy was reported as possessing the highest mechanical strength at 2200 K[5]. In the as-received state, sections of the alloy rods were ground to form dog bone shaped creep samples. Figure 5.1 shows the dimensions of the

creep sample.

5.2. Creep Testing Equipment and Creep Testing Procedures

To conduct high temperature creep tests of tungsten alloys, a vacuum better than 10^{-7} torr is required to prevent oxidation. A vacuum chamber evacuated by a cryogenic pump was constructed for this purpose. The creep samples were heated up to the test temperature by self-resistive heating. Figure 5.2 is a schematic diagram of the UHV high temperature creep test apparatus.

In order to establish the existence of threshold stress, high sensitivity and accuracy of the strain measurements are essential. In this study the sample elongation was measured directly from the TZM specimen grip inside the test chamber using an extensometer with two LVCs(linear variable capacitor). This requires the strain measuring system to withstand high temperatures over 600 K. A set of coaxial cable feedthroughs modified for UHV application were used to bring the signal from the LVC's inside the chamber to the outside signal amplifier. Cooling of the two LVC's was accomplished by two chilling blocks through which ethyl alcohol was circulated to remove the heat generated by the test sample.

The load inside the chamber was calibrated by a load cell mounted on the sample grip. The effects of vacuum and the bellow were eliminated via a correlation of the dead weight with load cell reading. There was a temperature distribution along the sample due to the resistive heating method employed. The temperature is uniform only in the middle section, and dropped sharply near the grips. This introduces difficulty in determining the effective gauge length of the test sample in the normal tensile test conditions. However, in the case of creep testing at very high temperature, the creep contribution decreases exponentially with temperature. The effective gauge length was determined by measuring the distance between the two points on both sides of

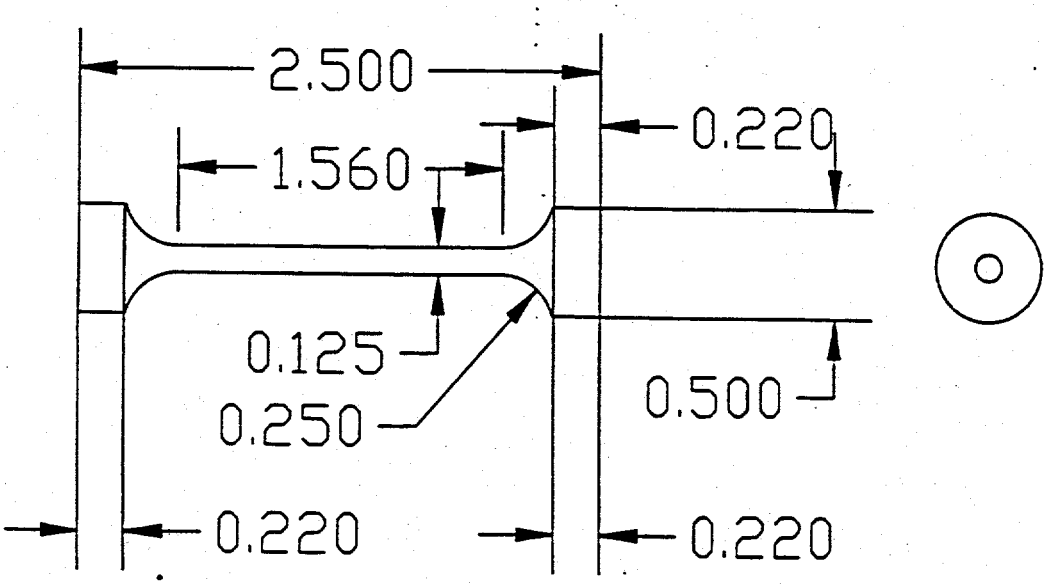

Figure 5.1 Dimensions of the creep specimens.

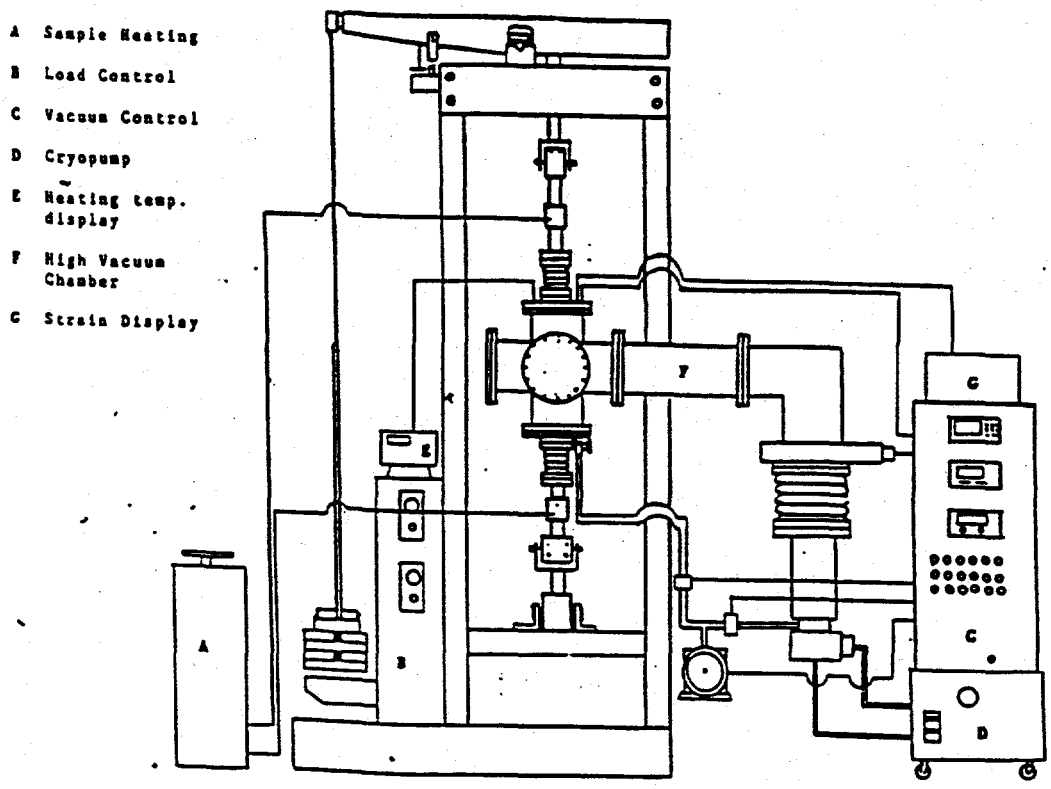

Figure 5.2 Experimental setup for high temperature creep testing.

the central high temperature zone beyond which creep was negligible. For the samples tested at different temperatures in this study, a laser micrometer was used to scan the permanent sample diameter change at room temperature after testing at elevated temperature. In all of the samples scanned, there is a section of 15 mm±1 mm in the middle of the gauge length within which sample diameter starts to thin gradually and reaches to a minimum at the center of the sample. For each of the crept sample, the total plastic elongation is less than 0.5 mm measured at above 2000 K. Thus the error of the strain calculation is below 10%. For this reason, the creep strain rate was calculated based on an effective room temperature gauge length of 15 mm plus the correction due to thermal expansion at the test temperature. Figure 5.3 shows a typical laser micrometer scanning of a crept sample and the effective gauge length is determined to be about 15 mm.

The creep test procedures are described as follows:

1) Before starting a creep test, the specimen was cleaned with acetone and methanol to remove grease and moisture.

2) The sample was mounted in the grips and surrounded with the tantalum heat shield. This shield was placed on top of lower specimen grip platform and was separated from the upper grip. A slot was opened on the shield to allow the temperature of the specimen to be measured by a dual wavelength infrared camera.

3) The insulation between the heat shield and the specimen was checked, as well as that between the heat shield and upper grip.

4) The chamber was sealed with a conflat flange and the chamber was evacuated with a roughing pump to 10^{-3} torr.

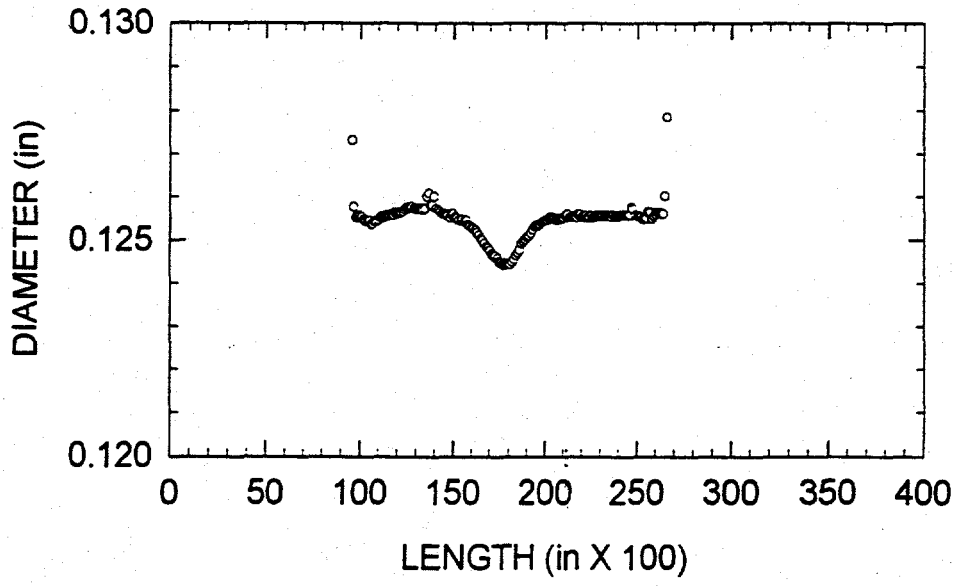

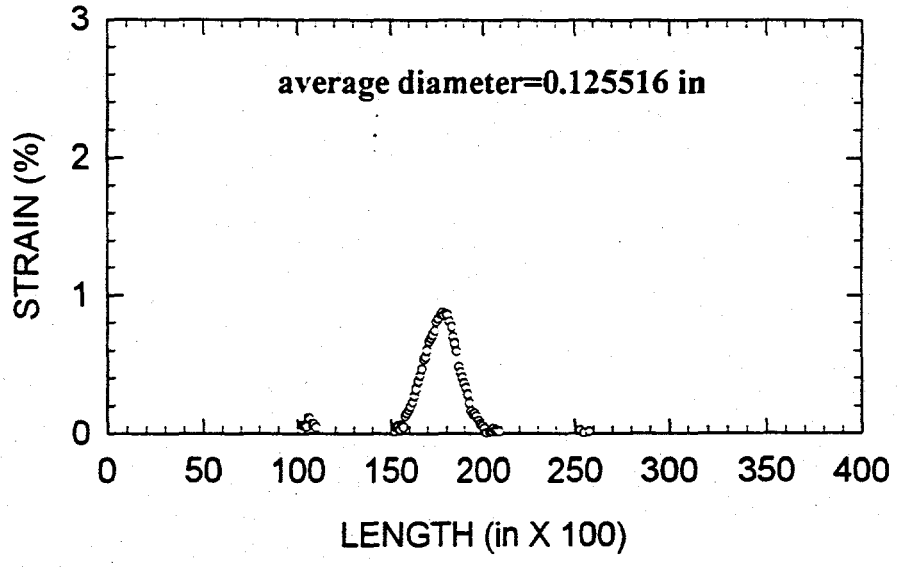

Figure 5.3 Laser micrometer scanning of crept sample.

5) The metal valve between the roughing line and the chamber was closed and then the high vacuum valve was opened so that the chamber was evacuated with a cryogenic pump.

6) When the pressure in the chamber drop to the low 10^{-7} torr range, the cooling bath for the ethyl alcohol was turned on, then the circulation pump to allow the liquid passing through the internal cooling system and the two chilling blocks for the two LVCs. The temperature of LVC was measured by a thermocouple.

7) The current adjustment knob was checked to make sure it was at the zero position before turning on the AC heating power unit.

8) The heating current was increased until the sample started to glow at about 1273 K. The sample and the chamber were allowed to outgass. At the same time, the strain signal amplifier and chart recording machine were turned on.

9) When the chamber pressure drop back to the low 10^{-8} torr range, the temperature of the specimen was increased to 1800 K and held for at least one hour to permit the entire system to reach thermal equilibrium (LVC temperature became stable).

10) The specimen temperature was increased to the desired recrystallization temperature for one hour then quickly reduced to the test temperature (if required). The sample was held at the test temperature for one hour prior to loading.

11) The chart recorder was turned on and set to a proper speed to record the sample elongation as a function of time.

12) A step-load test method was used in this study.

13) At the termination of the test, the specimen was cooled down under load and under the vacuum.

14) The high vacuum was closed to isolate the cryogenic pump from the chamber. The

chamber was let up to a nitrogen atmosphere. This prevent the absorption of the moisture by the inside surface of the chamber.

15) The specimen was removed and stored for further study.

16) Repeat steps 1 to 15 for another specimen.

5.3. Creep under Different Microstructures

Step-load creep tests were performed for the W-0.37HfC alloy with two different microstructures: 1) as-extruded and 2) recrystallized. Recrystallization annealings were conducted to some of the samples to study the microstructural effect on the creep behavior of the W-0.37HfC at temperatures between 2000 K and 2500 K. Other samples were tested under the as-received condition. Since in this condition, the substructure induced by hot extrusion is stabilized during creep by the HfC, the indirect strengthening is expected to contribute to the creep resistance of the material. In the recrystallized condition, the coarsened HfC particles in a matrix with a low dislocation density should provide direct strengthening only at the early stages of deformation. Conducting the creep tests in the above two conditions is intended to separate the effects of direct and indirect strengthening.

5.4. Parameters to be Determined

Many parameters can be identified from a creep test. However the creep parameters to be determined in this study are those that are directly related to the verification of the creep model described in Chapter 4. In the creep test of this study, the applied stress range started from the minimum stress the equipment could provide 5 MPa (according to the load cell calibration) and terminated below the yield strength of this alloy at the test temperature so that the plastic stain

was purely creep in nature.

Primary creep is a combination of anelastic strain and plastic creep deformation where work hardening dominates, thus displaying an ever-decreasing creep rate. The primary creep is sensitive to microstructure, deformation history and applied stress level[63]. Without enough information, direct comparison of these process between different alloys is difficult. However, the primary creep will be recorded during the creep tests to definitely identify the onset of steady state creep.

Steady state creep is a dynamic equilibrium of work hardening and thermal recovery. This creep behavior is usually used for theoretical analysis and for the comparison of creep properties between alloys. The steady state creep rates of W-Re-ZrC were plotted in a log-log manner as in Figure 4.2 and compared with the creep data of other PS (precipitation strengthened) and DS (dispersion strengthened) tungsten alloys. The stress sensitivity, denoted as "n", of the steady state creep equation can be determined by[64]

$$n = (\partial \ln \dot{\varepsilon} / \partial \ln \sigma)_T \qquad (5.1)$$

In the case of many ODS alloys, high n value is only an apparent stress exponent because of the presence of the threshold stress. If the creep of these alloys are expressed by the simple power law, the apparent activation energy $Q_{c\,app}$ corresponding to this apparent stress exponent n for creep can be determined by[64]

$$Q_{c\,app} = [\partial \ln \dot{\varepsilon} / \partial(-1/kT)]_\sigma \qquad (5.2)$$

where $\dot{\varepsilon}$ is the steady state creep rate, k is the Boltzmann constant.

For pure metal, the true activation energy of creep, Q_c, can be determined after considering the correction of temperature dependence of shear modulus, atomic volume of the material and other material parameters used in a proper creep model. For pure metals, Q_c can also be expressed as

$$Q_c = \Delta H_c - (n-1)(kT^2/G)(dG/dT) + (kT^2/\Omega)(d\Omega/dT) \quad (5.3)$$

where ΔH_c is the activation enthalpy of creep or is sometimes called the true activation energy of creep, Ω is the atomic volume of the materials. Because the effect of changing atomic volume to the activation energy is very small, the last term in Equation (5.3) is negligible. Therefore, the temperature dependence of modulus needs to be considered. Equation (5.3) can be simplified as

$$Q_c = \Delta H_c - (n-1)(kT^2/G)(dG/dT) \quad (5.4)$$

The exact expressions for DS tungsten alloys would follow the similar form as the Equation (5.4) plus the effect of the dependence of back stress on temperature[64]. In this study, Q_c for the model developed in Chapter 4 (Equation (4.5)) can be determined in the following manner. The threshold stresses (σ_{th})at different temperatures were obtained by the x-intercept of the plot $\dot{\varepsilon}^{1/4}$ versus σ plot of the creep data (see Chapter 4). The slope *K* of each line in the plot corresponds to the temperature dependence of creep. The real activation energy for the creep model used in the W-HfC was calculated from the negative slope of the fitted line of $\log(K^4G^3kT/b)$ and 1/T, that is

$$\log(K^4G^3kT/b) = \log(A'D_0) - (Q_c/2.303R)(1/T) \quad (5.5)$$

where K^4=A in Equation (4.3), and the y-intercept is $\ln(A'D_0)$. The indirect strengthening effect was determined by comparing the A' values for the two selected microstructures provided D_0 is known.

5.5. Microstructural Characterization of the Crept Specimens

The particle size used for the modeling was not measured in this study because detailed microstructural work has already been conducted by Ozaki[25] in the same material under the same fabrication condition. The average particle size will be estimated with Equation (3.9) obtained by Ozaki[25]. The interparticle spacing (L) was calculated by Equation (3.3). Extrapolated values of σ_{th} can be obtained using Gb/L at different temperatures for different microstructures.

X-ray diffraction was conducted on the transverse surface of the creep specimens which were recrystallized to confirm that recrytallization has occurred in these specimens. At the same time, optical microscopy was used to measure the grain size and monitor recrystallization.

6. RESULTS AND DISCUSSION

6.1. Creep of Recrystallized W-0.37HfC

Figure 6.1 shows the creep data from 2000 to 2500 K plotted in the form of log$\dot{\varepsilon}$ versus logσ for the recrystallized W-0.37HfC alloy. In this set of data, materials that recrystallized at 2773 K for one hour were tested between 2000 and 2300 K at 100 K interval. Materials that were recrystallized at 2673 K for one hour were crept at 2400 and 2500 K. The slope of all of the lines in this plot corresponds to the stress exponent n for the simple power law which varies from 5.5 to 9. Because the simple power law cannot provide a proper explanation of the creep in W-HfC alloys as mentioned in Chapter 4, the activation energy found in the simple power law model is referred to as the apparent activation energy. Following the idea of apparent activation energy (Equation (5.2)), the creep controlling mechanism in recrystallized W-0.37HfC was sought assuming that

$$\dot{\varepsilon} = \dot{\varepsilon}\,(T,\sigma) \tag{6.1}$$

Under the condition of constant stress, $Q_{C\,app}$ can be obtained by the following differential form[64]:

$$Q_{C\,app} = [\partial \ln\dot{\varepsilon}/\partial(-1/RT)]_{\sigma} \tag{6.2}$$

Here the $Q_{C\,app}$ is calculated on a per mole basis. To obtain the $Q_{C\,app}$ from the experimental data, the log of the steady state creep rates($\dot{\varepsilon}$) obtained for the recrystallized W-0.37HfC material under

selected stress levels were plotted against the reciprocal test temperature as shown in Figure 6.2. According to Equation (6.2), the activation energy $Q_{C\,app}$ corresponds to the slope of each of the lines at different stress levels. The resultant $Q_{C\,app}$ values are listed in the same figure. These values range from 663 kJ/mole to 1871 kJ/mole with an average of 1011 kJ/mole which is about 371 to 526 kJ/mole higher the activation energy for self-diffusion (485-640 kJ/mole) in pure tungsten[52].

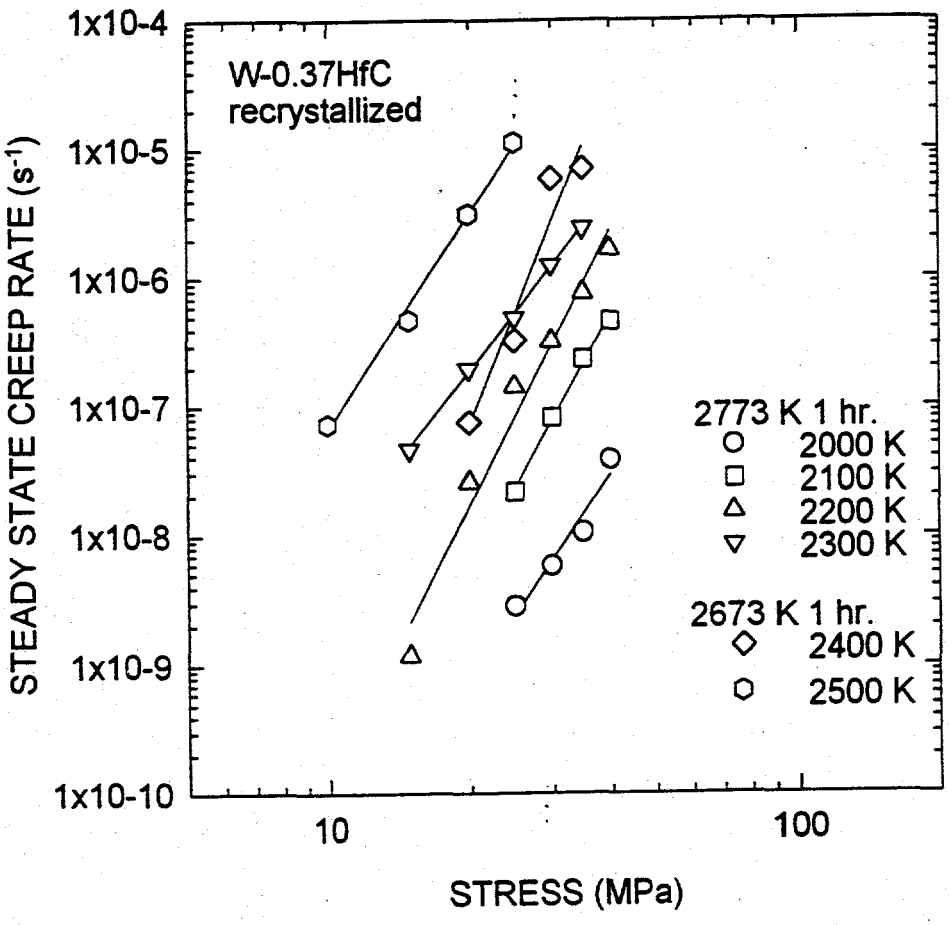

Figure 6.1. Stress-dependence of the steady state creep rate of recrystallized W-0.37HfC.

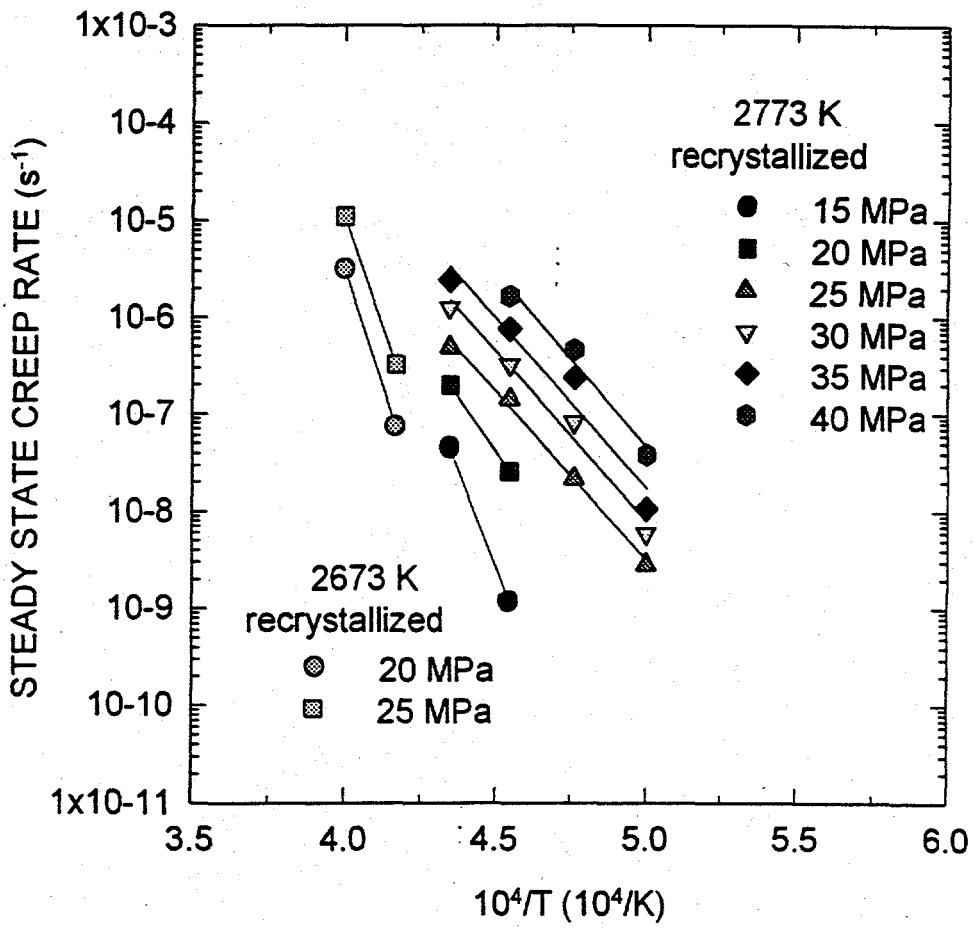

Figure 6.2. Effect of temperature on the steady state creep of recrystallized W-0.37HfC.

Apparent activation energy found to be between 648 to 1530 kJ/mole.

6.2. Creep of As-Received W-0.37HfC

Similar finding was obtained from the creep data of W-0.37HfC, tested in the as-received condition at temperatures

between 2019 and 2219 K. As shown in Figure 6.3, the stress exponent n ranges from 6 to 7. In this case, the average apparent activation energy $Q_{C\,app}$ is 947.5 kJ/mole (540 kJ/mole - 1,748 kJ/mole)as shown in Figure 6.4. These high and varying activation energy values were obtained under the assumption that steady state creep rate is only a function of temperature and the applied stress without considering any other structural and material factors. Factors such as Young's modulus and strengthening HfC particles in the W-0.37HfC alloy are also functions of temperature due to the temperature dependence of atomic bonding strength and particle coarsening. In the case of dispersion strengthened alloys, the increased interparticle spacing (L) due to particle coarsening with temperature will decrease the threshold stress σ_p according to Equation (4.4). This effect results in a situation where the material creeps under different equivalent stresses (σ-σ_p) under different temperatures even though the applied stresses are the same.

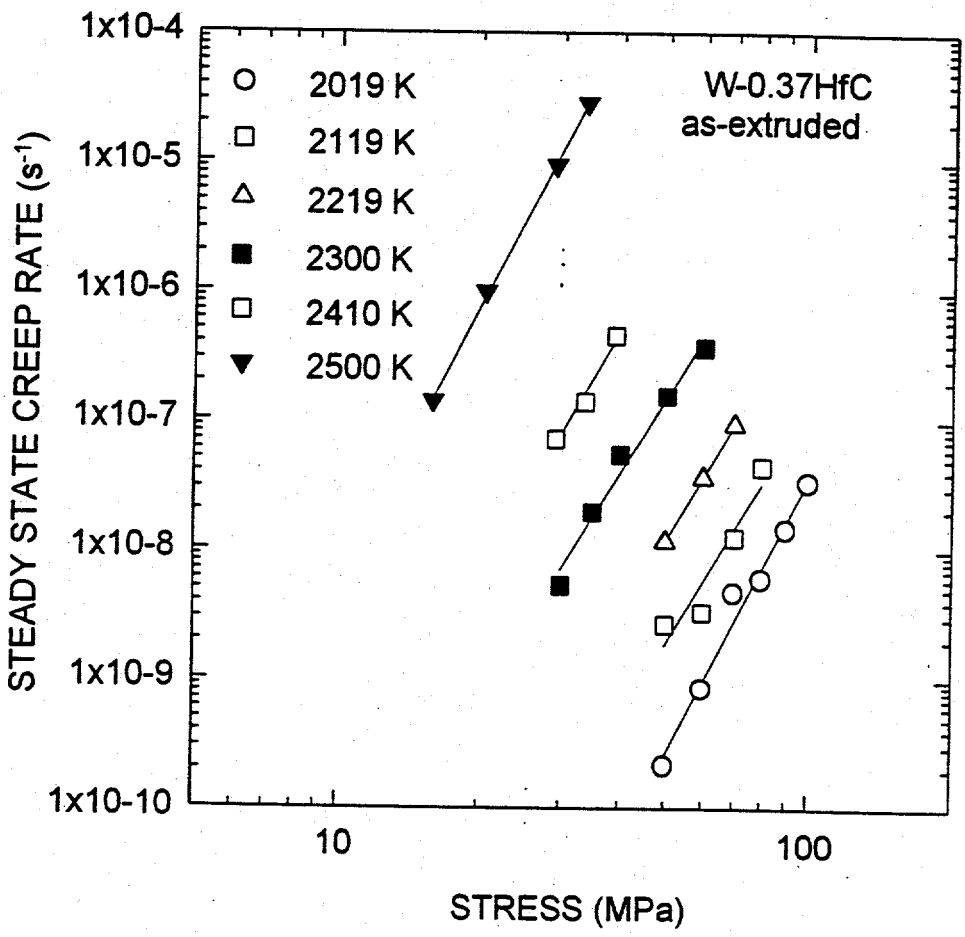

Figure 6.3. Stress-dependence of the steady state creep rate of the as-received W-0.37HfC.

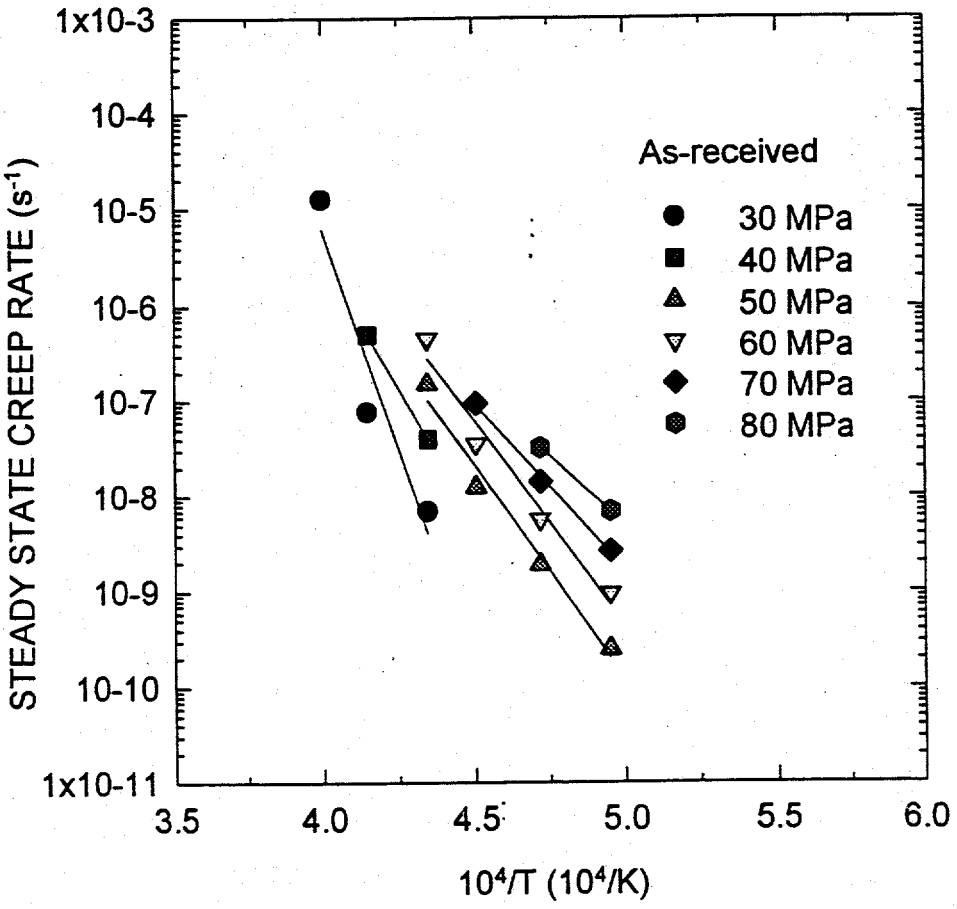

Figure 6.4. Effect of temperature on the steady state creep of the as-received W-0.37HfC. Apparent activation energies varies from 540 kJ/mole to 1748 kJ/mole, giving an average of 947.5 kJ/mole.

6.3. Verification of the Creep Model for Dispersive Carbide Strengthened Tungsten Alloys

To obtain a more meaningful activation energy using the equivalent stress approach, verification of the creep model developed for particle strengthened tungsten is necessary. Creep data at each temperature for the W-0.37HfC were fitted to the dispersion strengthened creep model developed for this class of material (Equation (4.3)):

$$\dot{\varepsilon} = A(\sigma-\sigma_p)^4 \tag{4.3}$$

where the constant A can be expressed according to Equation (4.5)

$$A = A'(Db/G^3kT) \tag{6.3}$$

Again A' is a material constant, k is the Boltzmann constant, b is the Burgers vector (equals to 0.274 nm for W) and G is the shear modulus. The diffusion coefficient D is expressed as $D_o\exp(-Q_C/RT)$ and Q_C is the activation energy in this model. However, the Q_C values obtained through this method may still contain the activation energy from other thermally activated processes in the materials which may occur during creep testing. As mentioned earlier, in both W-HfC and W-Re-HfC alloys, the strengthening effect of particles comes from two different contributions: "direct strengthening" and "indirect strengthening"[5,7,24]. The former refers to the resistance from the HfC particles to the gliding individual dislocation during deformation and the latter involves the stabilization of grains and subgrains by the particles. When the temperature is sufficiently high, loss of indirect strengthening due to particle coarsening may occur resulting in significant degradation of creep resistance. Furthermore, the parameter A' may also change when

dynamic recrystallization occurs.

Using Equation (4.3), the constant A was determined for the recrystallized W-0.37HfC samples tested at different temperatures by taking the fourth root of the strain rate ($\dot{\varepsilon}^{1/4}$) versus σ as shown in Figure 6.5. The threshold stress σ_p caused by the particles for each temperature can thus be obtained as the x-intercept of each line. The creep data for the recrystallized W-0.37 HfC also fits Equation (4.3) very well. These results are consistent with the modeling work described in Chapter 4 for W-Re-HfC and W-Re-ZrC.

Plotting the log(A) values versus 1/T will yield the required activation energy which is independent of stress if the temperature dependence of the shear modulus G is not considered. More accurate values were obtained by introducing the temperature dependence of shear modulus. This was accomplished by arranging the Equation (6.3) to the form:

$$AG^3kT/b = A'D_o\exp(-Q_C/RT) \qquad (6.4)$$

An examination of this equation indicates that if all the data points can be fitted in to a straight line in the plot of $\log(AG^3kT/b)$ versus 1/T, then Q_C can be calculated by multiplying the slope of the line by 2.303R. Both log(A) and $\log(AG^3kT/b)$ versus 1/T are plotted in Figure 6.6. Two straight lines are obtained. The calculated activation energies (575.8 and 582.1 kJ/mole) using the two methods are very close to that for the self-diffusion of pure tungsten (from 487 to 640 and averaged at 554 kJ/mole by seven reported values[52]). In both methods of analysis, the A' values were found to be relatively constant over the entire test temperature range from 2000 K to 2500 K. When calculating the creep activation energy of the recrystallized W-0.37HfC, the line was drawn based only on the four 2773 K recrystallized specimens which were crept between

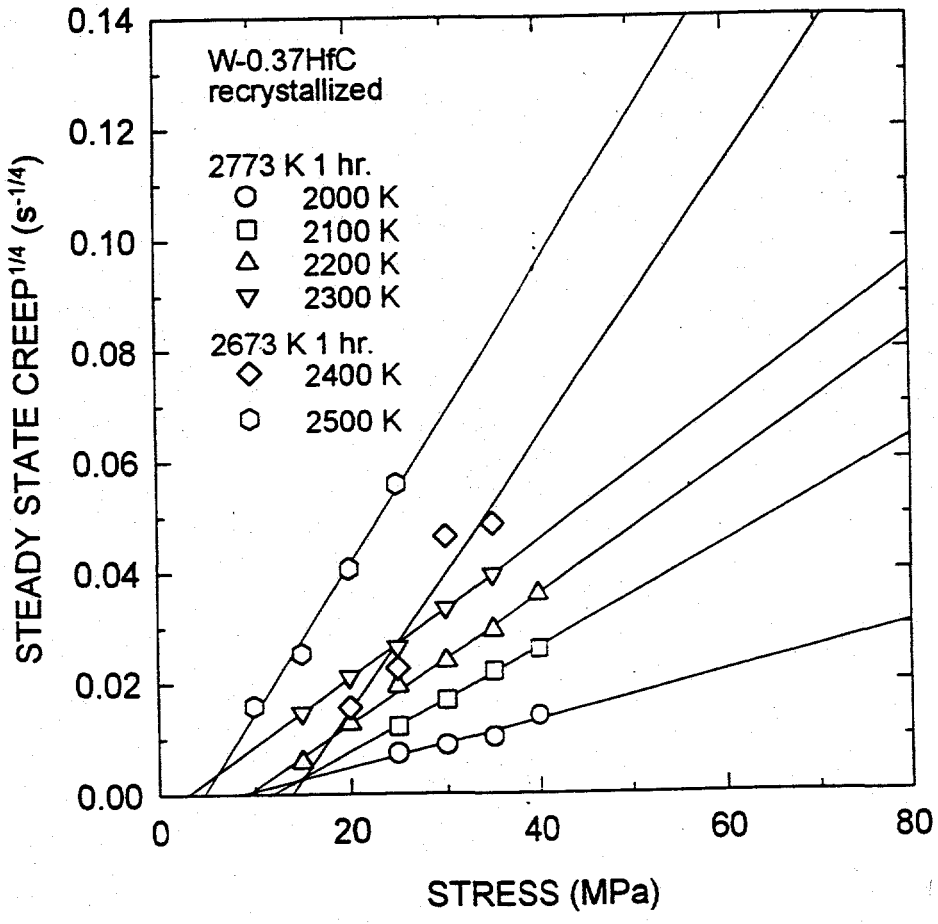

Figure 6.5. Creep data obtained from recrystallized W-0.37HfC plotted in accordance with the dispersion strengthened creep model given in Equation (4.3).

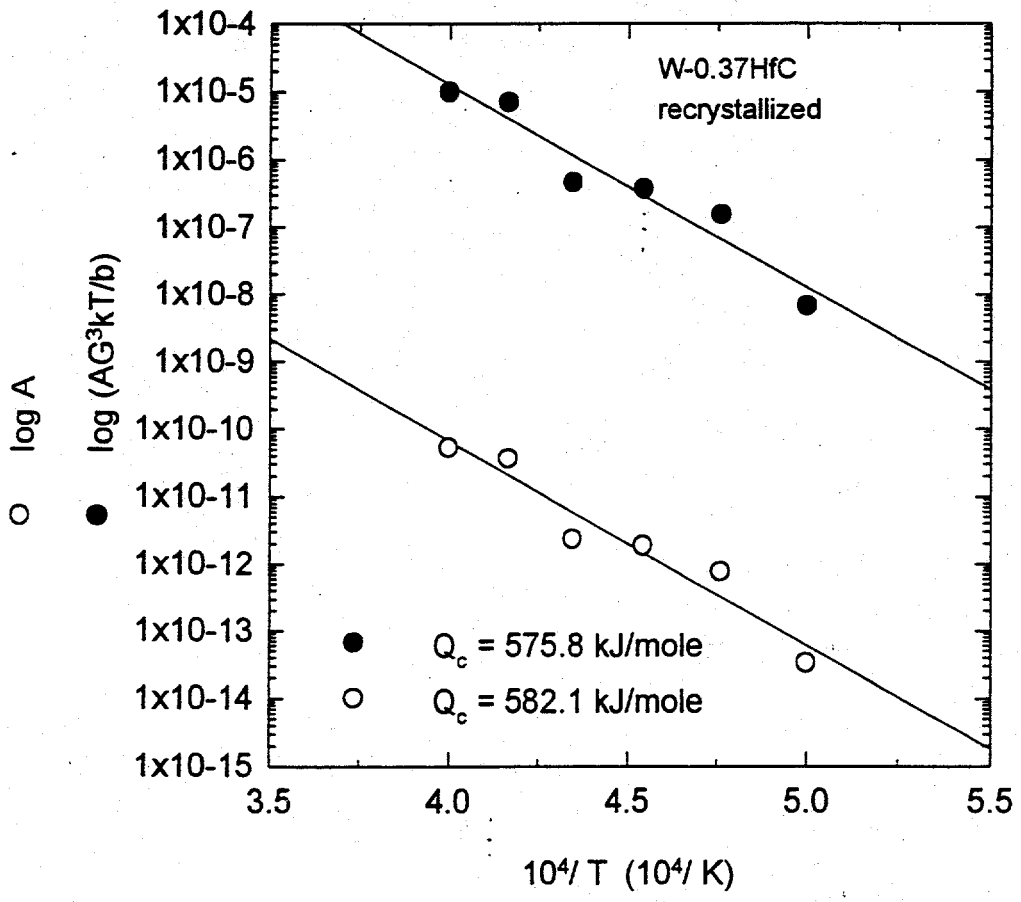

Figure 6.6. Activation energy for creep of recrystallized W-0.37HfC using equivalent stress approach.

2000 K to 2300 K. The other two high temperature (or low 1/T values) points (2400 K and 2500 K points) which still fall on the same line were from samples recrystallized at 2673 K. When the two points from the 2673 K recrystallized samples were also included in the activation energy calculation, the Q_c remained at around 585.2 kJ/mole. Since 2673 K is the reported one hour recrystallization temperature of W-0.4HfC alloy [25], this finding implies that A' does not depend on the temperature at which full recrystallization occurs. This results will be discussed further in the "Discussion" section. The creep of recrystallized W-0.37HfC can be expressed as:

$$\dot{\varepsilon} = 1.33\times10^{7}(b/G^{3}kT)\exp(-575800/RT)(\sigma-\sigma_{p})^{4} \qquad (2000\ K \le T \le 2500\ K) \qquad (6.5)$$

The A' in Equation (6.4) is influenced by cold working. This is supported by the experimental creep data of as-received W-0.37HfC and will be discussed in section 6.5.

Following the same method, the creep data of W-0.37HfC tested in the as-received condition were also analyzed in accordance with Equation (4.3) (Figure 6.7). The threshold stresses in the creep of the as-received W-0.37HfC under all test temperatures were obtained by extrapolation. However in this set of data, no single activation energy can satisfy all the data points when using the equivalent stress approach. As shown in Figure 6.8, at low temperature (2019 K to 2300 K) the slope of the curve still results in a reasonable activation energy value which is close to that obtained from the recrystallized samples. However at high temperature (2400 K - 2500 K) the activation energy (corresponding to the slope of the line in Figure 6.8) deviates significantly.

Plotting the values of $\log(AG^{3}kT/b)$ for both the as-received and the recrystallized

specimens against 1/T for all the test temperatures together, it was found that for specimens tested at 2500 K, the values of $\log(AG^3kT/b)$ from both microstructures were very close to one another (Figure 6.9). This result implies that the as-received specimens become fully recrystallized during creep testing at 2500 K. At 2400 K, partial recrystallization was believed to be the reason for the higher A value. To confirm this occurrence, all the crept samples were examined to determine their recrystallization state as will be described in the next section.

6.4 Recrystallization Study of Crept Specimens

In order to prove possible recrystallization for the as-received W-0.37HfC during creep, optical micrographs and x-ray diffraction (XRD) spectra were obtained from the transverse surface of all the crept samples. As shown in Figure 6.10, the material in the as-received sample possesses distorted grains and no equiaxial grain was observed. Significant texture was detected by XRD (Figure 6.11). However, this {110} texture disappeared in the as-received sample crept above 2300 K (Figure 6.12). Optical microscope observation shows that partial recrystallization occurs when samples are tested at 2300 K and 2400 K as shown in Figures 6.13 (a) and (b). Sample crept at 2500 K possessed fully recrystallized structures. Optical micrograph (Figure 6.14) shows that only equiaxial grains exist. On the other hand, samples that were recrystallized all exhibited recrystallized microstructure (Figures 6.15 and 6.16) with XRD spectra displaying multiple peaks that matched the spectrum for tungsten (Figures 6.17 and 6.18). Therefore, for the as-received W-0.37HfC, the activation energy for creep should be calculated based on the three low temperature points (2019 K, 2119 K an 2219 K) in Figure 6.8 where recrystallization has not occurred.

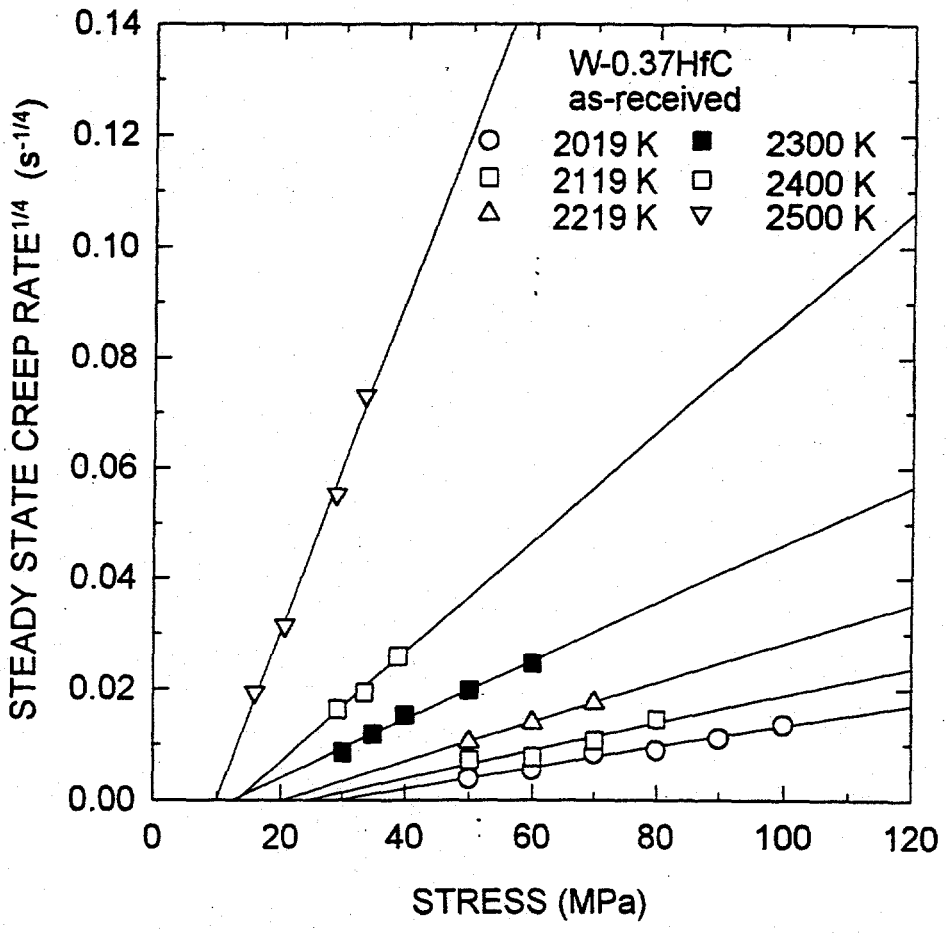

Figure 6.7. Creep data obtained from as-received W-0.37HfC plotted in accordance with the dispersion strengthened creep model given in Equation (4.3).

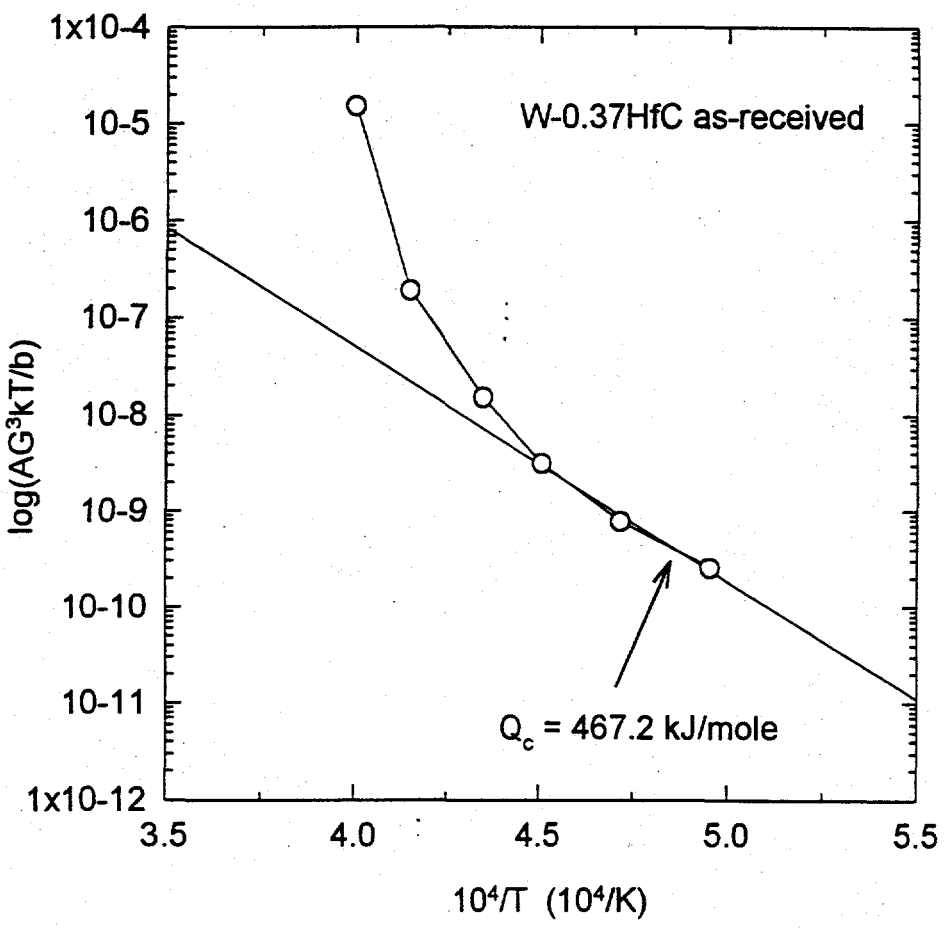

Figure 6.8. Creep activation energy of as-received W-0.37HfC using the equivalent stress approach.

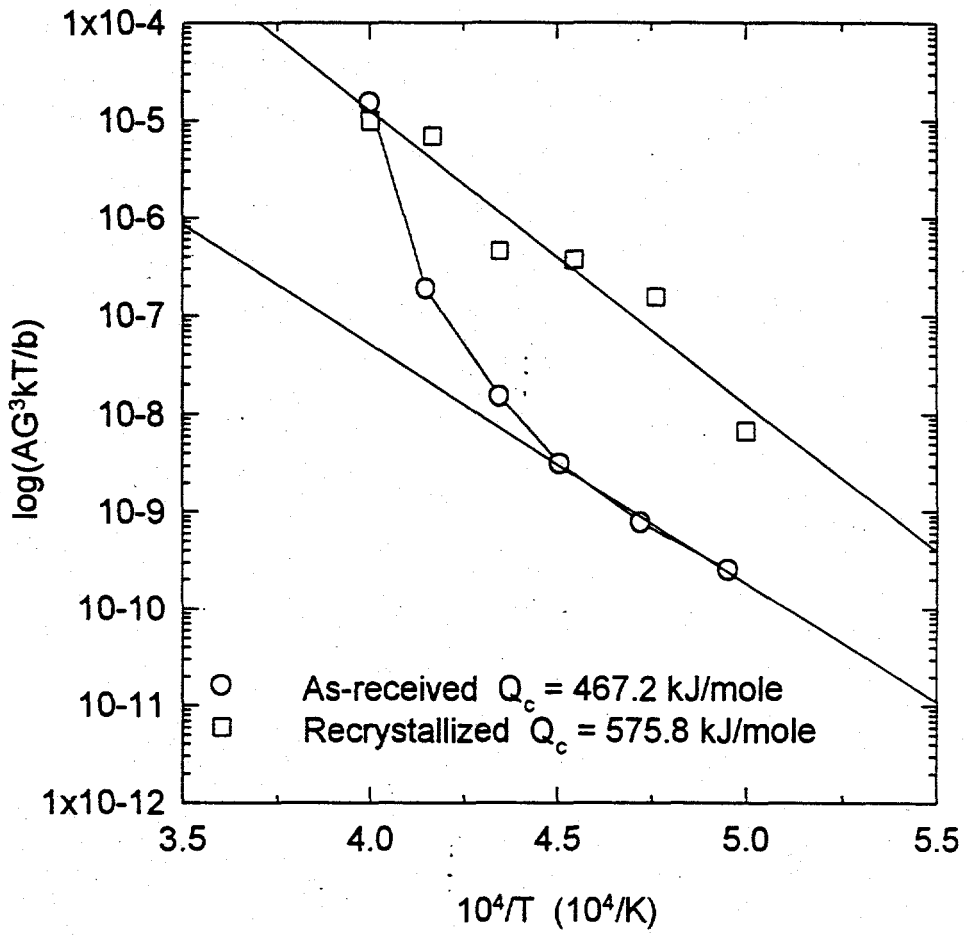

Figure 6.9. Comparison of the log(AG^3kT/b) values of W-0.37HfC in two different microstructure conditions.

Figure 6.10. Optical micrograph of the as-received W-0.37HfC.

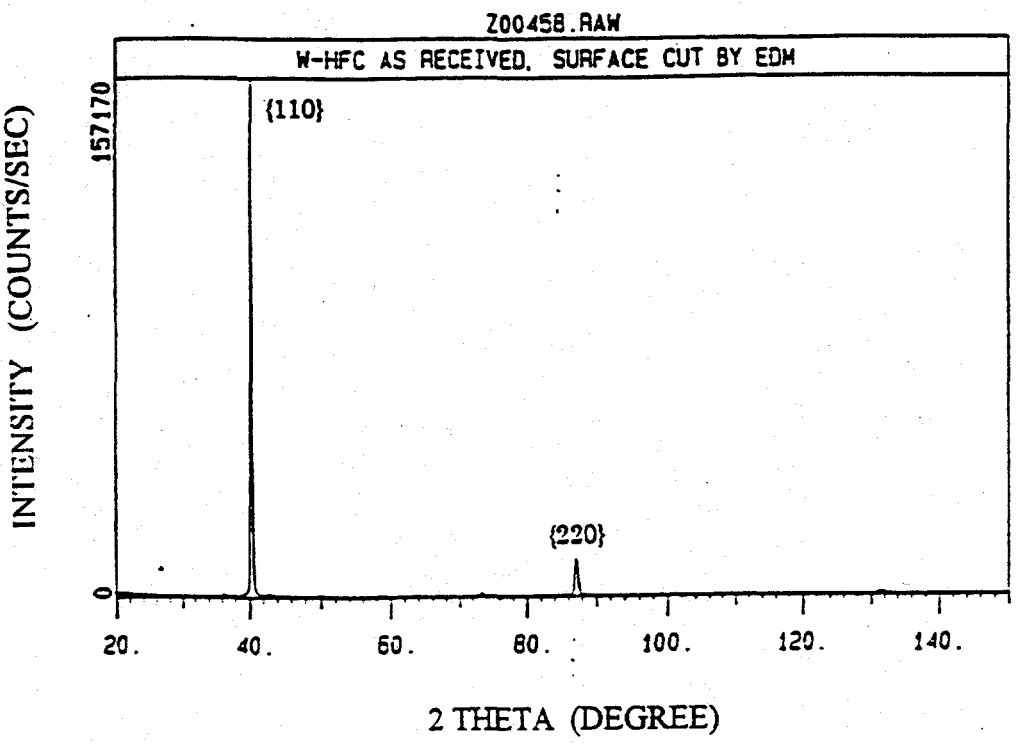

Figure 6.11. XRD spectrum of the as-received specimen.

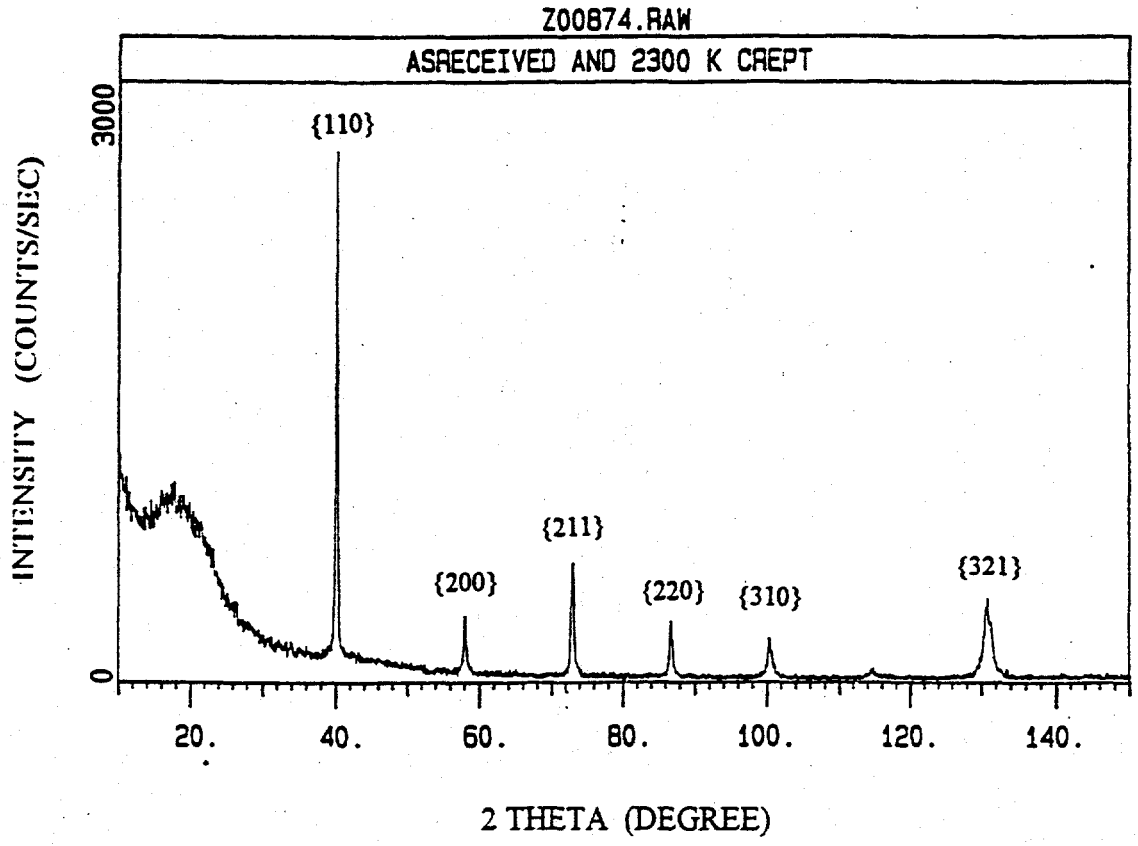

Figure 6.12. XRD spectrum of the as-received specimen crept at 2300 K.

Figure 6.13(a). Optical micrograph of as-received W-0.37HfC crept at 2300 K.

Figure 6.13(b). Optical micrograph of as-received W-0.37HfC crept at 2400 K.

Figure 6.14. Optical micrograph of as-received W-0.37HfC crept at 2500 K.

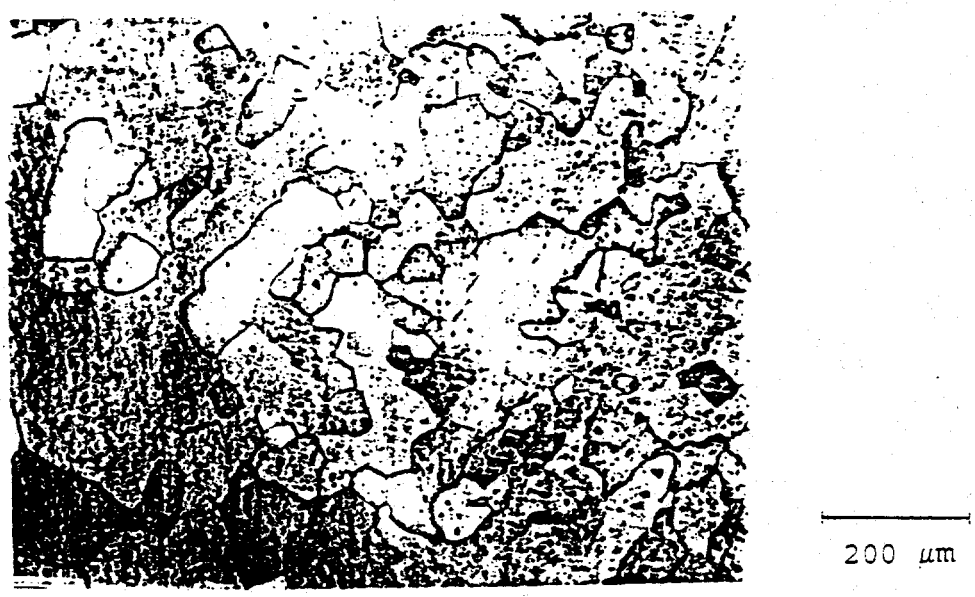

Figure 6.15. Optical micrograph of W-0.37HfC recrystallized at 2673 K and then crept at 2400 K.

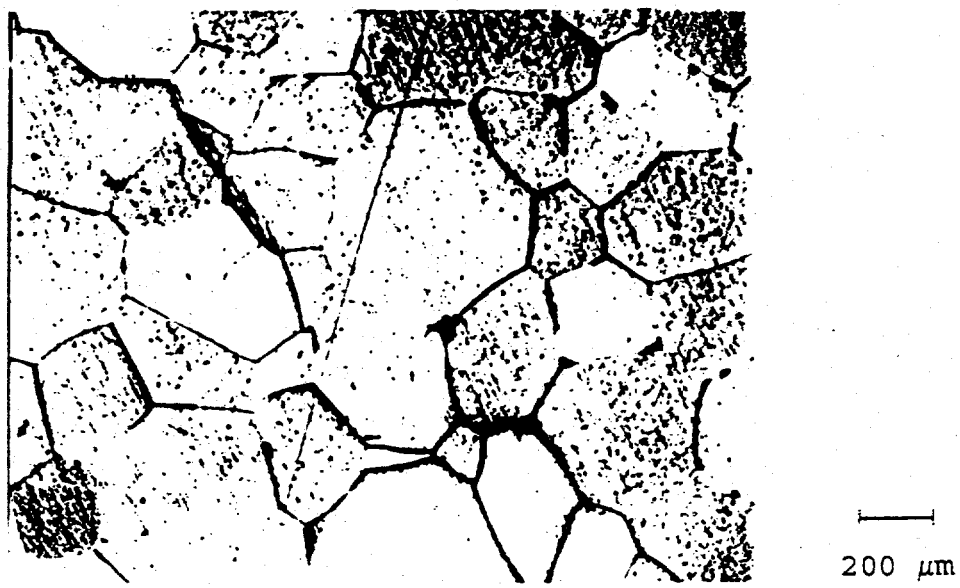

Figure 6.16. Optical micrograph of W-0.37HfC recrystallized at 2773 K and then crept at 2100 K.

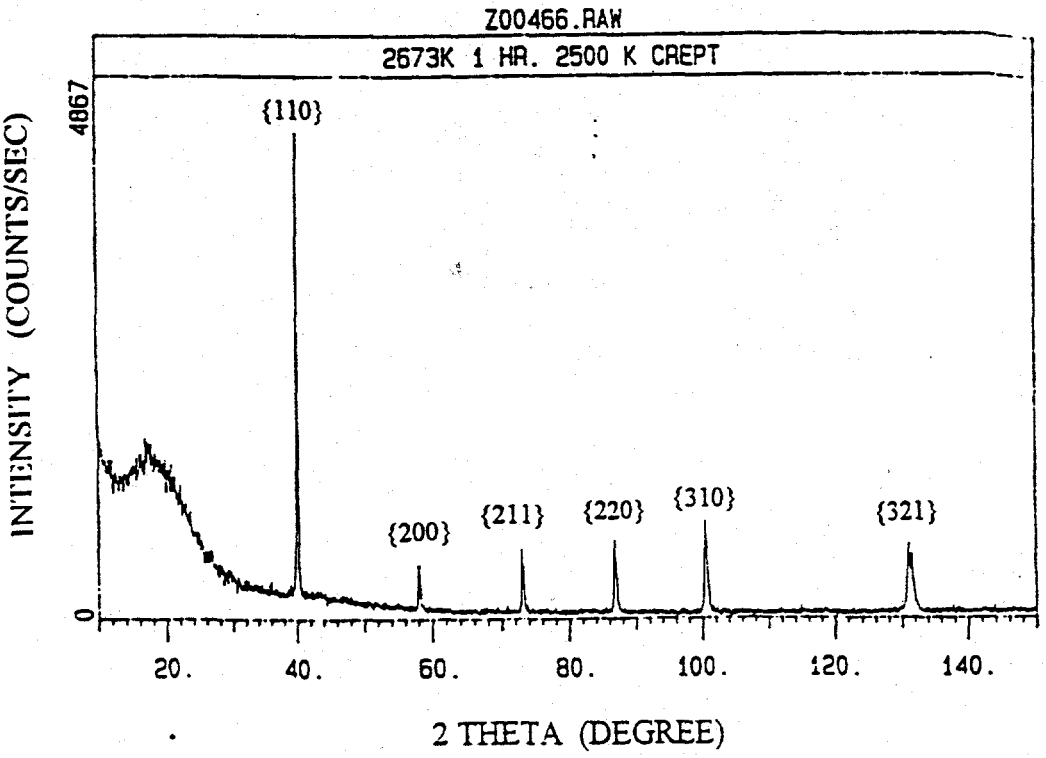

Figure 6.17. XRD spectrum of W-0.37HfC alloy 2673 K recrystallized and then crept at 2500 K.

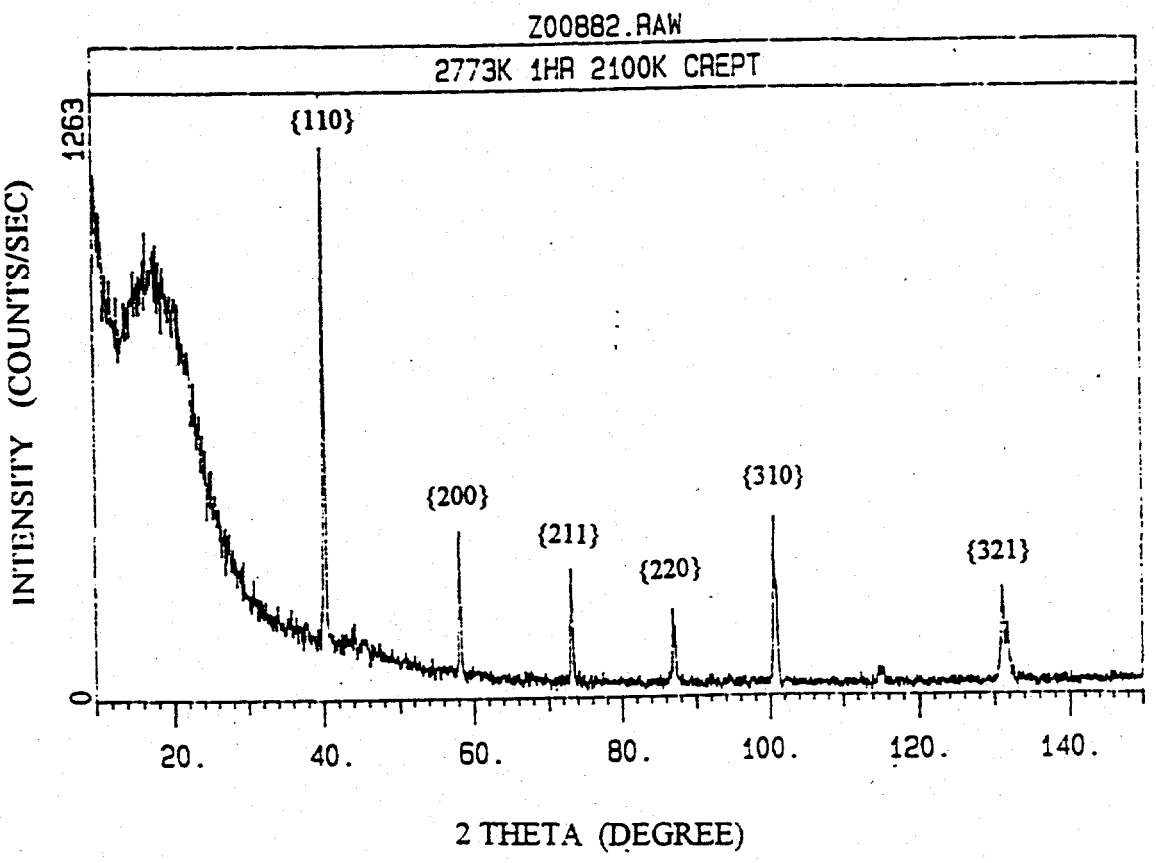

Figure 6.18. XRD spectrum of the W-0.37HfC specimen recrystallized at 2773 K and then crept at 2100 K.

6.5. Discussion

It is evident that the modified Lagneborg creep model can describe the creep behavior of W-Re-HfC, W-Re-ZrC and W-HfC alloys. Using the equivalent stress approach in accordance with this model yields reasonable value of the activation energy for creep. Comparing the $\log(AG^3kT/b)$ value of the recrystallized W-0.37HfC with those obtained from the as-extruded states, the A value of Equation (4.3) for the as-extruded material was about 1% of that for the recrystallized material tested at temperature below 2219 K. The particle stabilized worked structure decreases the A value. In order to further compare the A' values of the two microstructure states, the effect of activation energy for creep should be eliminated. Following the same method described in section 6.3, the value of $\log(A'D_0)$ was found to be 2.47 for the as-extruded W-0.37HfC alloy tested between 2019 K and 2219 K. The corresponding value for the recrystallized material is 7.12 between 2000 K and 2500 K. The activation energy for creep in the as-received W-0.37HfC between 2019 and 2219 K was found to be about 467 kJ/mole which is between the energy for lattice diffusion (585 kJ/mole) and dislocation core diffusion (378 kJ/mole). This activation energy value implies that both processes contribute to creep in the material in this tungsten alloy. Comparison of the activation energy values for creep between the recrystallized and the as-extruded materials indicated that the particle stabilized worked structure in the as-extruded material reduced the activation energy for creep by allowing more dislocations to participate in the diffusion process. Because of the significant contribution of the dislocation core to the diffusion process in the as-extruded W-0.37HfC samples, the corresponding D value in Equation (4.5) for this material should be D_{eff} as expressed by Equation (3.16)[35]. If the creep activation energy of this material between 2019 K and 2219 K is defined as $Q_{c\,eff}$, then the effective the D_{eff} can also be expressed as

$$D_{eff} = D_{0\,eff}\exp(-Q_{c\,eff}/RT) \tag{6.6}$$

where $Q_{c\,eff}$ equals to 467 kJ/mole. Equating Equation (3.16) and Equation (6.6) yields

$$D_{0\,eff}\exp(-Q_{c\,eff}/RT) = f_L D_L + f_D D_D \tag{6.7}$$

The value of $D_{0\,eff}$ can be estimated provided the values of f_L and f_D are known. According to Robinson and Sherby[35], f_L was found to be near unity. Using the lattice diffusivity of $D_L=5.6\text{x}10^{-4}\exp(-585200/RT)$ m^2/s and dislocation core diffusivity of $D_D=10^{-3}\exp(-378290/RT)$ m^2/s (R in unit of J/mole-K) given by Robinson and Sherby[35], the value of f_D is calculated to be $1.1\text{x}10^{-5}$ when assuming the $f_L D_L = f_D D_D$ at 2300 K. At this temperature, dynamic particle stabilized worked structure start to disappear in the as-extruded W-0.37HfC. Therefore the values of $D_{0\,eff}$ were found to be from $2.53\text{x}10^{-6}$ to $2.19\text{x}10^{-6}$ m^2/s between 2019 K and 2219 K with an average value of $2.33\text{x}10^{-6}$ m^2/s. Using the ratio of $\log(A'_{extruded}D_{0\,eff})/\log(A'_{recrystallized}D_0)$, which equals to 2.47/7.12, the A' for the as-extruded material is found to be

$$A'_{extruded} = 3.27\text{x}10^{-3}A'_{recrystallized} \tag{6.8}$$

This means that the A' is greatly reduced by the particle stabilized worked structure. Above 2300 K the A value increases drastically indicating that dynamic recrystallization has occurred. Therefore the creep of as-extruded W-0.37HfC alloy between 2019 K and 2219 K can be expressed as

$$\dot{\varepsilon} = 2.97\times10^{2}(b/G^{3}kT)\exp(-467400/RT)(\sigma-\sigma_{p})^{4} \qquad (2019\ K \le T \le 2219\ K) \qquad (6.9)$$

where G and σ are in unit of MPa.

Figure 6.19 shows a comparison of the $\log(AG^{3}kT/b)$ values between different recrystallized materials. The slope of the line for W-4Re-0.26HfC gives an activation energy of 613.8 kJ/mole which is different from that obtained for the W-0.37HfC by only 5% in the same temperature range. However the line for W-4Re-0.26HfC is below that of W-0.37HfC, showing a 3 to 5 times reduction in the corresponding A values over the entire test temperature range. The reason for this reduction was investigated by comparing the test conditions of the two materials. According to Chen and Tsao et al., W-4Re-0.26HfC become fully recrystallized after annealing at 2100 K for one hour[24,29]. The creep tests of the W-4Re-0.26HfC from 1955 K and 2500 K were all conducted after recrystallized at 2100 K. The initial particle radius was about 20nm. While for the W-0.37HfC, the creep tests were conducted after the material having been recrystallized from 2673 K to 2773 K for one hour. Thus the starting average particle sizes were estimated between 60 nm and 77nm according to Equation (3.9). But the particle size is not believed to be the reason for the higher A values. As shown in Figure 6.9, the $\log(AG^{3}kT/b)$ value for the as-extruded W-0.37HfC increases is larger than the corresponding reggretion value for the recrystallized material due to the dynamic recrystallization of the as-extruded alloy during the creep test. This value is even larger than the reggretion $\log(AG^{3}kT/b)$ value of the W-4Re-0.26HfC under the recrystallized condition. According to Ozaki[25], the average particle radius in the as-extruded W-0.37HfC alloy used in this study is also 20nm. However, this small particle size did not lead to smaller A value than the pre-recrystallized W-4Re-0.26HfC samples when it was tested at 2500 K. In fact, the A value for the W-0.37HfC is over 3 times as large as that for

the pre-recrystallized W-4Re-0.26HfC crept under the same temperature and W-0.37HfC has a higher HfC volume fraction than that of the W-4Re-0.26HfC. Therefore, particle size effect on A cannot explain such reduction. As illustrated in section 6.3, the A value does not depend on the grain size of the material as long as full recrystallization is achieved. Then only difference between the two materials is that the presence of 4 a/o Re in the W-4Re-0.26HfC. Thus the difference in the A value may be due to the solid solution strengthening effect of Re to the matrix. To provide a quantitative evaluation on the Re solid solution effect on the creep properties of the HfC particle strengthened tungsten alloys, further study is needed to separate the two strengthening mechanisms. Therefore the effect of solid solution atom on the creep tungsten should also be studied with the absence of HfC particles. This study will be conducted in the next chapter.

Similar to the above study on the creep data of the W-0.37HfC alloy, the analysis was also done to the W-3.6Re-0.33w/oZrC and W-4Re-0.33mol%HfC. The results of such an analysis for the W-3.6Re-0.33w/oZrC yielded Q_C value of 334 kJ/mole (as shown in Figure 6.19). This value is close to the activation energy for dislocation core diffusion of 378 kJ/mole. The value of f_D is calculated to be 1.7×10^{-5} at a transition temperature of 2400 K (the highest creep test temperature for W-3.6w/oRe-0.33w/oZrC). This corresponds to the condition that the contribution of dislocation core diffusion and lattice diffusion are equal at the transition temperature. Using the equation obtained by Robinson and Sherby[35], a dislocation density of 1.7×10^{13} m^{-2} was found necessary for pure tungsten to maintain the dislocation core diffusion as the dominating creep process up to 2400 K. This dislocation density corresponds to an applied stress of 82 MPa in pure tungsten according to Vandervoort and Barmore[46] who have measured the dislocation density of tungsten as a function of stress at 2073 K. However, most of the creep tests for both

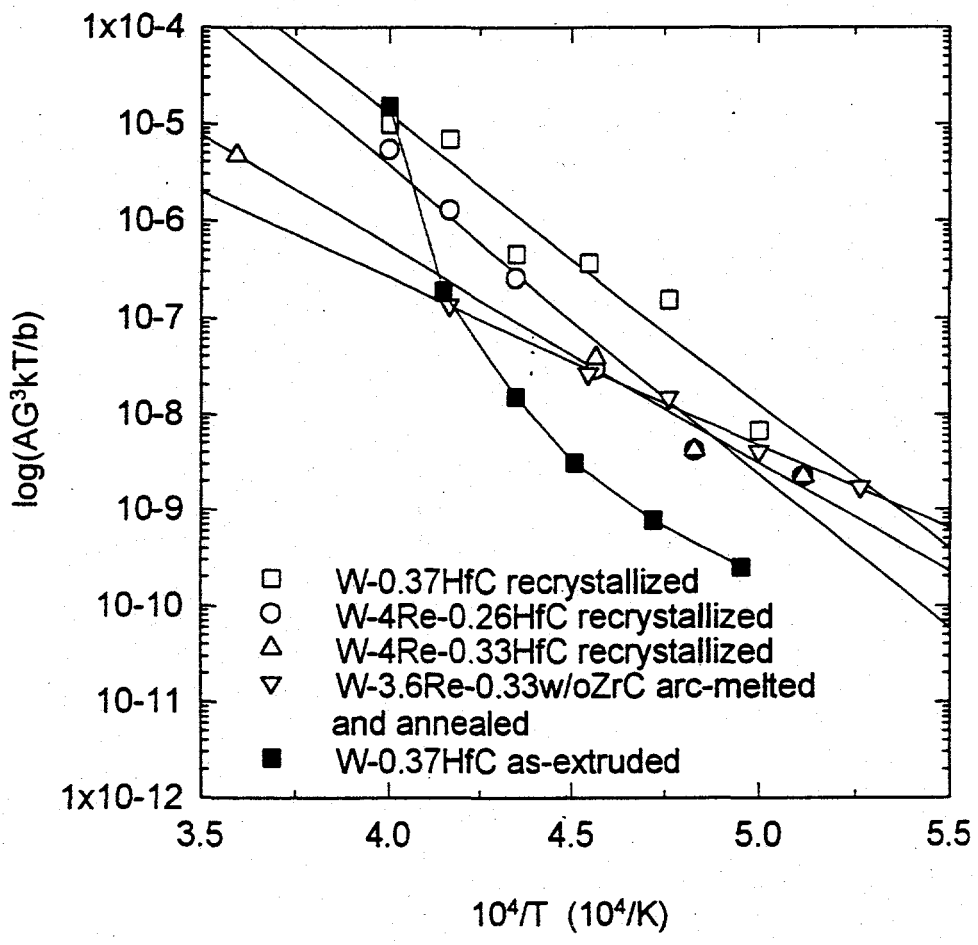

Figure 6.19. Comparison of the activation energy of particle strengthened tungsten alloys.

W-3.6w/oRe-0.33w/oZrC and W-4Re-0.33a/oHfC were conducted at stresses below 80 MPa. The reason for this material to have a high transition temperature of dominating creep controlling process may be due to high density of dislocations generated during the primary creep stage and retained by the particles during the steady state creep. In fact, in W-3.6w/oRe-0.33w/oZrC, there are estimated 1 vol% of ZrC particles (compared to 0.43vol% HfC in W-4Re-0.26 HfC and 0.6vol% HfC in W-0.37HfC). These ZrC particles are very fine (<100nm) even after annealing at 2473 K for two hours followed by testing at 2200 K for 200 hours[51]. The high volume percent and the presence of uncoarsened ZrC particles may be responsible for the low activation energy for creep observed. Another possible reason for the reduction of activation energy is the presence of alloying elements Zr in the W matrix which results in a decrease in the activation energy for diffusion of both solute and solvent. Povarova reported that the activation energy of diffusion for Zr in tungsten decreases by 167 kJ/mole due to the presence of Zr and it can be expected that the activation energy for the self-diffusion of tungsten will also be reduced with the presence of Zr[52].

An earlier study has examined the creep behavior in W-4Re-0.33mol%HfC alloy which contains 0.52 vol% of HfC particles. This concentration is very close to the reported volume percent at which this class of materials have shown the maximum high temperature tensile strength and creep strength[7]. As mentioned before, these high strengths are due to the high ability of HfC particles to resist dislocation motion and grain boundary and sub-boundary migration during deformation. Unfortunately, the author did not provide any microstructural information for their crept samples.

7. CREEP MODELING OF SINGLE CRYSTALLINE SOLID SOLUTION TUNGSTEN AND MOLYBDENUM ALLOYS

A recent report[17] stated that single crystal tungsten alloys had very high creep resistance which was an order of magnitude higher than that of W-4Re-0.33HfC at 2073 K. However, the authors did not mention the exact experimental conditions such as the crystal orientation of the specimens, the stress states and the stress direction relative to the orientation of the test specimens. These factors are important to the understanding of creep deformation in single crystals. Therefore, the analysis was first conducted based on an assumption that the growth of the single crystal were either in the [110] direction which is one of the conditions relevant to the geometry of the TFE or in [111] which provides six {110} planes on the circumference (maximum number possible). This (110) surface gives the best thermionic emission characteristics. The purpose of this research is to understand the creep behavior of TFE made of solid solution strengthened refractory single crystal alloys, especially molybdenum and tungsten. In such alloys, it is expected that the absence of grain boundary and the presence of solid solution will result in different creep deformation processes compared to dispersion strengthened polycrystals. The effects of the deformation geometry of the single crystal emitter and solid solution strengthening were examined separately.

7.1 Stress Analysis for Deformation of B.C.C. Single Crystalline Cylinderical Tube

The stress state experienced by the TFE cladding is more complex and resembles that of a thin wall cylinder subjected to an internal pressure. The wall of an internally pressured cylinder experiences a triaxial stress state with the circumferential stress (also called hoop stress or tangential stress) leading to creep in the diameter of the cylinder at high temperatures. Creep is usually measured by monitoring the outside diameter of the tube[49]. In this configuration, the

creep rate of the expanding outside diameter depends on the single crystal growth direction which is along the axis of the cylinder and the triaxial stress state. A stress analysis based on a single crystal cylindrical tube under an internal pressure was conducted.

In this study, we have only included the creep expansion in the outside diameter due to the effect of the hoop stress (resulting in the expansion of the diameter). Results, illustrated in Figure 7.1, show the resolved shear stresses in various possible planes on the surface of a single crystal cylinder with a [110] growth direction (coming out of the paper in Figure 7.1). The resolved shear stresses of three active slip systems under a hoop (or circumferential) stress, σ_h, were calculated around the perimeter of the cylinder. Two of the three slip systems belong to the $\{112\}\langle 11\bar{1}\rangle$ as indicated by the dotted and dashed lines. The third system is related to the basic $\{110\}\langle \bar{1}11\rangle$ slip and is represented by the solid line. Although the [110] direction possesses a two-fold symmetry, the resultant resolved shear stress distributions exhibit a four-fold symmetry due to the way that the circumferential (hoop) stress is projected onto the slip plane. The distribution of such resolved stresses provides information on the deformation around the circumference of the cylinder. There are alternating zones of large and small deformation within each slip system investigated. This is due to variations in the crystallographic orientation as a function of position around the cylinder. However the macroscopic stress distribution will be a summation of all the stresses from all the different available slip systems. This results in a relatively isotropic macroscopic stress distribution implying that the deformation observed in cylindrical single crystal with a [110] axis will be quite uniform. As pointed out by other authors[57], the increase in zone alternation results in a corresponding decrease in the effective

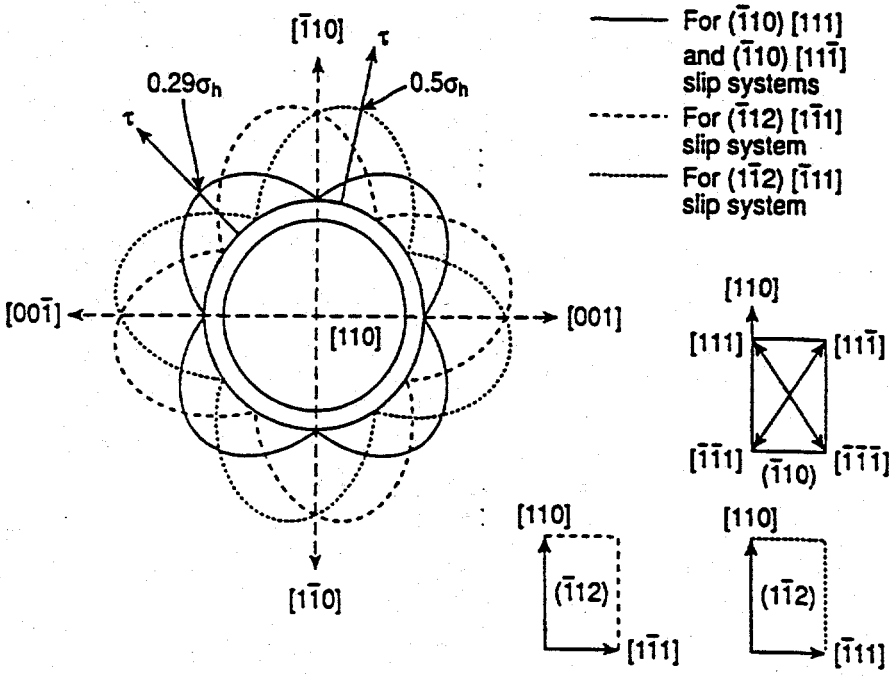

Figure 7.1. Resolved shear stress analysis for a BCC single crystalline thin-walled cylinder grown along the [110] axis.

dislocation free path generated by creep. This results in a reduction in the steady state creep rate. This effect was calculated for a cylinder with a [111] zone axis along its longitudinal direction. Similar to that shown in Figure 7.1, an analysis was also made on a single crystalline tube with a [111] growth direction. The resolved shear stress (τ) distributions for a [111] bcc single crystalline tube are shown in Figure 7.2. Three slip systems were considered, all of which were of the $\{1\bar{1}0\}<111>$ type. The three slip systems result in identical deformation (shown by the solid, dashed and dotted lines), but rotated 30° as expected due to the three-fold symmetry in the [111] direction. Consequently, the deformation due to a uniform hoop stress in cylindrical single crystal with a [111] axis is again quite uniform.

The above analysis is supported by the experimental study of Tachkova[49]. In Tachkova's work, the effect of solid solution strengthening on the creep expansion rates of the outside diameter single crystal cylindrical sample were reported and the results are summarized in Figure 7.3. In this figure, the steady state creep rate of the outside diameter is plotted against the resolved shear stress in a log-log manner so that the slope of the line is related to the stress exponent. The use of resolved shear stress instead of applied stress eliminates the directional dependence of the stress state. The tests were conducted using an internally pressurized thin wall tube configuration to simulate the service conditions of the TFE. The authors found, in pure Mo single crystals, the stress exponent (5.8) is independent of the crystal orientation (both in the [110] and [111] directions). This implies that the resolved stress distributions (similar to that given in Figures 7.1 and 7.2) for the two crystal directions are relatively similar.

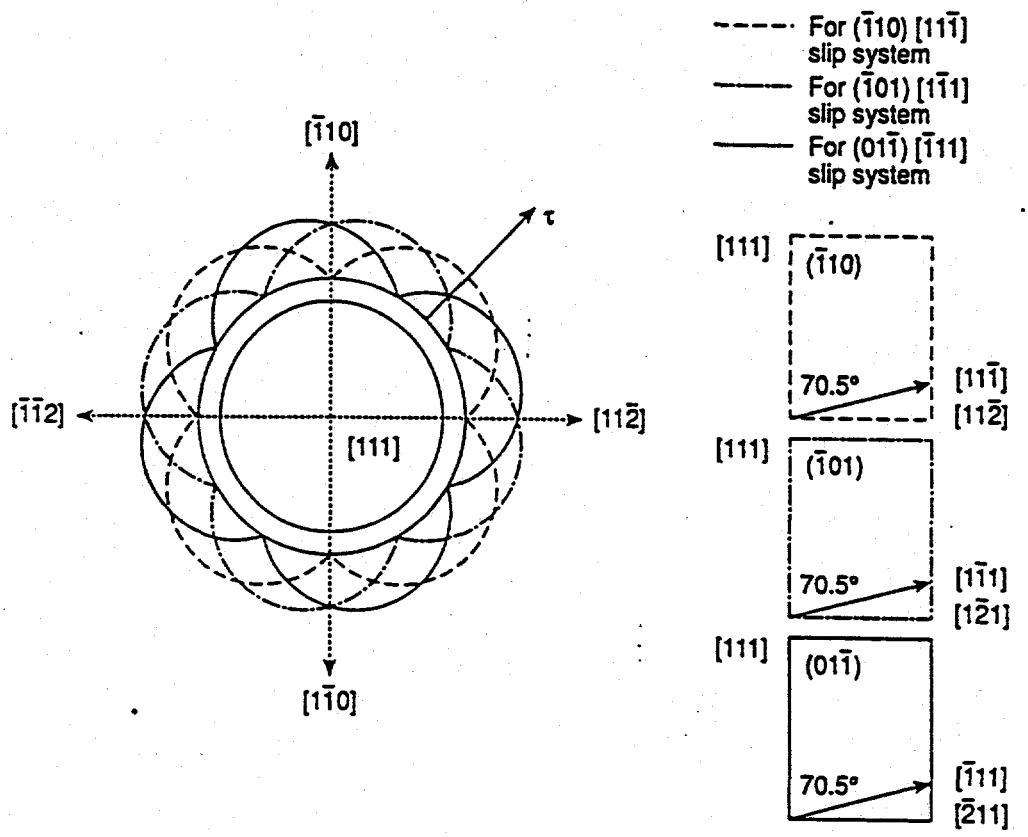

Figure 7.2. Resolved shear stress analysis for a BCC single crystalline thin-walled cylinder grown along [111] axis.

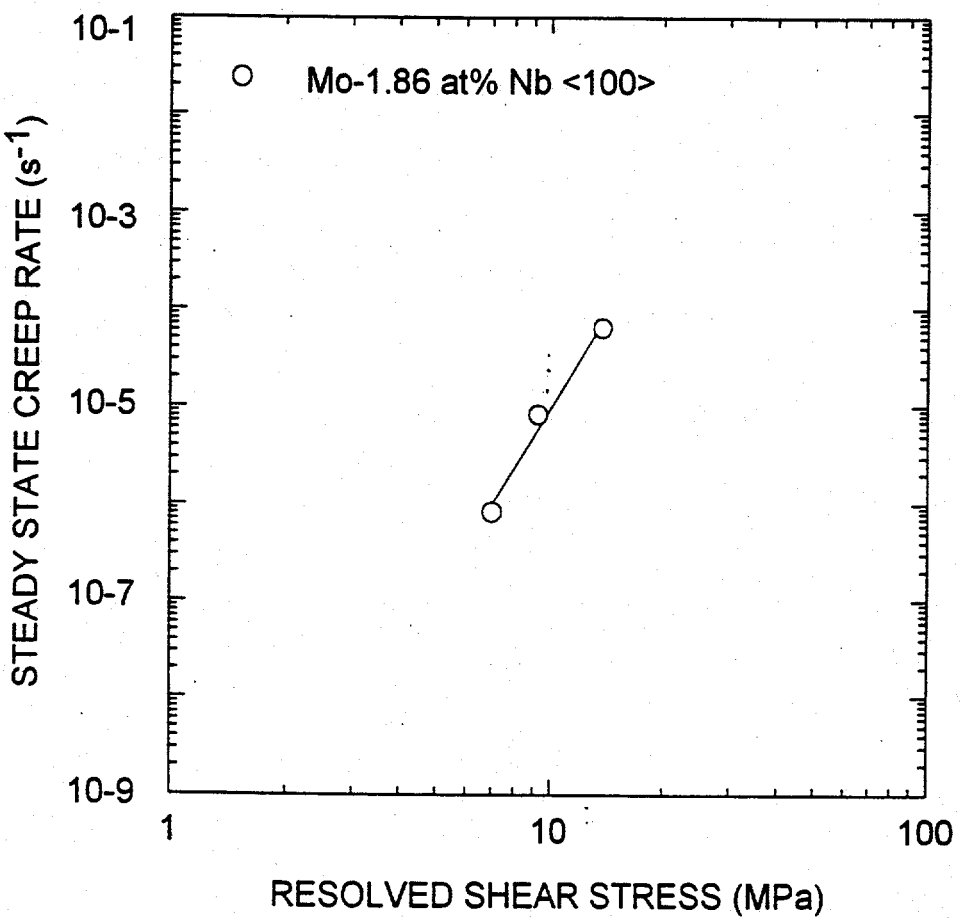

Figure 7.3. Creep of the outside diameter of a Mo-Nb single crystalline cylinder[49].

7.2 Creep Modeling of Tungsten and Molybdenum Single Crystalline Solid Solution Alloys

The effects of alloying on the creep behavior of solid solution alloys have been studied extensively. The addition of solute atoms not only increases the creep strength, but under certain conditions also leads to a change of the stress exponent of the steady state creep equation from 5 to a value of 3. This is especially the case for the creep of single crystalline Mo-Nb alloys at 1923 K reported by Tachkova[49]. They observed that the stress exponent of the alloys changed from 5.8 to 3 when the Nb content was increased above 3 wt%. This change in creep behavior is consistent with the classification by Sherby and Burke[32]. In their study, the steady state creep behavior of solids is divided into Class I and Class II solids by the two different stress exponent (n) values of 3 and 5 respectively. The transition of the creep behavior from Class II to Class I with the increase of solute concentration reveals a change of dominating creep mechanism from climb controlled (as modeled by Weertmann[48]) to glide controlled as modeled by Takeuchi and Argon[47]. The prediction of such a change with respect to the alloy type and alloy concentration depends on the modeling of the two distinct creep mechanisms. In Mo-Nb alloys, the effect of alloy concentration on Class I creep can be well explained by the T-A model as reported by Tachkova (Equation (3.19))[49]. However, the effect of alloying on the Class II creep of Mo-Nb alloys has not been formulated. Similar situation also exists in the solid solution tungsten alloys where many alloys exhibit Class II creep behavior, as reviewed in Chapter 3. Therefore the purpose of the following sections are to model the Class II creep behavior observed in tungsten and molybdenum alloys.

7.2.1. Modeling Approach

The creep strength of W-Re, W-Nb, and W-Hf at 2200 K has been determined by Raffo and Klopp[12]. They concluded that Hf was the most effective strengthener in tungsten while Re

was the least effective among the three elements considered as shown in Figure 7.4. The effect of strengthening was found to be governed by the atomic size difference between the solute atoms and tungsten. Unfortunately no quantitative model for these alloys has been developed. As shown in Figure 7.5, results from polycrystalline tungsten and its alloys show that Class II creep behavior exists in most alloys under the stress and temperature conditions of interest. The presence of solutes shifts the creep rate lower relative to that observed in pure tungsten. Thus a creep model was formulated for these materials that accounted for the alloying effect by a shift factor. The creep behavior of solution strengthened alloys is related to that of the pure material via the equation:

$$\dot{\varepsilon}_{alloy} = S_{alloy}\, \dot{\varepsilon}_{pure} \tag{7.1}$$

where $\dot{\varepsilon}_{alloy}$ and $\dot{\varepsilon}_{pure}$ are the steady state creep rate of the alloy and its matrix metal respectively, and S_{alloy} is the shift factor. This model requires that: (1) the creep of the dilute tungsten alloys has the same stress exponent (n) as that of pure tungsten, (2) atomic mismatch and alloy concentration being the dominate factors on creep, (3) the alloy shift factor S_{alloy} provides a smooth transition in terms of changes in composition and solute type.

To determine the form of the shift factor S_{alloy}, the observation that the addition of solute atoms leads to a reduction in creep rate or increment in creep strength is considered. The strengthening effect of the solute was assumed to originate from its interaction with climbing dislocations thus imposing an extra energy barrier for creep to occur in these alloys. This barrier was assumed to be a function of atomic mismatch (e) and alloy concentration (C) according to the conclusion of Raffo and Klopp[12]. Since creep is a thermally activated process, this extra energy barrier f(e,C) will affect the creep of the alloys through the term exp[-f(e,C)/(RT)]. Thus Equation (7.1) can be re-expressed as

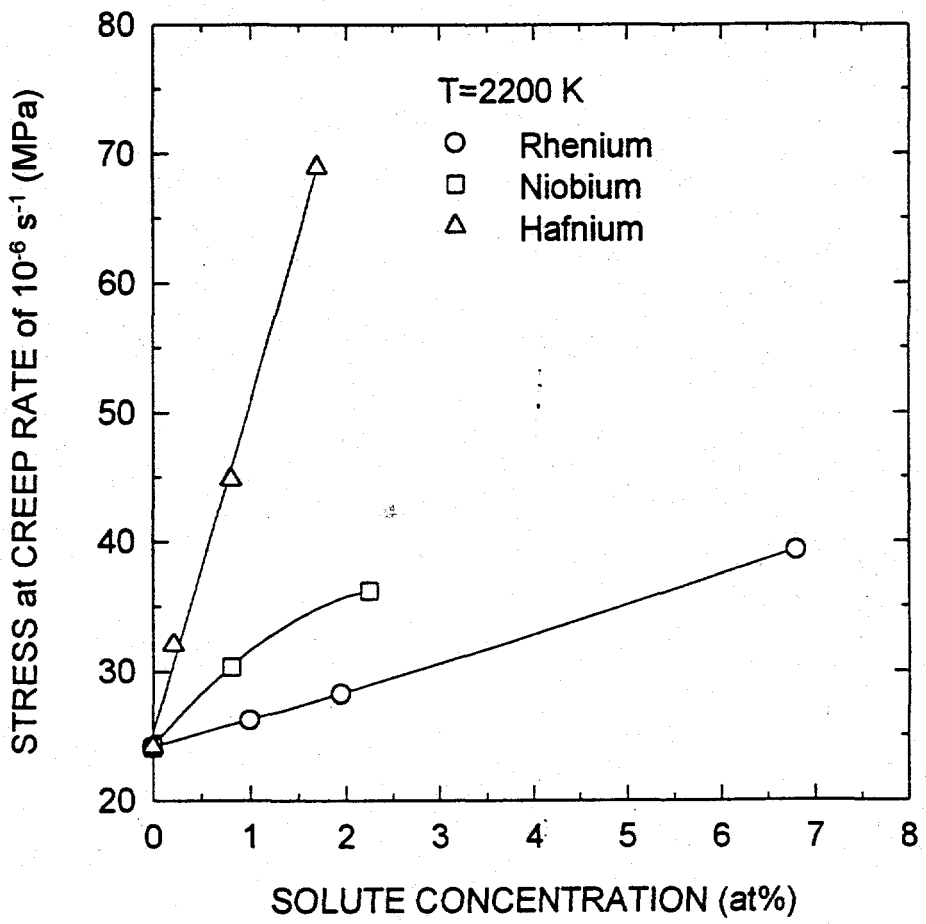

Figure 7.4. Effect of solute content on creep strength of solid solution strengthened tungsten alloys[12].

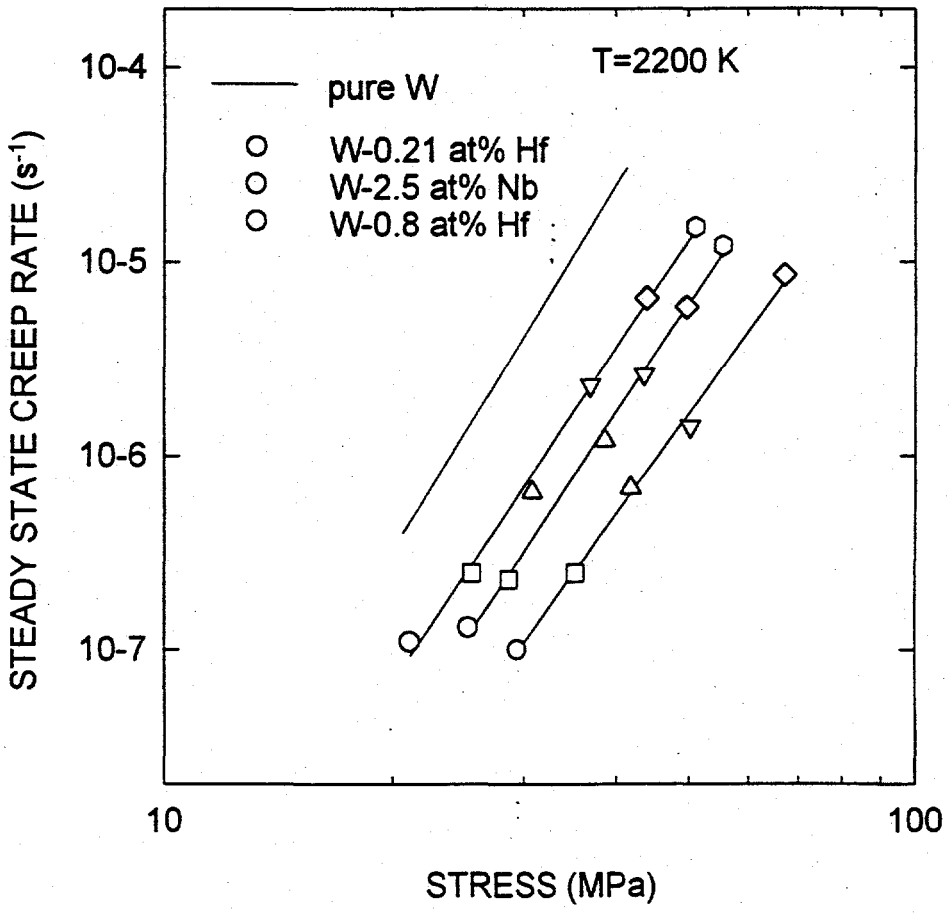

Figure 7.5. Steady state creep of tungsten and its solid solution alloys[12].

$$\dot{\varepsilon}_{alloy} = \dot{\varepsilon}_{pure} \exp[-f(e,C)/(RT)] \quad (7.2)$$

where R is the gas constant and T is the absolute temperature. The shift factor $S_{alloy} = \exp[-f(e,C)/(RT)]$ was assumed to be similar for materials in both the single crystalline and polycrystalline states.

7.2.2 Model Verification Based on Tungsten Alloys

The strengthening effect varies with solutes as illustrated in Figure 7.4. The value of the term $\exp[-f(e,C)/(RT)]$ at 2200 K can be obtained from the information provided in Figure 7.5 when both σ_{alloy}(creep strength of alloy) and σ_{pure} (creep strength of pure tungsten) at $\dot{\varepsilon}=10^{-6}$ s^{-1} are known for the given alloying solute and compositions. Hence, for any alloy that obeys the power law creep equation ($\dot{\varepsilon} = A_c\sigma^n$), the condition of constant creep rate of 10^{-6} s^{-1} yields the following relationship:

$$A_{c\ alloy}\sigma_{alloy}^{\ n} = A_{c\ pure}\sigma_{pure}^{\ n} = 10^{-6}\ s^{-1} \quad (7.3)$$

where n=5.8 in pure tungsten and its dilute alloys. From Equation (7.2), the condition of constant stress σ_{pure} gives:

$$A_{c\ alloy}\sigma_{pure}^{\ n} = A_{c\ pure}\sigma_{pure}^{\ n}\exp[-f(e,C)/(2200R)] \quad (7.4)$$

Taking the natural logarithm of both sides of the Equation (7.4) and combining with Equation (7.3), result in:

$$\ln\sigma_{alloy} = \ln\sigma_{pure} + f(e,C)/(2200Rn) \quad (7.5)$$

Through Equation (7.5), the relationship between e, C and σ_{alloy} can be obtained if the exact form of f(e,C) is known. The values of the atomic size mismatch (e) are given in Table 7.1 for use to determine the factor.

One of the boundary conditions of Equation (7.4) is that if the solute content C is zero (pure unalloyed material), $A_{c\ pure}$ should equals to $A_{c\ alloy}$. Furthermore, if the atomic size mismatch factor (e) is zero (same atomic radius and therefore no strengthening effect), we have $A_{c\ pure} = A_{c\ alloy}$. In both cases, the alloy behaves like a pure metal. The form of the parameter f(e,C) is thus expected to be a function of the product of e and C. Based on this phenomenological assumption, selecting different alloy concentrations and determining the creep strength at a constant creep rate of 10^{-6} s^{-1} and using the corresponding e values from Table 7.1, a master curve was obtained with the parameter f(e,C) taking the form of $eC^{1/2}$. This is shown in Figure 7.6. From this master curve, the creep strength of W-Re, W-Nb, and W-Hf alloys at 10^{-6} 1/s is governed by the product $eC^{1/2}$ through the relationship:

$$\ln\sigma_{alloy} = 66eC^{1/2} + 3.1 = 66eC^{1/2} + \ln\sigma_{pure} \quad (7.6)$$

Comparing the above equation with Equation (7.5), the parameter f(e,C) at 2200 K is given by $f(e,C) = 66eC^{1/2}$. Therefore, $f(e,C) = 145000nReC^{1/2}$ at 2200 K with C in mole fraction. The steady state creep rate of the binary solid solution strengthened tungsten alloys can be expressed as:

$$\dot{\varepsilon}_{alloy} = \dot{\varepsilon}_{pure} \exp(-145000neC^{1/2}/T) \quad (7.7)$$

where n equals to 5.8 for the arc-melted tungsten [3] and single crystalline tungsten [53]. Equation (7.7) shows that when either e or C equals to zero (which corresponds to a pure metal), f(e,C) vanishes, and the term exp[-f(e,C)/(RT)] equals to one. In this case, $\dot{\varepsilon}_{alloy}$ becomes $\dot{\varepsilon}_{pure}$ as required.

Table 7.1. Atomic Size Mismatch between Tungsten and Three Solutes

Element	Atomic Radius (R) (in angstrom) [65]	Atomic Size Difference (relative to W)	Atomic Size Mismatch (e) $e=\lvert r_W-r_{solute}\rvert/r_W$
W	1.38	0.00	0.00
Re	1.34	-0.04	0.029
Nb	1.44	0.06	0.042
Hf	1.55	0.17	0.123

*r_W is the radius of the tungsten atom and r_{solute} is the radius of the alloying solute.

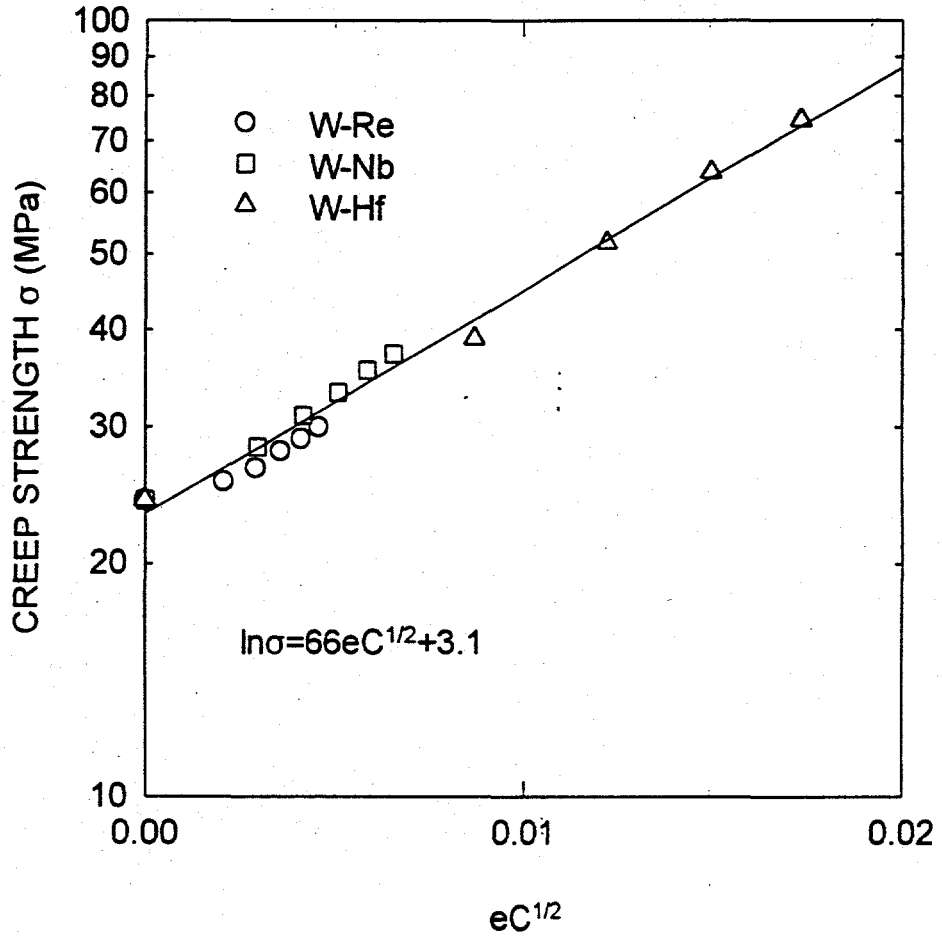

Figure 7.6. Master curve showing the dependence of creep strength of the tungsten solid solution alloys at $\dot{\varepsilon}=10^{-6}\,s^{-1}$ at 2200 K.

7.2.3 Model Verification Based on Molybdenum Alloys

The creep behavior of Mo-Nb and Mo-Hf solution strengthened single crystals is summarized in Figure (7.7). The data for the Mo-Nb alloys were obtained at 1923 K Tachkova[49] whereas the Mo-Hf study was conducted by Liu and Zee[66] at 1853 K. The creep response of an unalloyed Mo single crystal is included and it exhibits Class II creep with a stress exponent of 5.8. Two alloys (1.8 wt%Nb and 2 at%Hf) were found to possess Class II creep as shown in Figure 7.7. The same analysis outlined for the W alloys in the above section was conducted for these Mo alloys. The same objective is to determine the functional form of f(e.C) for Mo alloys. Figure 7.8 represents the shear stress dependence on the parameter $eC^{1/2}$ at a constant creep rate of 10^{-6} s^{-1} for the two Mo alloys of interest (similar to Figure 7.6 for W). Two lines were obtained due to the difference in temperature. The Mo-Nb alloy was tested at a higher temperature than the Mo-Hf material. Since creep is thermally activated, it is possible to correct for this temperature by the term $\exp(-Q_c/RT)$. Figure 7.9 represents a temperature corrected plot with an activation energy (Q_c) of 443 kJ/mol. This Q_c value corresponds to the activation energy for creep in Mo obtained from the literature[55]. From this analysis, the solution strengthening function was found to be $f(e,C)=260000RneC^{1/2}$. The Class II creep behavior of Mo-based alloys can therefore be described by

$$\dot{\varepsilon}_{alloy} = \dot{\varepsilon}_{pure} \exp(-260000neC^{1/2}/T) \qquad (7.8)$$

where C is the mole fraction of the solute.

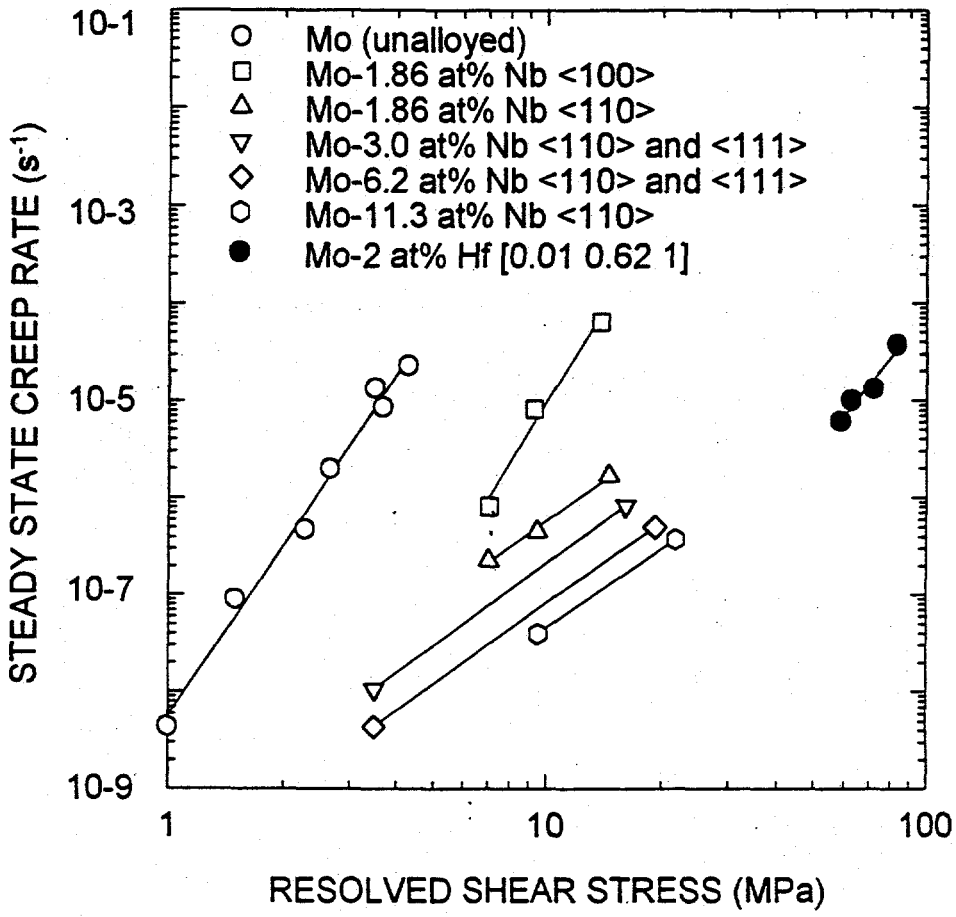

Figure 7.7. Steady state creep of molybdenum single crystal and single crystalline molybdenum alloys[49,66].

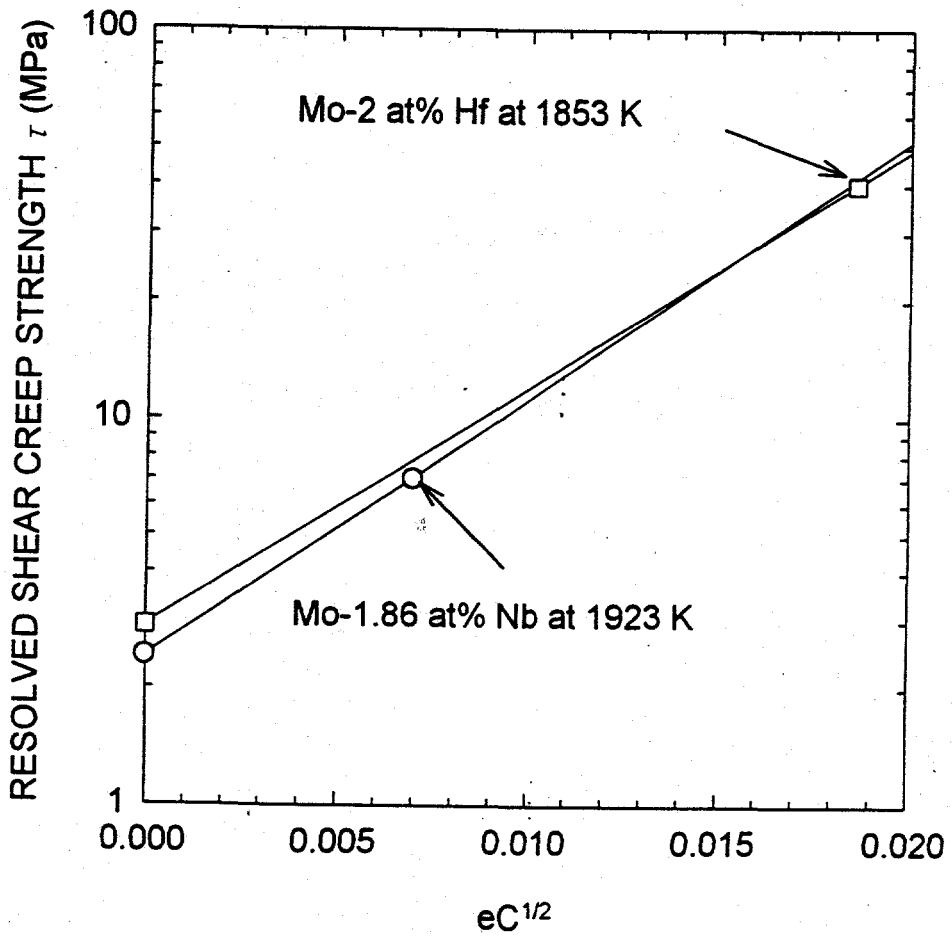

Figure 7.8. Dependence of creep strength of molybdenum alloys on alloy content and alloy type at $\dot{\varepsilon}=10^{-6}\,s^{-1}$.

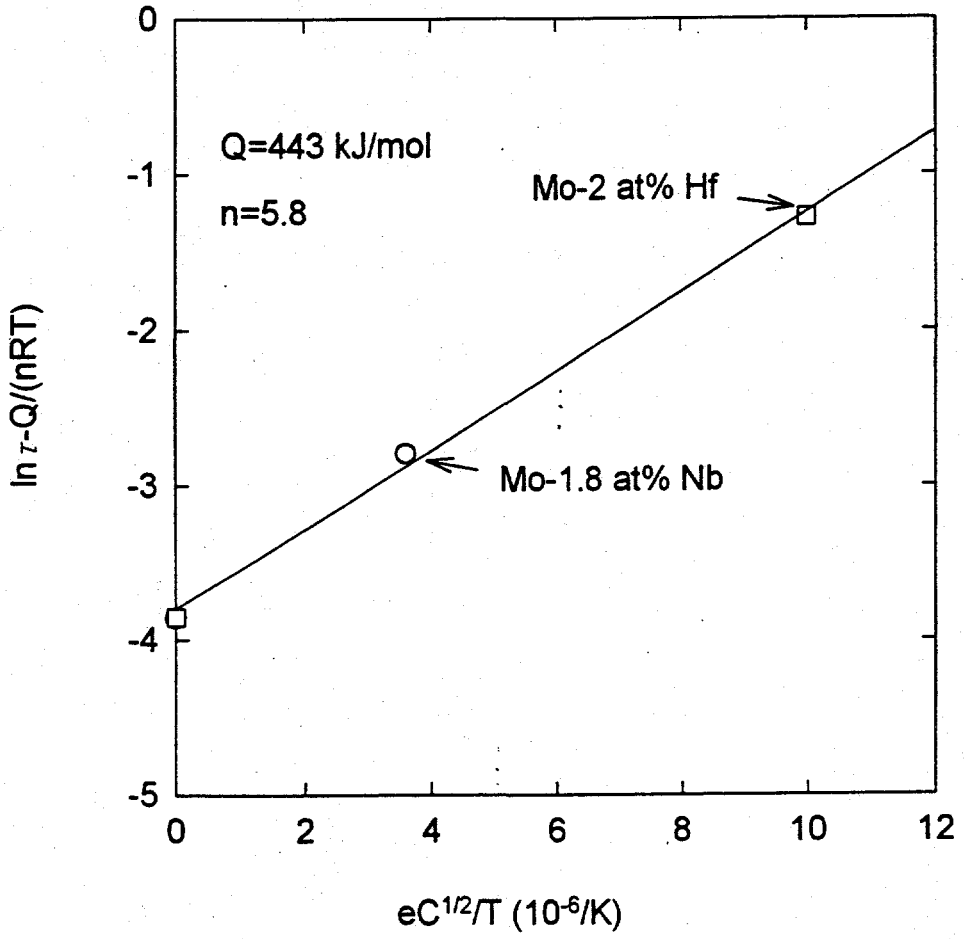

Figure 7.9. Same as Figure 7.8 but corrected by temperature.

7.2.4 Discussion

As mentioned earlier the physical origin of the factor f(e,C) is the additional energy barrier imposed on dislocation climb process caused by the solute atoms during creep. This implies that the process is thermally activated and the reduction of creep rate will drop exponentially as predicted by new model. Thus creep caused by dislocation climb will be reduced with increasing alloy concentration as compared to the creep induced by dislocation glide. Therefore there exists a point where creep mechanism changes from climb control to viscous glide control, the latter of which will dominate the creep when the solute concentration is high enough. This transition behavior was observed in Mo-Nb single crystalline alloys[49].

The creep model developed in this study for both tungsten and molybdenum alloys provides a good fit to the existing Class II creep data. For those alloys showing dislocation glide, there exists a point where creep mechanism changes from climb control to viscous glide control, the latter of which will dominate the creep when the solute concentration is high enough. This transitionbehavior was observed in Mo-Nb single crystalline alloys[49].

The creep model developed in this study for both tungsten and molybdenum alloys provides a good fit to the existing Class II creep data. For alloys showing Class I creep behavior, the creep caused by climb mechanism does not play a dominate role. For example, Raffo and Klopp[12] have examined a tungsten alloy with 0.8 at% Hf at 2200 K with the results shown in figure 7.10. Their data were in excellent agreement with the dislocation climb controlled model (Equation (7.7)) as illustrated in the same figure. As expected, the creep rate predicted by the Takeuchi and Argon[47] model ($\dot{\varepsilon} = \{kTD_s\sigma^3\}/[8Ce^2G^4b^5]$) is lower than the measured quantities indicating that the dislocation glide controlled creep is not a dominate process

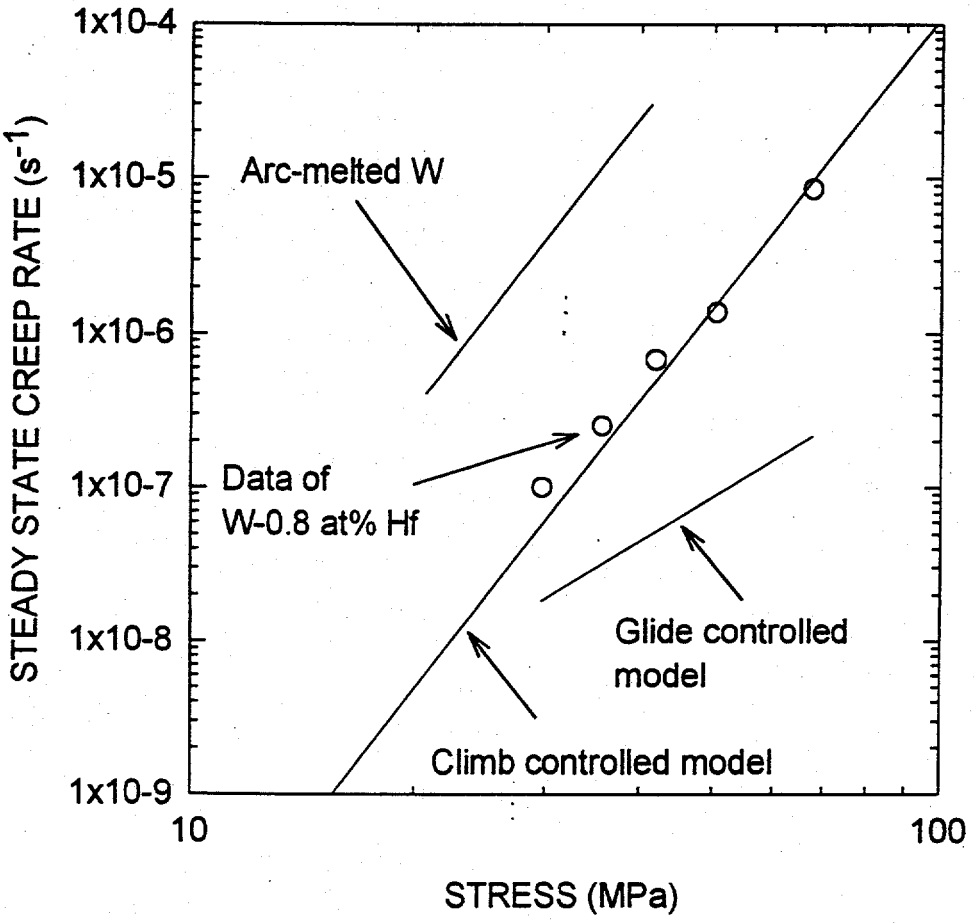

Figure 7.10. Comparison of creep rates of a W-Hf alloy predicted by the model with experimental data at 2200 K[12].

in this alloy. In this prediction, the solute diffusivity of Hf at 2200 K, $5.9X10^{-18}m^2s^{-1}$ was used according to Ozaki[25]. At stresses below 20 MPa, dislocation viscous glide will become the dominate mechanism as predicted by the Takeuchi and Argon. However, no creep data at such low stress levels are available. Especially, in W-25Re alloy where glide controlled creep (Class I) dominates[46], creep predicted by Equation (7.7) shown that the climb mechanism is not dominating which is consistent with the experimental data of W-25Re. In molybdenum alloys, Figures 7.10 and 7.11 show the excellent prediction of the dislocation climb model on Mo-Nb and Mo-Hf alloys respectively.

The physical origin of the shift factor in the above model has draw theoretical interest in this study. The presence of solute atoms enhances the creep resistance of the material by dislocation pinning. Under the conditions of high applied stress and high temperature, this strengthening effect is due to the resistance of dislocation climb by solutes. The size misfit between the solute and the solvent atoms is the source of dislocation pinning. The model developed is based on the excess energy for dislocations to bow around solute atoms. Figure 7.12 illustrates such an interaction. The solute atoms are assumed to be evenly distributed. Climbing dislocations (due to applied stress) are pinned when they encounter solute atoms due to the interaction of the strain field produced by the size misfit. The pinned dislocation line will bow upon increase in the applied stress. A balance in force will be established between the line tension of the

dislocation (T) and the resistance force of the solute (F). The bowing angle (ϕ) is a function of applied stress. The overall line length of the dislocation increases due to bowing. The force balance criterion yields:

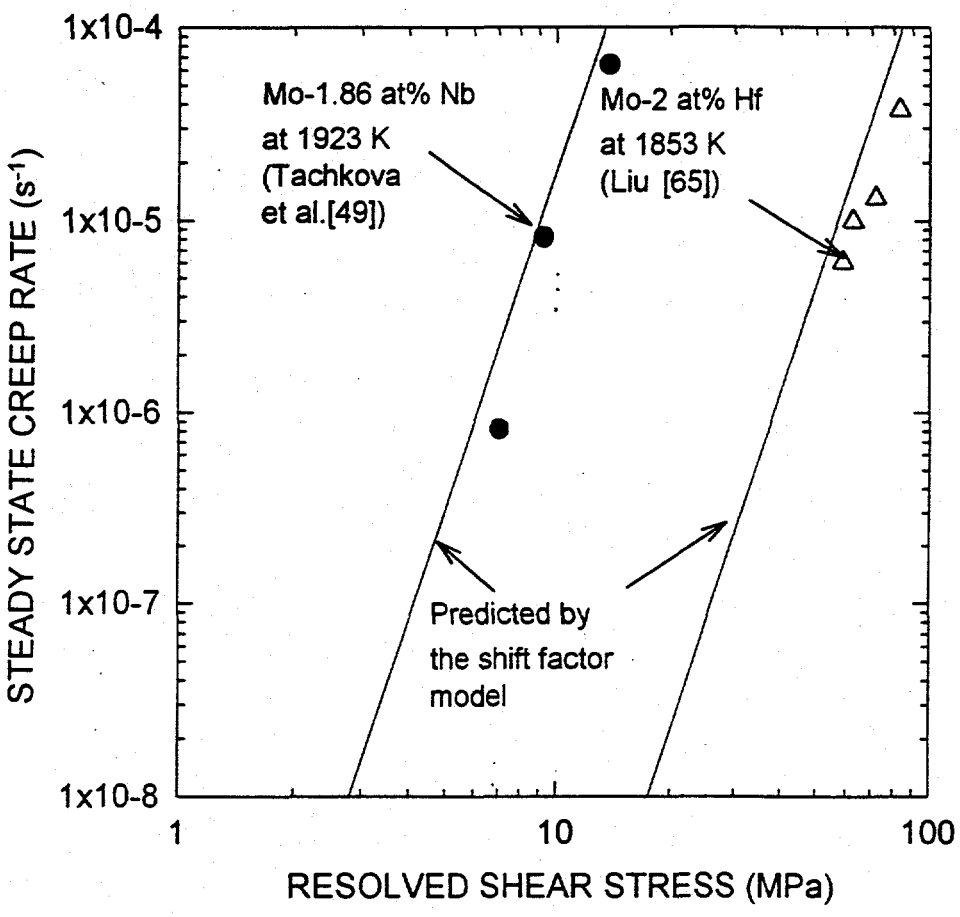

Figure 7.11. Comparison of creep rates of molybdenum alloys predicted by the model with experimental data[49,66].

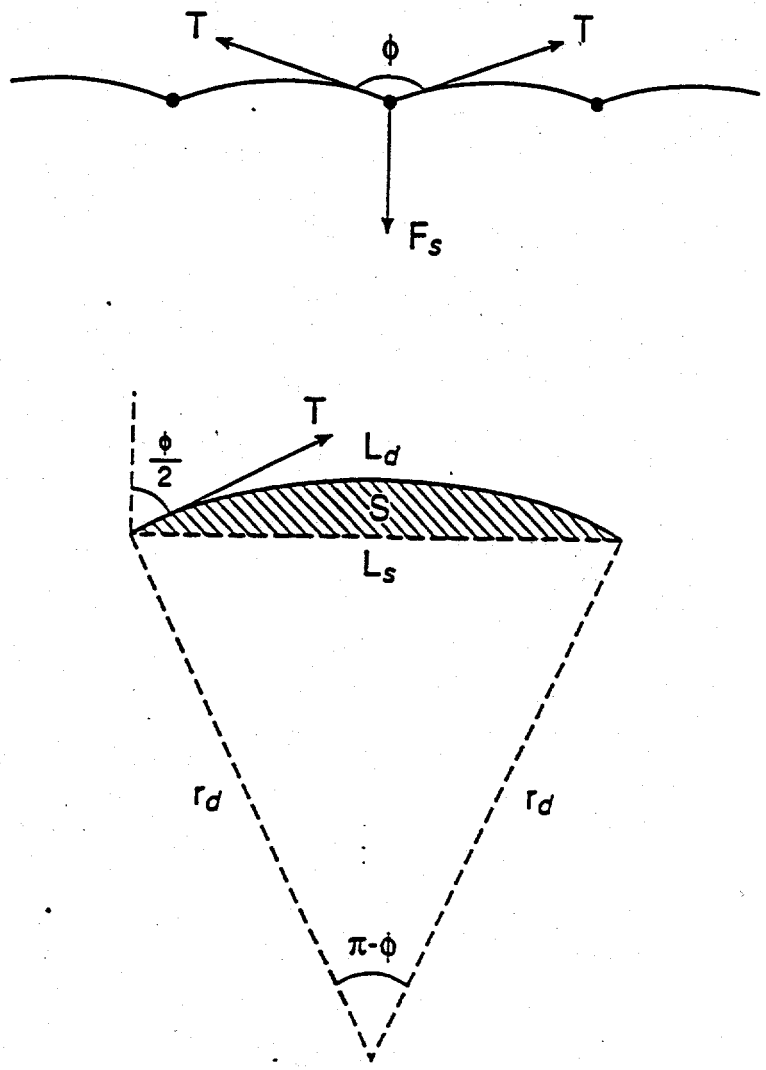

Figure 7.12. Schematic drawing of the interaction of climbing dislocation with solute atoms.

$$2T\cos(\phi/2) = F_s \tag{7.9}$$

The elastic interaction energy for a solute atom at a distance $\bar{r}$ and an angle θ from a dislocation can be described as[67]

$$U(r,\theta) = A(\sin\theta)/\bar{r} \tag{7.10}$$

where

$$A=(4/3)[(1+\upsilon)/(1-\upsilon)]Gber^3_{matrix} \tag{7.11}$$

and r_{matrix} is the atomic radius of the matrix, G is the shear modulus of the material (temperature dependent), b is the Burgers vector (0.274 nm for tungsten) and υ is the Poisson's ratio (0.28 for tungsten). The term e is the atomic size mismatch factor between the solute and the solvent (matrix) atoms as shown in Table 7.1. Absolute values of this parameter are given since the interaction between dislocations and solute atoms only depends on the magnitude of this mismatch and not its sign.

When a dislocation approaches a solute atom through the climb process, the interaction energy (given in Equation (7.10)) increases. The maximum interaction occurs at a θ angle of 90^0 (the dislocation approach the solute atom either from the top or bottom in Figure 7.12). Under this condition, the energy U is simply $A/\bar{r}$. The interaction force F that the solute atom exerts on the dislocation to impede its climb is related to the derivative of the interaction energy ($F=-dU/d\bar{r}$). This interaction force between solute and dislocation increases as the applied stress is

increased. The maximum force (F_c) that this interaction can provide prior to the breakaway of the dislocation from the solute atoms can be computed by first determining the interaction force through F=-dU/dr yielding:

$$F = (4/3)(1+\upsilon)Gber^3_{matrix}/[(1-\upsilon)\bar{r}^2] \quad (7.12)$$

Substituting the condition $r_{matrix} = \bar{r} = b/2$ and a Poisson's ratio of 0.28 into the equation yields:

$$F_c = 1.2Gb^2e \quad (7.13)$$

At the point of contact between the solute atom and the dislocation, the line tension T at the critical conditionjust prior to breakaway is given by[68]:

$$T_c = Gb^2[\ln(R_1/R_0)-1]/[4\pi(1-\upsilon)] \quad (7.14)$$

where R_1 is the spacing between dislocations and R_0 is the size of the dislocation core (which is normally approximately five times the Burgers vector. In the solution strengthened alloys of interest, the materials are normally in their well annealed state with an average dislocation density on the order of 10^{12} m^2. This yields a dislocation spacing (R_1) of 10^{-3} mm. Substituting $R_1=10^{-3}$ mm, $R_0=5b=1.2x10^{-6}$ mm and $\upsilon=0.28$ into Equation (7.14), the critical line tension for dislocation breakaway is:

$$T_c = 0.5Gb^2 \quad (7.15)$$

At this critical point, the parameters (F_c, T_c and ϕ_c) in Equation (7.9) will take on their respective critical values:

$$2T_c\cos(\phi_c/2) = F_c \tag{7.16}$$

From this equality, the critical bowing angle ϕ_c can be obtained. Combining Equations (7.13), (7.15) and (7.16), the critical bowing angle for tungsten strengthened with three types of solutes (Re, Nb and Hf) can be calculated. The parameter that distinguishes the three alloys is the misfit coefficient e. The (ϕ_c/2) values for the W-Re, W-Nb and W-Hf alloys are 89.0°, 88.6° and 85.8° respectively. These angles are related to the maximum bowing of the dislocations prior to breakaway.

The retardation of creep due to solution strengthening arises from the extra line length of the dislocation (due to bowing) that must be generated prior to the breakaway of the dislocation from the solute atoms. For a section of dislocation between two solute atoms separated by a distance L_s, the increase in energy ΔE to create this extra line length can be written as:

$$\Delta E = T_c(L_d - L_s)/N \tag{7.17}$$

where T_c is the critical line tension defined earlier, L_d is the line length of the bow (larger than L_s, the straight line distance) and N is the number of atoms within the volume that the bowing dislocation has swept through. The parameter N is related to the shaded area (S) in Figure 7.12 in the following manner:

$$N = Sb/(2R)^3 \tag{7.18}$$

The area S (in Figure 7.12) can be calculated using simple geometry and is related to the other parameters of interest through:

$$S = [\pi - \phi_c - \sin\phi_c]L_s^2/[8\cos^2(\phi_c/2)] \tag{7.19}$$

It is reasonable to assume that the solute atoms are distributed randomly in the matrix. The term L_s is the average nearest neighbor distance between these atoms and is equal to $b/C^{1/2}$ where C is the solute concentration. Substituting Equations (7.18) and (7.19) into (7.17), the following expression for the extra energy required to free the dislocation from the pinning of the solute atoms:

$$\Delta E = (32/3)Gr^3_{matrix} f(\phi_c)[(1+\upsilon)/(1-\upsilon)](eC^{1/2}) \tag{7.20}$$

where

$$f(\phi_c) = [\pi - \phi_c - 2\cos(\phi_c/2)] / [\pi - \phi_c - \sin\phi_c] \tag{7.21}$$

As illustrated earlier, the value of ϕ_c is relatively insensitive to type of solute. This implies that the term $f(\phi_c)$ is also quite insensitive to materials. For the three alloying elements selected, the value of $f(\phi_c)$ is approximately 0.25.

The extra energy needed to free a climbing dislocation from solute pinning sites (given in

Equation (7.20)) can be used to calculate the reduction in creep due to the presence of such solute atoms. Since ΔE can be treated as an extra activation energy for creep, it is feasible to account for this strengthening effect by introducing an additional rate limiting term of the form $\exp(-\Delta E/kT)$ to the creep for the pure material. The creep rate of a strengthened alloy ($\dot{\varepsilon}_{alloy}$) is therefore related to the creep rate of the pure materials ($\dot{\varepsilon}_{pure}$) via the equation:

$$\dot{\varepsilon}_{alloy} = \dot{\varepsilon}_{pure}\exp(-\Delta E/kT) \tag{7.22}$$

where

$$\Delta E = 1.2\text{x}10^{-29}(m^3)\ GeC^{1/2} \tag{7.23}$$

Creep data are available for three tungsten based alloys (W-Re, W-Nb and W-Hf). At 2200 K, the exponential term $\Delta E/kT$ becomes $4.10\text{x}10^{-10}GeC^{1/2}$. Comparing with the term $\exp(-145000neC^{1/2}/T)$ from Equation (7.7) at 2200 K with an n value of 5.8, a G value of 932 GPa was obtained. This value is about eight times the dynamic shear modulus of pure tungsten[43] at 2200 K. Therefore, pure elastic interaction can not explain the interaction between the solute and dislocation. In spite of this, the ability of this model to fit the available data strengthens the confidence of our assumption that the creep resistance of the solid solution alloy comes from the extra activation energy required for creep in tungsten alloys. Equations (7.7) and (7.8) can be used to serve as a guidance for further improvement of the above creep model and for new alloy development.

8. CONCLUSIONS

A comprehensive study was conducted to examine the strengthening effects in Mo and W alloys via an experimental-modeling approach. Both solution strengthening and dispersion strengthening concepts were investigated.

8.1. Carbide Particle Strengthened Tungsten Alloys

1) A semi-mechanistic phenomenological creep model was developed to describe the creep of precipitation strengthened tungsten and tungsten-rhenium alloys which is consistent with the microstructure.

2). High temperature creep tests of W-0.37HfC alloy were conducted under different metallurgical conditions. Direct and indirect strengthening effects of the HfC were separated by the model developed in this alloys. Dynamic recrystallization during creep significantly reduces indirect strengthening at temperature above 2300 K. Below this temperature, the indirect strengthening will provide about 20 fold reduction in the creep rate of the W-0.37HfC.

3). The activation energy of creep for the W-0.37HfC tested between 2000 to 2500 K is 585 kJ/mole, indicating that creep is lattice diffusion controlled under this condition.

4). Correlations between metallurgical state of W-0.37HfC and creep behavior were made as function of temperature and stress.

8.2 Solid Solution Tungsten and Molybdenum Alloys

1). A model was developed to describe Class II creep behavior in solution strengthened refractory alloys of tungsten and molybdenum. This model successfully explained the available data in

alloys based on these body-centered cubic materials.

2). The effects of alloying on the dilute binary refractory alloy were modeled with alloy concentration (C) and atomic size mismatch parameter (e) (being the main parameter) between tungsten and solute atoms. A shift factor was developed and employed to predict the creep behavior of these alloys. Results show that Class II creep behavior of the binary tungsten alloys can be expressed as

$$\dot{\varepsilon}_{alloy} = \dot{\varepsilon}_{pure}\exp(-145000neC^{1/2}/T) \tag{8.1}$$

while the Class II creep behavior of the binary molybdenum alloys can be expressed as

$$\dot{\varepsilon}_{alloy} = \dot{\varepsilon}_{pure}\exp(-260000neC^{1/2}/T) \tag{8.2}$$

where $\dot{\varepsilon}_{pure}$ and $\dot{\varepsilon}_{alloy}$ are the steady state creep of the pure single crystalline tungsten and binary alloys respectively.

The model gives satisfactory predictions to existing creep data in solution strengthened tungsten and molybdenum alloys and provides insights into the development of high creep strength single crystals of refractory materials.

REFERENCES

1. T. Lamp and B. Donovan, "Advanced Thermionics Technology Programs at Wright Laboratory", American Institute of Physics Conference Proceedings 246, 1992 617-622.
2. Iain Le May, Principles of Mechanical Metallurgy, New York: Elsevier North-Holland, 1981.
3. P.L. Raffo, W.D. Klopp and W.R. Witzke, "Mechanical Properties of Arc-Melted and Electron-Beam-Melted Tungsten-Base Alloys", NASA TN D-2561 (1965).
4. W.D. Klopp, W.R. Witzke, and P.L. Raffo, "Mechanical properties of Dilute Tungsten-Rhenium Alloys", NASA TN D-3483 (1966).
5. W.D. Klopp and W.R. Witzke, "Mechanical Properties of Arc-Melted Tungsten-Rhenium-Hafnium-Carbon Alloys", NASA TN D-5348 (1969).
6. W.D. Klopp, P.L. Raffo and W.R. Witzke, "Strengthening of Molybdenum and Tungsten Alloys with HfC", Journal of Metals, June 1971, pp. 27-38.
7. L.S. Rubenstein, "Effect of Composition and Heat Treatment on High Temperature Strength of Arc-Melted Tungsten-Hafnium-Carbon Alloys", NASA TN D-4379 (1968).
8. W.R. Witzke, "The Effect of Composition on Mechanical Properties of W-4Re-Hf-C Alloys", Metallurgical Transactions 5, Feb 1974, pp. 499-504.
9. J.F. Morris and D.L. Jacobson, "Materials Considerations for Ultrahigh Temperature Thermionic Conversion in Space Nuclear Power", 21st Intersociety Energy Conversion Engineering Conference (IECEC) (1986) pp. 1326-1330.
10. J.F. Morris, "Ultralloys for Nuclear Thermionic Conversion", 18th Intersociety Energy Conversion Engineering Conference (IECEC) (1983) pp. 208-214.
11. J.F. Morris, "Decreased Creep for Increased Space Power", Engineering Fracture

Mechanics 24 (1) (1986) pp. 77-95.

12. P.L. Raffo and W.D. Klopp, "Mechanical Properties of Solid Solution and Carbide-Strengthened Arc-Melted Tungsten Alloys", NASA TN D-3248 (1966).

13. G.W. King and H.G. Sell, Trans. TMS-AIME, **233** (1965) pp.1104-1113.

14. CRC Handbook of Chemistry and Physics, 76th edition, D.R. Lide Ed., Ch. 12, pp. 172-189.

15. P.L. Raffo and W.D. Klopp, Refractory Metals and Alloys IV - Research and Development, Gordon and Breach, New York (1965) pp. 501-518.

16. A. Luo, Ph.D Dissertation, the Arizona State University, (1990).

17. Y.V. Nikolaev, V.S. Kolesov, P.V. Zubarev, A.G. Sintzov, N.G. Tachkova, A.A. Yastrebkov and A.S. Gontar, "Molybdenum and Tungsten Single Crystal Alloys with Abnormally High Creep Strength for Space Nuclear Power and Propulsion System", American Institute of Physics Conference Proceedings 271, Mohamed S. EL-Genk and Mark D. Hoover, eds., Albuquerque, NM, (1993), part one: 267-274.

18. G.S. Ansell, "The Mechanism of Dispersion-Strengthen - A Review", AIME Conference on Oxide Dispersion Strengthening, Bolton Landing, N.Y. June 27-29, 1966.

19. J.R. Low, Jr., Relation of Properties of Microstructure, ASM, P163.

20. K.H. Westmacott, C.W. Fountain and R.J. Stirton, "On Spacing of Dispersed Obstacles", Acta Metall., 14(1966) 1628-1629.

21. E. Orowan, Symposium on Internal Stress in Metals and Alloys, the Institute of Metals, London, 1948, p.451.

22. W.D. Klopp, W.R. Witzke and P.L. Raffo, "Effects of Grain Size on tensile creep Properties of Arc-Melted and Electron-Beam-Melted Tungsten at 2250°F to 4140°F",

Trans. Met. Soc. AIME, 233 (1965) 1860-1866.

23. A.J. Ardell, "Further Applications of the Theory of Particle Coarsening", Acta Metall., 15(1967) 1772-1775.

24. B.L. Chen, "High-Temperature Creep Behavior of Second-Phase Particle-Strengthened Tungsten Rhenium Alloys", Dissertation, Arizona State University, 1990.

25. Y. Ozaki, "Thermal Properties of Refractory Metals for Advanced Energy Conversion Systems", PhD Dissertation, Auburn University, 1994.

26. B.A. Dainyak, and V.I. Kostikov, Diffusion and Defect Data, 16(1978)66.

27. V.N. Yeremenko, T.Y. Velikanova, L.V. Artyukh and A.S. Vishnevsky, "Phase Diagram of Ternary System Hafnium-Tungsten-Carbon. Solidus Surface Projection", Rev. Int. Htes. Temp. Et Refract, 12 (1975) 209-213.

28. W.D. Klopp and P.L. Raffo, "Effect of Purity and Structure on Recrystallization, Grain Growth, Ductility, Tensil, and Creep Properties of Arc-Melted Tungsten", NASA TN 2503 (1964).

29. B.H. Tsao, M.L. Ramalingam, D. Tang, B.L. Chen, and D.L. Jacobson, "The Effect of ThO_2 and HfC on the Recrystallization of W-Re Alloys," Tungsten and Tungsten Alloys, Recent Advances, Andrew Crowson and Edward S. Chen Ed. 1991.

30. C. Zener, quoted by C.S. Smith, "Grains, Phases, and Interfaces: An Interpretation of Microstructure", Trans. Met. Soc. AIME, 175(1948) 47-49.

31. F.R.N. Nabrro, Report on Conference on Strength of Solids, Phys. Soc., Landon, 1948.

32. O.D. Sherby and P.M. Burke, "Mechanical Behavior of Crystalline Solids at Elevated Temperature", in Progress in Materials Science, 13(1967) 325-390.

33. J.W. Pagh, L.H. Amra and D. T. Hund, "Properties of Tungsten-Rhenium Lamp Wire"

ASM Trans. 55(1962) 451-461.

34. B. Harris and E. G. Ellison, "Creep and Tensile Properties of Heavily Drawn Tungsten Wire", Trans ASM, 59(1966) 744.

35. S.L. Robinson and O.D. Sherby, "Mechanical Behavior of Polycrystalline Tungsten at Elevated Temperature", Acta Metall. 17 (1969), 109-125.

36. J.W. Pugh, Trans ASM, 47(1955)984.

37. W.V. Green, Trans. AIME, 215, 1507(1959).

38. E.C. Sutherland and W.D. Klopp, "Observations of Properties of Sintered Wrought Tungsten Sheet at very High Temperatures", NASA TN D-1310, Lewis Reseearch Center, Cleaveland, Ohio, (1963).

39. E.R. Gilbert, J.E. Flinn and F.L. Yagee, paper presented at Fourth Symposium on Refractory Metals, French Lick, Indiana. Oct. 1 (1965).

40. P.N. Flagella, "High temperature creep -rupture behavior of unalloyed tungsten", Third High Temperature Technology Symposium, Asilomar, California, September (1967).

41. J.L. Taylor, D.H. Boone and O.W. Simmons, in Refractory Metals 1117, edited by W.A. Krivsky, pp.491-505. Gordon & Breach (1968).

42. P.E. Armstrong and H.L. Brown, Trans AIME, vol. 230, 962 (1964).

43. R. Lowrie and A.M. Gonas, J. appl. Phys., **36** (1965) pp.2189-2192.

44. W.D. Klopp, "Summary, NASA-Lewis Research Center Program on Refractory Metals for 1963-1974", NASA-Lewis Research Center, Cleveland, Ohio, (1974).

45. R.R. Vandervoort, "The Creep Behavior of W-5Re", Metall Trans. **1**(1970) pp.857-864.

46. R.R. Vandervoort and W. L. Barmore, "Elevated Temperature Deformation and Electron Microscope Study of Polycrystalline Tungsten and Tungsten-Rhenium Alloys",

Proceedings of 6th Plansee Seminar, Metallwerk Plansee Ag., Reutte-Tyrol, (1969) 108-137.

47. S. Takeuchi and A.S. Argon, "Steady-State Creep of Alloys due to Viscous Motion of Dislocations", Acta Metallurgica, 24 (1976): 883-889.

48. J. Weertman, "Natural Fifth Power Creep Law for Pure Metals", Proc. Second Int. Conf. Creep and Fracture in Engineering Materials and Structures, B. Wilsire and D.R.J. Owen (Eds), Prinerdge Press, Swansea, 1984, pp. 1-13.

49. N.G. Tachkova, P.V. Zubarev and A.A. Yastrebkov, "High temperature Creep of Monocrystalline Mo-Nb Alloys," Russian Metallurgy, (1987)1, 149-153.

50. B.L. Chen, A. Luo, K.S. Shin and D.L. Jacobson, " High Temperature Mechanical Properties of W-Re-HfC Alloys", Refractory Metals: State-of-the-Art 1988, P. Kumar and R.L. Ammom Ed. TMS 1989.

51. A. Luo, D.L. Jacobson, and Kwang S. Shin, "Particle Strengthened Tungsten for Space Power Applications', Proc. 26th Intersociety Energy Conversion Engineering Conference, Boston, Massachusetts, August 4-9, 1991, pp.142-147.

52. K.B. Povarova, "Diffusion and Stability of Strengthening Phases in Tungsten. Review.", Russ. Metall., 2(1981)134-147.

53. M.M. Myshlyaev, Y.A. Romanov, O.N. Sen'kov, I.I. Khodos and V.G. Glebovskii "High-Temperature Creep and the Dislocation Structure of Tungsten Single Crystals", Strength of Metals, (1979)11: 476-485.

54. A. Gindin et al, Fiz. Metal. Metalloved. 28, No. 6, (1969)1046.

55. A.H. Clauer, B.A. Wilcox and J.P. Hirth, "Creep Behavior of Molybdenum Single Crystals", Acta Metallurgica, 18 (1970) 367-379.

56. V.A. Kononenko et al., Fiz Metal. Metalloved., No. 4, (1991) 181.

57. YU.S. Belomyttsev et al., Russian Metallurgy, No. 1, (1984) 90.

58. J. Čadek, Creep in Metallic Materials, pp. 238-238, Elsevier, New York, (1988).

59. G.S Ansell and J. Weertmann, Trans. AIME **215** (1959) 838.

60. R.W. Lund and W.D. Nix, Acta Metall., **24** (1976) pp. 469-481.

61. R. Lagneborg, "Bypassing of Dislocation Past Particles by a Climb Mechanism", Scripta Metall. 7 (1973)605-613.

62. E. Arzt and M.F. Ashby, Scripta Met., **16** (1982) pp. 1285-1290.

63. A.J. Kennedy, Process of Creep and Fatigue in Metals, pp.147-280, Oliver and Boyd, Edinburgh 1962.

64. J. Čadek, Creep in Metallic Materials, pp. 50-51, Elsevier, New York, (1988).

65. F. Laves, "Crystal Structure and Atomic Size", Theory of Alloy Phases, American Society of Metals,(1956) pp.124-193.

66. J. Liu and R. Zee, to be published

67. A.H. Cottrell and B.A. Bilby, Proc. Roy. Soc., A62, 49(1949).